LIÈGE université Library

https://lib.uliege.be https://matheo.uliege.be

Master thesis : Clarifying the Neuronal and Neurovascular Properties of the fMRI Global Signal Amplitude During Mind-Blanking Reports

Auteur : Strizhneva, Varvara
Promoteur(s) : Phillips, Christophe; Demertzi, Athina
Faculté : Faculté des Sciences appliquées
Diplôme : Master en ingénieur civil biomédical, à finalité spécialisée
Année académique : 2024-2025
URI/URL : http://hdl.handle.net/2268.2/24912

Avertissement à l'attention des usagers :

Tous les documents placés en accès ouvert sur le site le site MatheO sont protégés par le droit d'auteur. Conformément aux principes énoncés par la "Budapest Open Access Initiative"(BOAI, 2002), l'utilisateur du site peut lire, télécharger, copier, transmettre, imprimer, chercher ou faire un lien vers le texte intégral de ces documents, les disséquer pour les indexer, s'en servir de données pour un logiciel, ou s'en servir à toute autre fin légale (ou prévue par la réglementation relative au droit d'auteur). Toute utilisation du document à des fins commerciales est strictement interdite.

Par ailleurs, l'utilisateur s'engage à respecter les droits moraux de l'auteur, principalement le droit à l'intégrité de l'oeuvre et le droit de paternité et ce dans toute utilisation que l'utilisateur entreprend. Ainsi, à titre d'exemple, lorsqu'il reproduira un document par extrait ou dans son intégralité, l'utilisateur citera de manière complète les sources telles que mentionnées ci-dessus. Toute utilisation non explicitement autorisée ci-avant (telle que par exemple, la modification du document ou son résumé) nécessite l'autorisation préalable et expresse des auteurs ou de leurs ayants droit.

University of Liège
School of Engineering and Computer Science

Clarifying the Neuronal and Neurovascular Properties of the fMRI Global Signal Amplitude During Mind-Blanking Reports

Master's Thesis

Submitted in partial fulfillment of the requirements for the degree of Master of Science in Biomedical Engineering by **Strizhneva Varvara**

Supervisors:

Profs Christophe Phillips and Athena Demertzi

2024–2025

Abstract

Spontaneous thinking can be seen as the internal mechanisms of consciousness that arise unintentionally and without deliberate effort. These thoughts include the dynamic processes that occur during wakefulness, but notably, they also involve periods where active cognition is absent. One such example of spontaneous thinking is mind-blanking, which refers to moments when a person experiences a complete lack of cognitive activity. Based on previous studies, this state is linked to increased slow-wave activity, which refers to low-frequency brain oscillations associated with deep sleep or drowsiness during wakefulness.

Research using functional magnetic resonance imaging (fMRI) has found that during episodes of mind-blanking, there is a noticeable increase in the fMRI global signal amplitude, which is defined as the time course across all voxels, and can reflect various underlying physiological and neuronal processes. However, because the global signal is complex and can be influenced by multiple factors such as physiological (e.g., heart rate), neuronal, and technical artifacts, it has been unclear which specific components are responsible for the observed increases during mind-blanking.

The objective of this study is to identify and clarify the specific components of the fMRI global signal during mind-blanking. Understanding how these components contribute to the phenomenon can shed light on the underlying neural and physiological mechanisms driving this state.

To achieve this, we analyzed multimodal data collected from electroencephalogram (EEG), fMRI, and electrocardiogram (ECG) recordings. Participants performed the Sustained Attention to Response Task (SART) and were asked to report their mental state and level of alertness throughout the experiment. From these data, key features were extracted: fMRI global signal amplitude, heart rate variability from ECG, and the amplitude of EEG oscillations across different frequency bands (delta, theta, alpha, gamma).

Then, we used linear mixed-effects models to examine the relationships between these physiological and neuronal signals and the global signal amplitude. Our analysis focused especially on how these relationships present during mind-blanking, but also considered other mental states such as mind-wandering and the on-task condition.

The results indicated that during reports of mind-blanking, the global signal amplitude was significantly negatively correlated with delta and theta EEG activity, meaning that as slow-wave activity increased, the global signal amplitude decreased in these bands. Conversely, there was a modest positive correlation with ECG variability, suggesting a physiological contribution. When examining the entire dataset regardless of mental state, we found that the global signal amplitude positively correlated with theta oscillations and negatively correlated with alpha oscillations, consistent with some previous studies.

In summary, these findings suggest that mind-blanking, which is associated with increased slow-wave EEG activity, can also involve a physiological contribution, particularly heart rate variability as reflected by the global brain signal. The observed increase in the global signal amplitude appears to be primarily driven by physiological changes, which can provide insights that mind-blanking is not a purely neuronal process and can be associated with increased heart rate activity as well.

Acknowledgments

This Master's thesis was my first long-term project in computational neurobiology, giving me the opportunity to step into the world of scientific research in this field and work alongside inspiring scientists. The work involved multi-level research and data processing, which would not have been possible without the guidance and support of many important individuals to whom I am sincerely grateful.

First, I would like to thank Prof. Christophe Phillips, my supervisor at the University of Liège, and Prof. Athena Demertzi, Head of the Physiology of Cognition Laboratory. They guided me throughout the project, provided professional support, and taught me valuable lessons not only related to my research but also about conducting scientific correctly.

I am also deeply grateful to the Physiology of Cognition Laboratory for welcoming me into a friendly and supportive atmosphere and for introducing me to the specific topic of my thesis. I thank Prof. Athena Demertzi for giving me the opportunity to work on such an interesting and meaningful project. I would like to extend my thanks to Federico Raimondo, postdoctoral researcher in the Applied Machine Learning Group, Institute of Neuroscience and Medicine, Brain Behaviour (INM-7), Research Centre Jülich, Germany, for supervising me on specific aspects of data processing and providing software support.

My special thanks go to Paradeisios Alexandros Boulakis, postdoctoral researcher at the Physiology of Cognition Lab, who mentored me throughout the project, guided me in statistical analysis and EEG processing, and patiently answered all my questions. The realisation of this project would never have been possible without his help.

I am also thankful to Dr. Christina Schmidt, who supported me with hardware-related questions, guided me with software issues, and was always friendly and available to help.

I wish to thank the Cyclotron Research Centre, where I carried out my work and participated in many lab events during my thesis period. This experience gave me the chance to meet an international scientific community, which was truly unique. I am also grateful to the University of Liège for the opportunity to pursue my Master's degree here, fulfilling my dream of studying internationally. Special thanks to Geris Liesbet, who introduced me to Prof. Phillips at the beginning of my studies and helped me integrate into the scientific field.

Finally, I would like to thank my husband for his constant support from a distance and for helping me with all technical problems. His encouragement and support meant a lot to me.

Contents

List of Figures

List of Tables

Abbreviations

Abbreviation	**Full Form**
fMRI	Functional Magnetic Resonance Imaging
EEG	Electroencephalography
ECG	Electrocardiogram
rs-fMRI	Resting-State Functional Magnetic Resonance Imaging
NREM	Non-Rapid Eye Movement Sleep
MB	Mind-Blanking
MW	Mind-Wandering
REM	Rapid Eye Movement Sleep
DMN	Default Mode Network
PFC	Prefrontal Cortex
ACC	Anterior Cingulate Cortex
AG	Angular Gyrus
Broca	Broca's Area
CE	Cerebellum
HC	Hippocampus
IFG	Inferior Frontal Gyrus
MPFC	Medial Prefrontal Cortex
SFG	Superior Frontal Gyrus
SMC	Supplementary Motor Cortex
CBF	Cerebral Blood Flow
CBV	Cerebral Blood Volume
$CMRO_2$	Cerebral Metabolic Rate of Oxygen
ATP	Adenosine Triphosphate
BOLD	Blood Oxygenation Level-Dependent
Hb	Hemoglobin
dHb	Deoxygenated Hemoglobin
GSR	Global Signal Regression
GSS	Global Signal Subtraction
LFP	Local Field Potentials
GS	Global Signal
HRF	Hemodynamic Response Function
GSA	Global Signal Amplitude

Table 1: List of abbreviations used in the thesis

Chapter 1

Introduction

Spontaneous thoughts, which are described as mental experiences that arise unintentionally and without deliberate effort, have become a widely researched topic in recent years. This is because they offer valuable insights into how our consciousness generates mental activity independently of environmental input.

Moreover, spontaneous thoughts are closely linked to attentional lapses, which occur when individuals disengage from the surrounding events, which affects cognitive performance in tasks that require attention. Investigating these mental states may help clarify how fluctuations in attention impact perception, memory, and decision-making.

Two prominent forms of spontaneous thought are mind-wandering (MW) and mind-blanking (MB). Both occur when attention drifts away from external stimuli, but they differ in content and experience (McCormick et al., 2018; Kawagoe et al., 2019). MW refers to self-generated thoughts that are unrelated to the task at hand but maintain internal mental content. MB, by contrast, is characterized by a subjective absence of thought, as if the mind "goes blank" without any discernible content.

MW has been extensively studied and is often described as a state less constrained than goal-directed thinking but more structured than dreaming (Christoff et al., 2016). It has become the dominant term in literature for describing spontaneous mental activity (Callard et al., 2013; Andrillon et al., 2019). MB, on the other hand, is a more recently characterized state. It is considered a distinct, spontaneous cognitive state, which, unlike MW, where thoughts drift away from an ongoing task but remain internally generated, MB is characterised by a seeming lack of mental content. In this sense, MB represents a unique state, which raises questions about whether it can be as an intermediate state between wakeful consciousness and unconsciousness. Although the psychological profile of MB is quite straightforward, the neural mechanisms underlying this state have only now started to be elucidated. Recent work by Andrillon et al. (2021) demonstrated that MB is associated with slow waves oscillations during wakefulness. Understanding this association is important, as it suggests that MB may provide a useful model for studying the neural dynamics of slow waves outside of sleep, thereby helping to bridge the gap between active cognitive processing and unconscious states.

Recent work by Mortaheb et al. (2022) suggested that MB may indeed act as such an intermediate state. Their findings showed that fMRI global signal amplitude (GSA) was significantly higher during MB reports compared to both stimulus-dependent and stimulus-independent thoughts. They proposed that this elevated GSA might reflect neuronal silencing during wakefulness. Importantly, MB was characterized by a pattern of globally positive functional connectivity, indicating high inter-areal coherence across brain regions. This suggests that MB reflects a state in which cortical networks communicate more uniformly, possibly due to reduced differentiation of neural activity. In addition, they demonstrated that the removal of the global signal disrupted the coherence of the interregional brain, reinforcing the idea that the global signal plays an important role in the neural signature of MB.

However, what remained unresolved is whether the increased GSA observed during MB is a result of neural activity or driven by physiological signals such as cardiac or respiratory fluctuations. This distinction is crucial, as the fMRI BOLD signal reflects changes in blood oxygenation that are influenced both by neural activity and systemic physiological factors. These include respiration, heart rate, and blood pressure, all of which can introduce variability unrelated to cognition (Liu et al., 2017).

This ambiguity extends to the global signal (GS), which represents the average BOLD signal across the brain. GS is often treated as a nuisance variable in fMRI research, but recent studies suggest that the GS carries meaningful neural information that may be relevant to understanding spontaneous cognitive states like MB. For instance, Wong et al. (2013) showed that global signal amplitude correlates positively with low-frequency EEG activity (delta, theta) and negatively with higher-frequency bands (alpha, gamma) during resting-state fMRI. These findings support the hypothesis that the GS may partly reflect neural activity (Liu et al., 2017; Bolt et al., 2024), particularly, it can track the levels of arousal. Since the BOLD signal is sensitive, it is influenced not only by neuronal activity but also by systemic physiological processes. This makes it challenging to determine whether the increased GSA observed during MB reflects a true neural correlate of this state or is a physiological signal.

A promising approach to disentangle the neural vs. physiological contributions to MB is the simultaneous use of EEG and fMRI. While fMRI provides excellent spatial resolution, it indirectly measures brain activity through hemodynamic responses, which are slow and susceptible to non-neural influences. EEG, on the other hand, captures real-time neuronal activity by measuring electrical potentials generated by neuronal firing, with the sampling frequency much higher than in fMRI.

EEG obtains rich information about neural and physiological components during different mental states. That way, MB was linked with delta and theta oscillations profiles, the latter of which are associated with oscillations which are pronounced during slow-wave activity (Andrillon et al., 2021). These frequency bands are prominent in sleep and drowsiness but have also been linked to spontaneous thought during wakefulness (da Silva, 2022). Using the EEG method, it is possible to learn the components of mental states in more detail. Studying MB through EEG–fMRI integration not only addresses key methodological challenges but also advances theoretical understanding of consciousness. From a methodological standpoint, it allows researchers to better isolate neuronal contributions in fMRI (Power et al., 2018). Theoretically, it informs models of consciousness by characterizing MB not just as an absence of thought, but as a state with distinct neural and possibly physiological signatures.

Identifying such markers contributes to the broader field of spontaneous cognition and stream-of-consciousness research, revealing how the mind transitions between thought-rich and thought-free states. Understanding MB in this context could shed light on the dynamic architecture of consciousness during wakefulness.

In the following chapters, we describe our approach to investigating these questions using a combined EEG–fMRI dataset. We focus on amplitude-based metrics of the global signal, ECG and EEG and explore their relationships during MB, MW, and on-task states. Specifically, we test whether slow-wave EEG oscillations are associated with increases in GSA during MB, and whether fluctuations in ECG are correlated with GSA. Finally, we examine whether these associations are specific to particular mental states or remain consistent across conditions.

Chapter 2

Background

2.1 Spontaneous Thoughts

One of the interesting features of the human brain is that, even in the absence of external stimuli, mental activity continues to process. In addition to this, the brain often has thoughts and feelings that are completely unrelated to events happening around us now. This process, when the mind generates mental process independently of surrounding conditions, is called self-generated mental activity (Smallwood, 2013). This term is used to describe an overarching category encompassing various phenomena – including mind-wandering, daydreaming, fantasy, task-unrelated thought, and stimulus-independent thought. Despite this variability, the term "self-generated mental activity" describes a common phenomenon: conscious experience is driven more by an individual's concerns, preoccupations, and hopes (i.e., self-generated) rather than by immediate sensory input (i.e., perceptually generated) (Callard et al., 2013).

Studying self-generated mental activity was ignored for a long time due to the dominance of a task-centric view of mental processes. More than this, rest states, where spontaneous activity can be learn, were mainly considered as noise and were tried to minimise the effects of task-unrelated thought (Christoff et al., 2016). Generally, rest was used just as a baseline, and mental activity during it was not considered necessary. A crucial turning point was the meta-analysis of Shulman et al. (1997), which made a breakthrough by showing that a specific set of brain regions (posterior cingulate/precuneus, parietal cortex, frontal cortex, inferior temporal gyrus, and amygdala) is always more active during rest conditions, rather than during task-based acquisitions requiring external attention, thereby supporting their association with internally driven thought processes. Moreover, another study also supported the idea of informative brain signal during rest, showing that the same brain regions were consistently involved in memory and complex thinking (Andreasen et al., 1995; Binder et al., 1999). Later, these brain regions will be considered as default mode network (DMN)

Now, already, many researchers acknowledge that brain signals during rest have broad implications for many elements of psychological and neural function. For example, research has focused on how self-generated thought might be related to both physical and psychological aspects (Callard et al., 2013). Particularly, the broader context of self-generated thought has expanded into the study of spontaneous thought, which encompasses a wide range of internally arising mental experiences.

Christoff et al. (2016) defines spontaneous thought as a mental state or a sequence of mental states that arises relatively freely due to an absence of strong constraints on the contents of each state and on the transitions from one mental state to another. They propose that the content of mental states and the transitions between them can be constrained mainly through two methods: comprehensive cognitive control and automatic constraints. (Fig. 2.1). That gives an understanding that spontaneous thought is a broader umbrella, which includes self-generated thoughts, but

also mental activity that may be less deliberately initiated or structured.

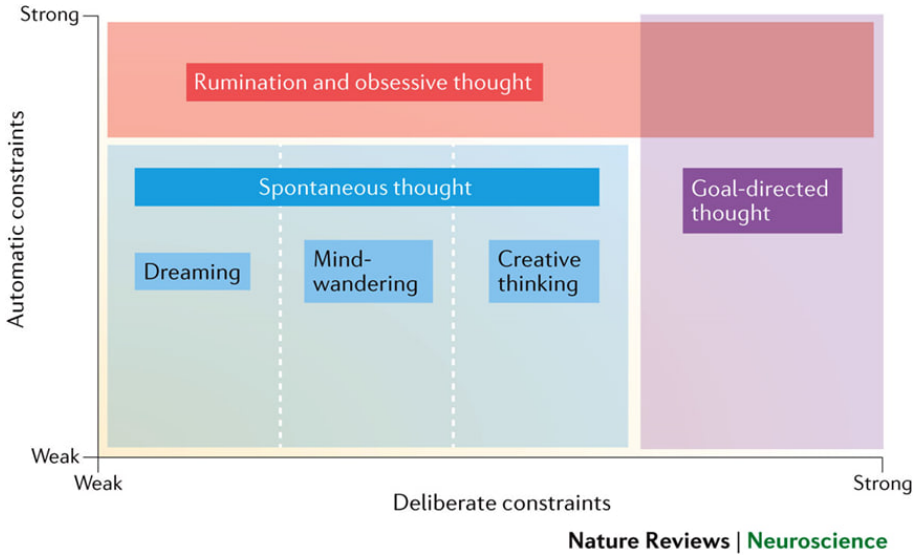

Figure 2.1: Conceptual space relating different types of thought (Christoff et al., 2016)

Basically, there are two types of attention constraints: flexible and deliberate, which involve cognitive control to focus on tasks (like, during a boring lecture), and automatic constraints, which can draw attention involuntarily due to factors, like emotional or sensory salience, making it hard to ignore distractions (e.g., a buzzing fly in a quiet space) (Christoff et al., 2016).

Furthermore, the neuronal profile of spontaneous thought has been associated with dreaming for a long time, marking some similarities between these two states (Foulkes and Fleisher, 1975). This similarity is particularly evident in phenomena like daydreaming, which, much like dreaming, involves internally generated imagery and narratives detached from immediate sensory input. Unlike dreaming, however, daydreaming occurs during wakefulness, making it part of the broader category of spontaneous thoughts. While sleep and wakefulness are generally considered distinct states, these parallels suggest that these states are not as independent as traditionally assumed, but rather exist on a continuum of conscious states.

Within this continuum, sleepiness represents an intermediate state characterized by low activity and reduced responsiveness to the environment. Sleepiness has particular behaviour patterns, like Non-Rapid Eye Movement (NREM) sleep, which amounts to 75–80% of sleep in healthy adults (Carskadon and Dement, 2005) and has high-amplitude slow oscillations. These oscillations can also be called "slow waves" which will characterize alternations between moments of neuronal silencing and firing synchronized across the entire cortex (Vyazovskiy and Harris, 2013). Another pattern of sleepiness is characterised by low-amplitude, theta (4–7 Hz) and mixed-frequency oscillations in Rapid Eye Movement (REM) sleep (Andrillon et al., 2019). Importantly, local modulations of sleep-like activity can affect the contents or structure of subjective experience during sleep (Andrillon et al., 2019). That way, local slow waves could act as a functional switch enabling or disabling specific cognitive processes during sleep, directly impacting oneiric contents and the ability to process external stimuli (Andrillon et al., 2016).

On the other hand, wakefulness is characterised by a pattern of brain activity dominated by fast, low-amplitude, desynchronized oscillations. In past years, it was found that local modulations of sleep-like activity can impact behavioural performance during wakefulness and not only during sleep. It was shown that local sleep-like slow waves can be observed outside of NREM sleep (Andrillon et al., 2019). Because slow-wave oscillations are spatially and temporally limited, they can be overlooked by looking at more global characteristics of wakefulness and sleepiness. Existing studies suggest that local slow waves occur in the frontal and parietal regions, with more oscillations in the parietal areas (Andrillon et al., 2019). Such findings raise an important question: how can spontaneous thoughts, which occur during wakefulness, be linked to brain activity patterns

resembling those of sleep?

Mind-wandering research offers one possible connection. Mind-wandering can be defined as a special case of spontaneous thought that is more deliberately constrained than dreaming yet less constrained than creative thinking and goal-directed thought (Christoff et al., 2016). Nowadays, the term "mind-wandering" is the dominant term researchers use to characterize the self-generated mental activity in which they are interested (Callard et al., 2013). The DMN, one of the most researched brain networks in cognitive neuroscience, is primarily linked to mind-wandering and spontaneous thought. Initially, scientists identified the DMN as a collection of brain regions that deactivate when individuals are engaged in tasks requiring external focus, indicating its involvement in internally directed cognitive functions (Christoff et al., 2016). Yet, the DMN is not solely connected to spontaneous cognition; it also remains active during purposeful, goal-oriented mental activities, including episodic memory retrieval, thinking about personal future scenarios, and mentalizing (Andreasen et al., 1995; Binder et al., 1999).

The discovery that local sleep-like slow waves can intrude into wakefulness suggests that elements of the sleeping brain's physiology can influence ongoing cognition even when awake. These overlapping mechanisms, which have shared neural patterns and similar network involvement, provide a foundation for understanding self-generated mental activity across states. This approach is particularly relevant for interpreting phenomena such as mind-blanking, which is the focus of this work.

2.2 Mind-Blanking

Besides MW, which is the most common spontaneous thought, a state has also been reported where the mind drifts away and becomes blank. During this state, people experience an decoupling of perception and attention, one in which attention fails to bring any stimuli into conscious awareness (Ward and Wegner, 2013). This state is referred to as mind-blanking.

Even though in one report it was noted that MB is a distinct cognitive state from MW (McCormick et al., 2018), it remains unclear whether the two experiences are readily distinguishable. For this purpose, an additional study was conducted. The idea was to find out whether participants could recognize the difference between the experiences of MB and MW.

As part of the experiment, participants were asked to read, and during the task, they were asked questions regarding their mental states at random times. As a result, across all tests, all participants reported both MW and MB, indicating that people are familiar with the differences between these two states. It was also shown that the duration of MB may be shorter, unlike MW, which can be pronounced for a longer period. Another distinction between the states was observed when participants were asked to recall the text after reporting their thoughts. During mind wandering, they often failed to remember the material. In contrast, during MB, they were still able to recall it, suggesting that MB involves a brief lapse of attention but does not impair the ability to return to the task when required (Ward and Wegner, 2013).

While mind-wandering refers to a state in which attention is disengaged from the current task and directed toward internally generated, task-unrelated thoughts, mind-blanking is characterised by the absence of reportable mental content. In this state, the individual does not merely shift focus to alternative stimuli but instead experiences a subjective sense of mental emptiness (Ward and Wegner, 2013).

MB is particularly important because it challenges the traditional view that wakefulness is always filled with ongoing thoughts. It can be described as a continuous process with time gaps (blanks) at which our consciousness goes away and then comes back. In MB, consciousness does not disappear entirely but rather shifts to a state where experiences are minimal or cannot be reported, even though the person remains awake and responsive (Andrillon et al., 2024). Despite the similarities of MB with the process that can be observed during mediations (Ward and Wegner, 2013), Andrillon et al. (2024) highlights that practices like open monitoring meditation involve

deliberately maintaining awareness and observing experiences without focusing on specific objects, like a controlled and intentional process. In contrast, spontaneous MB occurs without deliberate effort and is marked by a lack of intentionality. There is also "deliberate MB," where people intentionally try to think of nothing, but this likely involves different neural mechanisms, reflecting active thought suppression rather than spontaneous MB.

Kawagoe et al. (2018) investigated whether individuals could intentionally clear their minds, and what neural changes accompanied this process. Participants were instructed to "think of nothing" during resting-state fMRI scans. Results showed that, compared to MW, there was decreased connectivity among major brain networks such as the DMN, frontal, and visual regions. Participants reported being in a blank state for approximately 58% of the scan duration, suggesting that MB can be voluntarily achieved, though the precise neural signature remained unclear at that stage (Kawagoe et al., 2018).

Following the line of the research, they provided the first investigation of the neural correlates of MB (Kawagoe et al., 2019). In this study, participants again reported MB during nearly 57% of the experience sampling probes. However, when asked to distinguish between "truly blank" and "attempted to be blank" states, only 32% of responses were confirmed as genuine MB, indicating that the ability to enter this state deliberately varies and can not be clear for participant (Kawagoe et al., 2019). Kawagoe et al. (2019) mentioned that the blank mind may be obscured by internal self-examination. Any attempt to assess one's own mental states will necessarily find conscious thoughts and thus fail to find a blank mind.

The review article of Boulakis and Demertzi (2025) summarised the neuroimaging studies on MB (Fig. 2.2). fMRI consistently shows that MB reports are associated with widespread deactivations spanning frontal, parietal, occipital, and thalamic regions, including the angular gyrus and medial anterior regions, when contrasted with stimulus-dependent and stimulus-independent thoughts. Importantly, Broca's area, involved in inner speech, and the hippocampus, typically engaged during MW, exhibit consistent deactivation during MB. In contrast, other nodes of the DMN, such as the anterior cingulate cortex (ACC), remain active, suggesting a selective shutdown of self-referential and linguistic processing, which could explain the subjective absence of thoughts (Kawagoe et al., 2019; Boulakis et al., 2023).

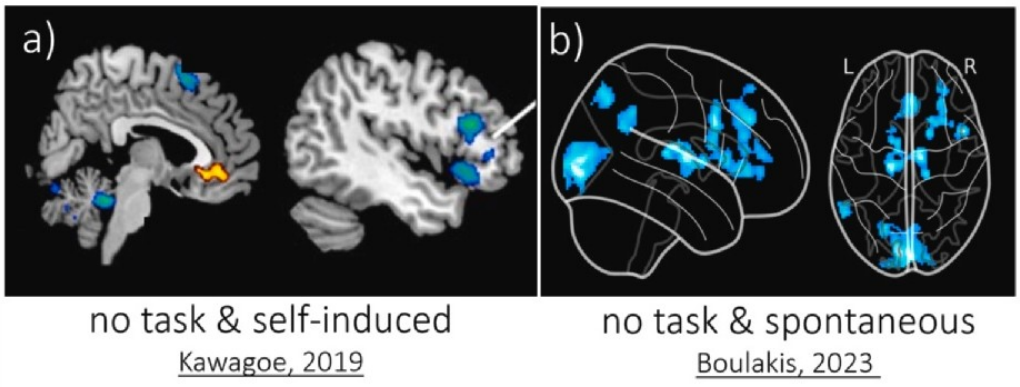

Figure 2.2: Neuroimaging evidence of MB **(a)** Self-induced MB during no-task conditions, adapted from Kawagoe et al. (2019), shows deactivation in Broca's area and the hippocampus (blue), with preserved activity in the anterior cingulate cortex (yellow). **(b)** Spontaneous MB during no-task conditions, adapted from Boulakis et al. (2023), reveals widespread deactivations across frontal, parietal, occipital, and thalamic regions (blue). These patterns support the view that MB is associated with reduced cortical engagement and altered connectivity (Boulakis and Demertzi, 2025)

Mind-blanking has unique neural correlates, but the nature and driving forces of this state remain an area of unresolved research. One of the ways to untangle this phenomenon is through functional magnetic resonance imaging, which provides a non-invasive means to observe brain activity across the entire brain. To better understand the mechanisms behind mind-blanking, it is

essential to first explore how fMRI works, particularly how it captures neural activity through the BOLD signal; afterwards, additional neuronal correlates of MB will be introduced.

2.3 fMRI and BOLD signal

fMRI has become a widely used technique for exploring brain organization in humans and non-human subjects. The principle of the main fMRI contrast relies on changes in blood oxygenation levels, which occur when populations of neurons are activated and begin to fire. This neuronal activity increases the oxygen demand, leading to the consumption of oxygenated hemoglobin. After the consumption of oxygenated hemoglobin by neurons, hemoglobin changes its form to deoxygenated hemoglobin (dHb) by releasing oxygen and picking up carbon dioxide, then moving through the veins back to the heart and lungs. Importantly, oxygenated hemoglobin is diamagnetic, which means it resists the external magnetic field and does not disturb it. At the same time, the paramagnetic properties of deoxygenated hemoglobin allow the local magnetic field around blood vessels to change. In this way, local hydrogen nuclei experience a different magnetic field, which results in a change in the signal around activated regions of neurons. This leads to a faster loss of phase coherence and a quicker decay of transverse magnetization, a process known as T2* decay (Huettel et al., 2004).

Particularly, higher concentrations of deoxygenated hemoglobin not only change the local magnetic field but also induce changes in cerebral blood flow (CBF), cerebral blood volume (CBV), and cerebral metabolic rate of oxygen ($CMRO_2$). In this way, changes in oxygenated and deoxygenated hemoglobin, along with these three characteristics, serve as an indirect way to measure neuronal activity in a specific brain region. In that sense, a positive BOLD response is achieved due to a significant increase in oxygen delivery and a subsequent rise in blood flow, which leads to a decrease in deoxygenated hemoglobin.

This process happens with a delay, which is due to the delayed response of the cardiovascular system. Initially, there is a small dip in the signal, which indicates a rise in deoxyhemoglobin, followed by a steady positive increase due to the rise in oxygen and blood flow. This is then followed by a gradual decrease back to baseline (Fig. 2.3). The effect is most noticeable near blood vessels, where dHb levels are higher and the magnetic field disturbances are stronger (Huettel et al., 2004).

fMRI can be broadly categorized into two main types: task-based fMRI and task-free fMRI. Task-based fMRI involves designing specific tasks or stimuli that participants perform or respond to during the scan, enabling the assessment of brain regions involved in particular functions or processes. In contrast, task-free fMRI, also known as resting-state fMRI, does not require participants to perform specific tasks; instead, it measures spontaneous brain activity when the subject is at rest. As mentioned above, spontaneous thoughts usually occur during rest, but they can also be detected during task-based acquisition, where patients report the states they experienced while engaged in the task.

Functional connectivity is determined by evaluating the temporal similarity between BOLD signals from different brain regions. This similarity is typically quantified using metrics such as the correlation coefficient. Voxels with correlation coefficients above a statistical threshold are considered functionally connected, revealing spontaneous shared fluctuations. However, because these time series are measured simultaneously, non-neural processes can influence the signals and introduce artifacts into functional connectivity measurements. These artifacts can lead to spurious results, either increasing functional connectivity by introducing false similarities between time series or reducing it by introducing differential confounds between regions (Murphy et al., 2013).

The important confound in fMRI studies is the so-called global signal. The GS is defined as the mean time course computed over all voxels within the brain (Liu et al., 2017). Since it is the global signal, it can consist of variable components, including instrumental and non-neuronal sources present within the whole brain. The unwanted terms can be referred to as “nuisance components” (Liu et al., 2017).

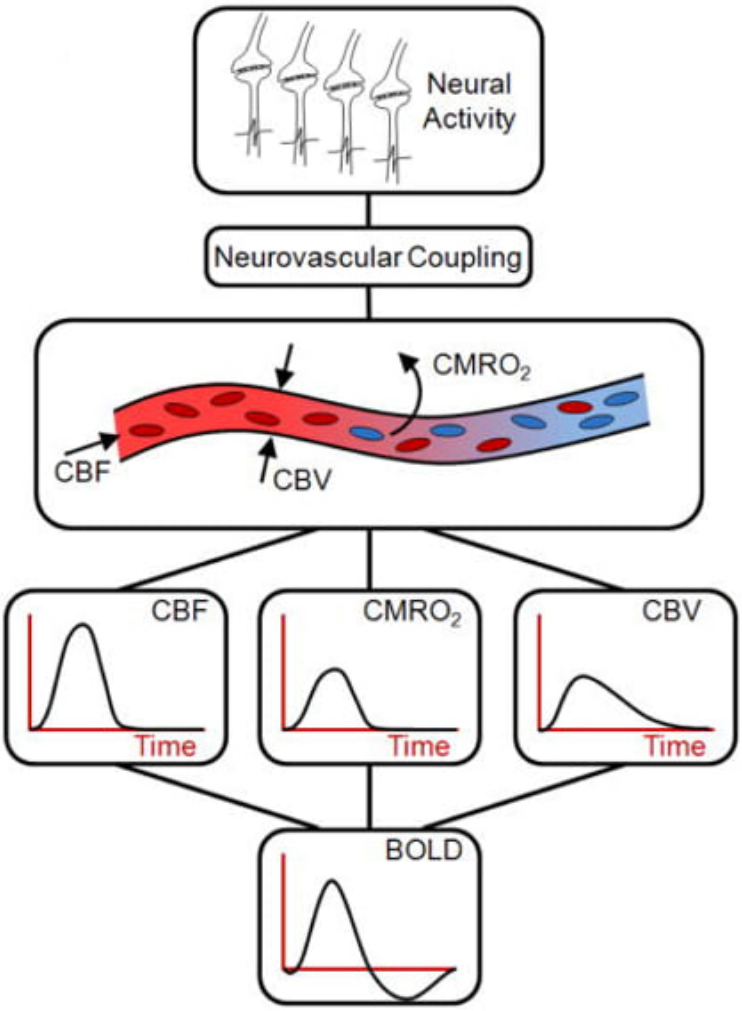

Figure 2.3: A relationship between an increase in neural activity and the corresponding BOLD signal is shown. When neural activity causes increased oxygen consumption (CMRO2), neurovascular coupling mechanisms alter the state of the vasculature changing CBF and CBV. The complicated interaction between these 3 parameters leads to the BOLD signal as measured with fMRI (Murphy et al., 2013)

Since fMRI signals are indirect, they can be influenced by many sources of noise. This kind of noise can be structural and arises from specific sources, like hardware, lung expansion during respiration, or the motion of the subject during the acquisition (Power et al., 2018). Another type of noise is random, like thermal noise, which is induced by the random movement of the molecules and is intrinsic. All these types of non-neuronal signals can significantly vary the interpretation of the signal during resting-state fMRI, as they can obscure or distort true neural functional connectivity (Liu et al., 2017). However, these effects have more impact on resting-state fMRI than on task-based fMRI, because task-based analysis can better isolate task-related activity, whereas resting-state data lacks clear timing.

Generally, BOLD fluctuations must be interpreted with caution. While decreases in neural activity can lead to negative BOLD responses, the complex interactions between excitatory and inhibitory processes can produce unpredictable effects. Neurovascular coupling varies across different brain regions and can also be altered in certain pathological conditions, such as epilepsy, cortical spreading depression, brain ischemia, and Alzheimer's disease (Attwell et al., 2010). In

the review article, the authors have also focused on determining which aspects of neuronal activity are most accurately reflected in BOLD signals. Additionally, other cell types, such as astrocytes, play a role in regulating hemodynamic fluctuations, and physiological processes like cardiac and respiratory cycles can introduce confounding factors in BOLD measurements (Jorge et al., 2014).

One of the primary focuses of the fMRI research field remains mitigating the effects of noise. One of the most widespread techniques is still removing the global signal component, which is known as global signal regression (GSR) or global signal subtraction (GSS), despite ongoing debate. While GSR can reduce widespread noise and motion-related artifacts by removing the global signal from the time series of each voxel through linear regression, it can also disregard the signal of neuronal origin impacting on observed functional connectivity patters. Fox et al. (2009) demonstrated that applying GSR can introduce prominent anti-correlations between intrinsic brain networks, such as the DMN and task-positive network (TPN) (Fox et al., 2009). Their analysis revealed that these anti-correlations, while robust, may partially result from mathematical artifacts introduced by the regression process itself—essentially shifting correlation values downward and potentially converting some weak positive correlations into negative ones.

While global signal fluctuations are known to reflect non-neuronal noise sources, such as head motion or physiological rhythms (e.g., cardiac and respiratory cycles), Fox et al. (2009) emphasized that removing the global mean does not necessarily disentangle all sources of noise. In fact, indiscriminately regressing the global signal may distort the underlying connectivity structure and complicate interpretation. Nevertheless, evidence also points to a neuronal component within the global signal, suggesting that it may carry functionally relevant information.

Interestingly, subsequent work has shown that anti-correlated networks can still be detected even in the absence of GSR. For instance,Wong et al. (2012) reported that caffeine administration led to the emergence of DMN–TPN anti-correlations similar to those typically seen after GSR. This finding implies that certain anti-correlated patterns may arise from genuine physiological changes rather than regression artifacts, reinforcing the idea that GS contains both noise and meaningful neuronal information.

Li et al. (2019b) revealed that individual differences in GS topography contain sufficient neural information to be associated with individual variation in behaviors. This suggests meaningful differences in functional MRI sources of variance (GS topography versus connectivity) that are associated with behavior. In other words, GS can contain neural data and contribute to interpreting the results on subject-level analysis.

The other study also linked the global signal to neuronal activity. Schölvinck et al. (2010) conducted a study on an anaesthetised monkey during resting-state fMRI and simultaneous local field potentials. The study showed that the fMRI signal highly correlated with neural activity, which was pronounced across the cerebral cortex. This coupling was consistent across different cortical regions (occipital, parietal, and frontal electrodes) but varied based on behavioural state, being stronger and anticipatory when the monkeys' eyes were closed. These results suggest that the global signal can carry some useful neuronal information and should not be disregarded from the signal (Schölvinck et al., 2010).

Despite such findings, disentangling the different components within the global signal remains technically challenging. Several studies, particularly by Power and colleagues, have characterised the properties of the global signal in fMRI and proposed methods to mitigate nuisance contributions. In the recent article of Power et al. (2018) they used multi-echo ICA to separate motion and respiration components from global signal, motion artifacts were successfully removed using ICA, but respiration components, that are were highly correlated with movement, was impossible to decompose using multi-echo ICA, due to this the most reasonable way was to exclude global signal entirely because respiration showed high correlation with global signal (Power et al., 2018). It is important to mention that the choice of eliminating all global signal was made primarily due to the high correlation of respiration components with GS.

Not only multi-echo ICA showed such results, but it was also observed with other statistical methods, such as regression of multiple models of respiratory variance, and after regression of

motion estimates and nuisance compartment signals, global respiratory signals persist through these denoising approaches (Power et al., 2018)

Therefore, rather than relying solely on global signal removal, a more nuanced approach involves characterising the GS and understanding its constituent sources to avoid misinterpretation of brain connectivity measures. That way, it is possible to retrieve the accurate brain signal without loss of important information.

2.4 EEG and slow waves

When a stimulus or change occurs, it triggers activity in populations of neurons that is detected by our sensory system. When we record an EEG, we measure the electrical potential at the scalp, which reflects synchronized activity in a specific area of the brain. EEG electrodes detect the voltage differences created by synchronized brain activity, but the electrical signals must pass through the brain and skull. This process, known as volume conduction, alters the signals before they reach the electrodes (Murta et al., 2015)

Therefore, scalp EEG serves as another indirect method of measuring brain activity. But the complication, according to the volume conduction issue, makes it more difficult to determine the exact locations of the electrical potentials on the scalp. While the neural activity sources are located within the three-dimensional brain, EEG only captures data from the two-dimensional surface. The signals recorded on the scalp do not pinpoint the exact location of the active neurons producing them (Murta et al., 2015). However, EEG has the advantage of tracking brain activity on a millisecond timescale due to very high sampling frequency, allowing researchers to observe the fast-changing dynamics of neuronal populations. This attribute has made EEG an important tool for studying brain function for nearly a century (Warbrick, 2022). Interestingly, even though EEG is often mentioned as a direct measure of neuronal activity, the complete understanding of its underlying neurophysiological correlations has in fact not yet been achieved (Jorge et al., 2014).

Niedermeyer and Silva (2005) explained this change in potential, which we register in EEG, that neuronal activity is mediated by synaptic interactions and action potential propagation (spiking). Neurons generate time-varying electrical currents upon activation, primarily through ionic currents across cellular membranes, known as transmembrane currents, that give rise to intra and extracellular currents along the membrane. The latter generate the so-called local field potentials (LFPs) and can be seen as equivalent electric dipoles between the stimulated dendrites and sub-synaptic regions (Jorge et al., 2014).

Neuronal activation occurs in two main forms. The first is the rapid depolarisation of neuronal membranes, leading to action potentials mediated by voltage-dependent sodium and potassium conductances (gNa and gK). This process results in a brief shift of the intracellular potential from negative to positive, which quickly returns to resting levels within 1–2 ms. To note: action potentials propagate along axons and dendrites without a loss in amplitude. The second form of neuronal activation involves slower changes in membrane potential due to synaptic activity, mediated by various neurotransmitter systems. These postsynaptic potentials are classified as either excitatory or inhibitory, depending on the neurotransmitter involved, its receptor interactions, and subsequent effects on ionic channels and intracellular signalling pathways. In each neuron, synaptic inputs tend to induce transmembrane ionic currents (postsynaptic activity) (da Silva, 2022). These membrane potential changes also contribute to LFPs.

EEG signals are characterized by complex temporal patterns that reflect specific transient responses to applied stimuli, as well as the varying frequency composition known as brain rhythms. These rhythms result from synchronous oscillatory activity in different brain regions, and their mechanisms vary significantly depending on the targeted frequency range (Niedermeyer and Silva, 2005). Fluctuations within specific frequency bands may occur in response to external stimuli, leading to phenomena known as event-related synchronization or desynchronization (Jorge et al., 2014).

The power spectra of LFP and scalp EEG signals follow a power law distribution, that is, they may be broadly represented by a straight line on a logarithmic scale. The 1/f power law distribution characterizes the brain arrhythmic activity, and the conspicuous peaks characterize the brain rhythms (so-called oscillations). These oscillatory patterns are visible in electrophysiological signals recorded either from the scalp or directly from within the brain; they are commonly categorized as delta (0.5–4 Hz), theta (4–8 Hz), alpha (8–12 Hz), beta (12–30 Hz) and gamma (>30 Hz) (Murta et al., 2015; da Silva, 2022). The temporal characteristics of brain rhythms are phylogenetically preserved across mammalian species, despite significant differences in brain size. This preservation throughout evolution suggests that brain rhythms serve a specific functional role. Among these, slow wave oscillations (1–4 Hz) are the hallmark of deep, non-REM (NREM) sleep, particularly Stage N3. During this phase, neurons across the cortex oscillate between active “up-states” and "down-states" of reduced firing, leading to a synchronised rhythm that turns down consciousness and limits external inputs from reaching higher-order awareness. However, occasional theta (4–8 Hz) or even delta (1–4 Hz) frequencies can transiently appear during normal wakefulness, particularly during drowsiness.

2.5 Artifacts of EEG signal

EEG, like fMRI, is a discrete-time system that records continuous biological signals. These signals originate as analog electrical activity generated by neuronal firing and are then digitized for subsequent analysis. However, EEG data are particularly susceptible to a wide range of artifacts, which can compromise the quality and interpretability of the recordings. These artifacts can generally be categorized into three types: instrumental, environmental, and biological.

Instrumental artifacts are typically caused by hardware-related issues. For example, malfunctioning or poorly attached electrodes can generate high-amplitude fluctuations or unstable signals that are not reflective of underlying brain activity. Additionally, when EEG is recorded simultaneously with fMRI, it introduces specific types of instrumental artifacts. These include gradient artifacts caused by the rapid switching of magnetic gradients during fMRI data acquisition, and cardioballistic artifacts, which are induced by the physical movement of electrodes due to pulsatile blood flow from the heartbeat. These scanner-induced artifacts are typically periodic and can significantly distort EEG signals if not properly corrected. These artifacts are typically attenuated using specialised algorithms that model and subtract the artifactual waveforms associated with the scanner (Chowdhury et al., 2019).

Environmental artifacts include power line interference (50 or 60 Hz), mechanical vibrations from the surroundings, and electromagnetic noise from devices, like phones or elevators. Such artifacts are commonly removed using high-pass filtering (e.g., at 0.1 Hz) or notch filters targeting specific frequencies. Biological artifacts originate from the body and are more diverse: eye blinks produce slow, high-amplitude deflections primarily at frontal electrodes due to corneal-retinal potential shifts; eye movements cause deflections near temporal sites; and both are prominent in delta and theta bands (Croft and Barry, 2000). Muscle artifacts, typically from teeth clenching or jaw, generate high-frequency noise above 20 Hz, extending up to 300 Hz and affecting the full spectrum (Xun Chen, 2025). Besides this, moderate body movements can also alter electrode impedance and can induce large voltage shifts.

Artifact handling strategies generally fall into three categories: rejecting affected segments, ignoring them, or repairing the data through attenuation techniques, including filtering (high-pass, low-pass, notch) or re-referencing affected channels. Since EEG data contains mixtures of neural and non-neural signals, ICA is widely used to statistically separate these components; this way, it is possible to enable the identification and attenuation of different types of artifacts while preserving meaningful brain activity (Fig. 2.4).

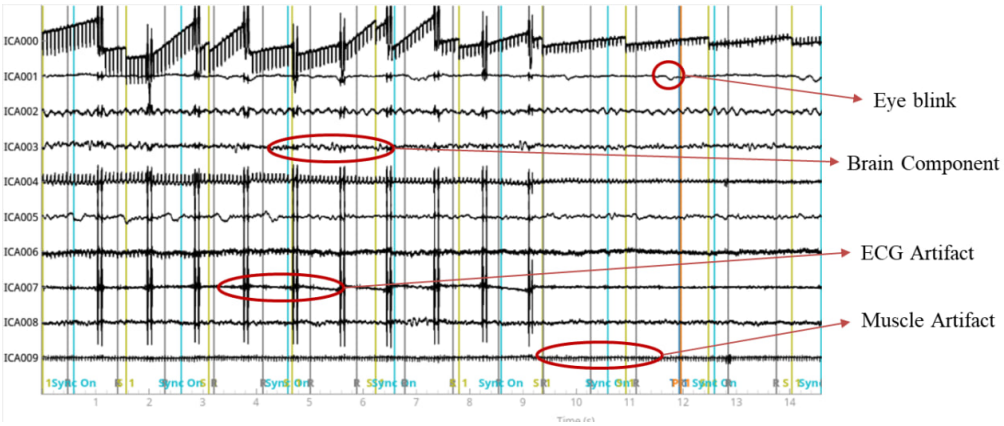

Figure 2.4: Example of separation using ICA with 61 components

2.6 Link between EEG and fMRI

Both fMRI and EEG described above have their pros and cons, and a combined approach was offered to combine the strengths of these two methods. Using a combined approach, it is possible to reach high temporal resolution from EEG and high spatial resolution from fMRI. That way, we can combine two approaches of indirect neuronal activity to benefit from both. This is especially useful in fMRI acquisition with several blocks or sessions, so reaching more convincing results for neuronal activity is possible. Moreover, simultaneous EEG-fMRI provides several practical benefits, including a reduction in experimental duration, the removal of habituation effects, and the maintenance of a consistent sensory environment across different modalities. These advantages have enabled EEG-informed fMRI techniques, allowing EEG to identify specific temporal patterns (such as epileptic spikes, seizure activity, or sleep rhythms). At the same time, fMRI helps identify where these patterns come from, providing important information about the brain networks involved in neurological disorders and different mental states. This combined approach allows researchers to build spatiotemporal maps that visually localize particular EEG signals across brain regions, enabling the investigation of the nature of these signals in three dimensions (Warbrick, 2022).

This combined approach has proven especially valuable in understanding the physiological relevance of brain signals. For instance, Wong et al. (2013) used simultaneous EEG–fMRI recordings to demonstrate that global signal amplitude—measured as its standard deviation—varies systematically with EEG-defined vigilance. Specifically, higher vigilance states were associated with lower global signal amplitudes across individuals and experimental runs. Moreover, there was an additional session with caffeine, which is known to elevate alertness; they observed a significant reduction in global signal amplitude, further supporting its link to arousal levels.

On the other hand, simultaneous EEG-fMRI acquisitions comes with several challenges. The strong and rapidly fluctuating magnetic fields in an MRI scanner introduce substantial artifacts into the EEG signal, such as gradient and ballistocardiogram artifacts, it require additional preprocessing steps in EEG data. Additionally, metal electrodes and leads in the high-field MRI environment can include potential heating and induced currents; therefore, specialised hardware is required. Motion artifacts further complicate data acquisition, as physical vibrations and scanner noise can distort EEG readings, while even small participant movements pose greater challenges in a simultaneous setup. A final critical issue is ensuring precise synchronisation between EEG and fMRI data streams, which can be achieved by the correct placement of scanner triggers, which are reflected in the EEG recording as well. (Warbrick, 2022).

This combined fMRI-EEG approach can be useful for studying slow-wave processes during wakefulness, such as MB, because its neural characteristics are not appropriately defined, and this technique overcomes this.

2.7 Characteristics of Mind-Blanking

After investigating techniques useful for studying MB, this section will present some characteristics from MB studies.

Research by Vyazovskiy et al. (2011) has shown that during sleep deprivation, a subset of brain regions may display EEG signatures of NREM sleep, despite the individual being behaviourally and physiologically awake (Vyazovskiy et al., 2011). This "local sleep" phenomenon occurs when sleep-like slow waves (delta and theta range) emerge in specific cortical regions while the rest of the brain remains in a wakeful state. The emergence of these localized slow waves in task-critical areas can lead to attention lapses, microsleeps, or MB, as the ability to maintain conscious processing diminishes. Notably, slow wave sleep (N3) is characterized by high-voltage (>75 μV) delta frequencies. The authors also propose that local modulations of slow waves affect both wakeful performance and subjective sleep experiences. This study forced to reconsider the concept of the line between wakefulness and sleep.

In a recent review of Andrillon et al. (2021), they authors identify that MB can be associated with slow-wave activity in the brain, because unlike mind-wandering (where one's attention drifts to internal thoughts), MB shows EEG patterns remind of lower-vigilance or "offline" states: namely, increased low-frequency or slow-wave power and a relative disintegration of large-scale cortical networks. These findings suggest that MB may represent transient "micro-shutdowns" of higher-order cognition, during which conscious contents are effectively absent. If large enough portions of the cortex synchronize in slow-wave oscillations, conscious content may drop out entirely, resulting in the subjective experience of "nothingness" or blankness (Andrillon et al., 2021). This mechanism likely contributes to day-to-day episodes of MB or losing track of one's surroundings (attention lapses), underscoring that the boundary between wakefulness and sleep is more permeable than often assumed (Andrillon et al., 2021).

Occasional slower theta (4–7 Hz) or even delta (1–3 Hz) frequencies may be seen during normal wakefulness, but usually these slower activities only become prominent during drowsiness (Louis et al., 2016). During drowsiness, the first prominent change is a gradual loss of frequent muscle and movement artifacts and a reduction of blinks and rapid lateral eye movements (Louis et al., 2016). However, delta oscillations can occur in some parts of the human cortex when they are completely conscious. But the authors Sachdev et al. (2015) concluded also that the occurrence of delta oscillations during wakefulness is mostly linked to inattentiveness and unconsciousness, which supports the previous findings of Andrillon et al. (2019) between delta oscillations and MB.

fMRI studies also revealed unique neuronal correlates of MB. Mortaheb et al. (2022) conducted a study with 36 healthy participants using a 3-T MRI scanner while they were at rest with their eyes open. During the session, participants were randomly presented with 50 auditory probes that required them to report their current mental state by pressing a button. The mental states included MB, sensory perception (Sens), stimulus-dependent thoughts (SDep), and stimulus-independent thoughts (SInd).

After analyzing the frequency of reported mental states, MB occurred significantly less often than the other states (Fig. 2.5). For the reaction time analysis it was shown that participants responded more quickly when reporting MB compared to SDep and SInd, while no significant difference was found between MB and Sens.

To understand how MB is connected to brain activity by examining the role of the GS, a measure of widespread brain activity that has been linked to neural processes. Since the GS might have functional significance, they analyzed its amplitude (strength) in different regions of interest (ROIs) around the time participants reported MB.

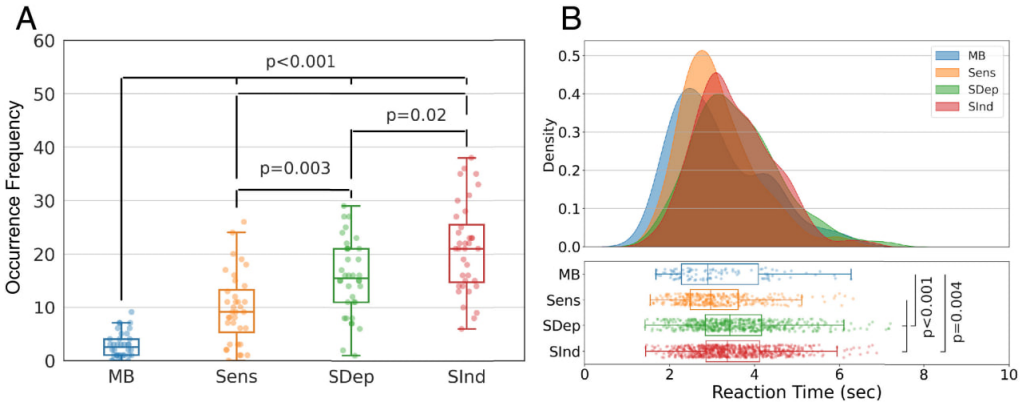

Figure 2.5: MB is characterized by a distinct behavioural profile (Mortaheb et al., 2022)

To do this, they measured the GS amplitude over a 10.2-second window (covering five fMRI scans: two before the MB report and three after) to account for how BOLD signals change over time. Their analysis showed that the GS amplitude was higher during MB compared to other mental states like SDep and SInd, suggesting that MB is associated with stronger global brain activity (Fig. 2.6).

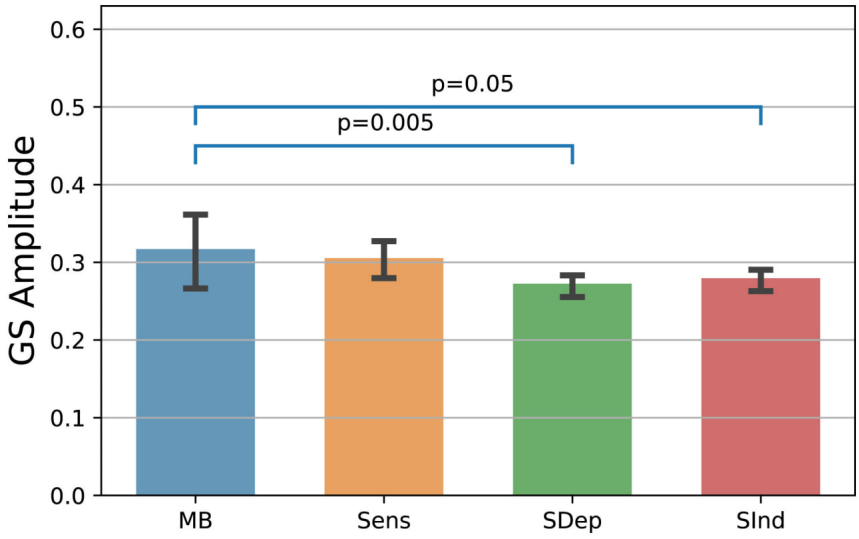

Figure 2.6: Volumes labeled as MB are characterized by high GS amplitude (Mortaheb et al., 2022)

To ensure the reliability of this finding, they repeated the analysis with different time windows (from five scans before the MB report up to three scans after) and found similar results.

To find out if MB has a unique neural signature, they analyzed functional connectivity dynamics by looking at how the brain activity changes across different moments during rest. For this they combined all the brain connectivity data from multiple participants into a single dataset, and using a k-means clustering method, they grouped these connectivity patterns into four distinct types that consistently appeared in resting-state brain activity (Fig. 2.7). They found that Pattern 3 —the globally positive connectivity pattern—was the one most strongly associated with MB reports, this suggests that when people experience MB, their brains tend to be in a state where most brain regions are positively connected (Mortaheb et al., 2022).

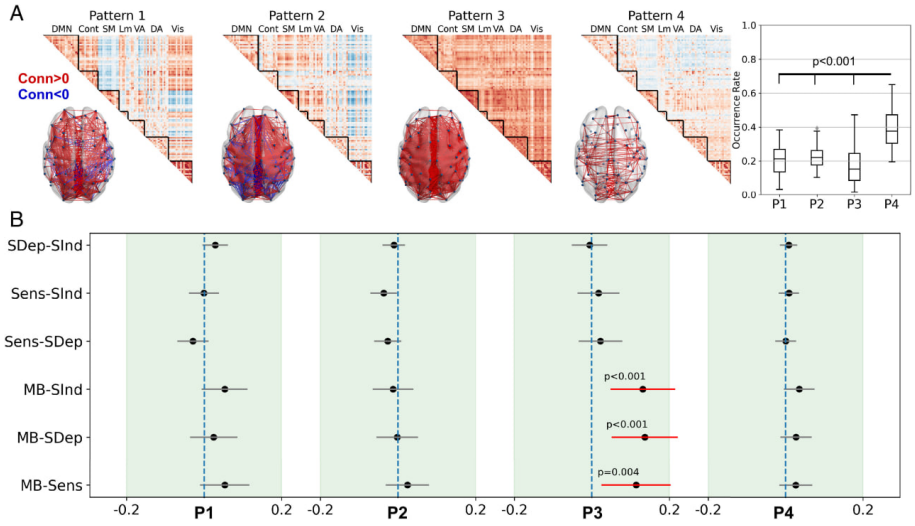

Figure 2.7: MB is associated with an overall positive interregional brain connectivity pattern (Mortaheb et al., 2022)

Moreover, Kawagoe et al. (2019) also found that deactivation of Broca's area (a key region for inner speech) was the most significant neural signature of MB. Since Broca's area is essential for semantic articulation and verbal thought, its suppression suggests that MB arises when inner speech is silenced, preventing individuals from identifying any psychological content. Moreover, increased activity in the medial prefrontal cortex (PFC), a core DMN region, was observed during MB, which may indicate a weak connection to spontaneous cognition or a transient disengagement from self-referential thought, which was also supported by the fact of deactivation of the hippocampus, a region linked to spontaneous thought generation, because it has been reported that the hippocampus is the region that spontaneous thoughts emerge from.

To better understand the role of the global signal in MB, they also decided to remove the GS from brain activity data using two different methods - GSR and GSS. In both cases, they found that the connectivity structure of P3 shifted towards more negative values, meaning that removing the GS enhanced anticorrelations. So, removing it alters the neural signature of MB, particularly by shifting the P3 connectivity pattern, which was originally associated with strong global coherence. These results suggest that the GS carries partially independent neural information and contributes to the cerebral profile of MB reportability.

It is important to note that the GS is a complex measure that includes not only neural activity but also physiological components such as respiration and cardiac effects. This means that while MB was found to be associated with GS fluctuations, this does not necessarily prove that MB reflects purely neural activity. Instead, it is possible that the observed GS changes during MB are partly influenced by physiological factors, such as increased blood pressure or other systemic processes, rather than being solely driven by brain function.

Chapter 3

Goals and Objectives

3.1 Goals

Previous work (Mortaheb et al. (2022); Section 2.7) examined the role of the GS, the average signal intensity across all voxels in the brain, during MB. They found that GS amplitude, measured over a 10.2-second window around MB reports, was significantly higher during MB than during other mental states such as SDep and SInd thought (Fig. 2.6). This effect was consistent across different time windows.

Using dynamic functional connectivity analysis, they identified four recurring brain connectivity patterns. Among them, Pattern, characterized by globally positive (all-to-all) correlations, was most strongly associated with MB (Fig.2.7). Removing the GS from the data (via GSR and GSS) shifted P3 toward more negative connectivity, indicating that the GS contributes to the coherent connectivity profile observed during MB.

However, the GS is not purely neural signal, it also contains physiological components such as respiration and cardiac effects. Thus, while MB is linked to GS fluctuations, the extent to which these changes reflect intrinsic neural dynamics versus physiological processes remains unclear.

These findings motivate the present study, in which we aim to investigate the neural mechanisms underlying MB using simultaneously acquired EEG–fMRI data. In particular, we focus on separating neural and physiological components of the EEG signal and relating them to GS amplitude, to determine whether MB reflects intrinsic neural dynamics or is partially driven by physiological fluctuations.

A combined fMRI–EEG approach is particularly well suited for this purpose, as it allows us to study MB, whose neural characteristics are still not well defined, during wakefulness, while also disentangling their physiological contributions. In the study of Wong et al. (2013), using particularly simultaneous EEG-fMRI recording, using this approach they managed to identify a negative correlation between global fMRI signal and arousal levels, suggesting that the global BOLD signal may serve as an indicator of vigilance fluctuations (Wong et al., 2013).

Based on this, investigating the correlation between the global fMRI signal and EEG activity during MB could help characterise the main neural oscillations associated with MB. Based on the section describing characteristics of MB (Section 2.7), it is likely that slow-wave activity (particularly in the delta range, 1–4 Hz) will be prominent during MB episodes. Furthermore, through the correlation analysis, it is possible to determine the reason for the increase in GS amplitude during MB reports.

3.2 Hypothesis

The GS components related to MB reports will incorporate both neuronal and neurovascular information. However, the extent of contributions of each component requires further investigation.

3.3 Objectives

Therefore, our objectives are the following:

- To analyze EEG recordings acquired during simultaneous EEG–fMRI sessions and separate them into their neural and physiological components (in this study ECG), in order to isolate the neuronal signal and physiological signal of interest.
- To preprocess and denoise task-based fMRI data, extract the GSA
- To examine correlations between GSA and different EEG bands, with a particular focus on identifying the EEG features most strongly associated with MB reports
- To examine correlations between GSA and ECG, with a particular focus on periods during MB reports
- To extend this analysis to other mental states reported during the experiment (MW and on-task), allowing for comparison of EEG–GSA relationships across different cognitive states.

Chapter 4

Methods

This Chapter first describes the data used and its characteristics, including the experimental protocol, and then outlines the preprocessing steps applied to the data. Finally, the methods for analysing the preprocessed data are provided.

4.1 Participants

For this study, collaborators from Monash Centre for Consciousness and Contemplative Studies provided the data. The data consists of 38 subjects with simultaneous task-based fMRI and EEG data. 27 subjects out of 38 also have resting state fMRI and EEG data. The mean age of the 38 participants is 26.4 (range from 18 to 32), and 24 of the subjects were females. All participants reported normal or corrected-to-normal vision and no neurological or psychiatric disorders.

4.2 Experiment Design

The experiment design was first introduced by Andrillon et al. (2021). The entire experiment consisted of 4 blocks of EEG-fMRI acquisition, each lasting around 12 minutes. Participants were allowed to rest between blocks, so the experiment lasted about 50 minutes. The task in each block consisted of an SART, in which participants were instructed to pay attention to a series of human face images, each probe repeated 10 times. Each participant responded to 40 probes across four blocks. These human faces were selected from the Radboud Face Database (Radboud University Nijmegen).

In each probe, participants were instructed to press a button in response to neutral faces ('Go trials') and to withhold their response when presented with the smiling face ('NoGo trials'). After around 1 minute, the presentation of stimuli was interrupted by a sound and the appearance of the word "STOP" on the screen. During these interruptions, participants were asked about their mental state with three questions, with multiple possible answers. For the first question, participants were asked "Where was your attention focused?" and forced to select one of the following options: (1) "task-focused" (on-task, ON), (2) "off-task" (mind-wandering, MW), (3) "mind-blanking" (MB), or (4) "don't remember." Since the "don't remember" option accounted for only 1.1% of all responses and previous studies often do not differentiate between these options, the third and fourth categories were combined into MB for all analyses (Andrillon et al., 2021). If participants selected the Off-Task option, they were additionally presented with the following question: "Just before the interruption: What distracted your attention from the task?" Available options were: (1) Something in the room, (2) Something personal, and (3) Something about the task. For the last question, participants were asked to rate their level of vigilance over the past

few trials using a 4-point scale ranging from 1 ('Extremely Sleepy') to 4 ('Extremely Alert'). The whole experimental protocol is illustrated in Fig. 4.1.

Participants were informed about the nature of the interruptions and the questions before the experiment began. Explanations of the mental state categories (ON, MW, and MB) were provided both orally and in writing. The responses during the probes were recorded using an MRI-compatible button box. Behavioural data were synchronised with the MRI acquisition through trigger pulses sent by the scanner, so that it is possible to align neural and behavioural measurements.

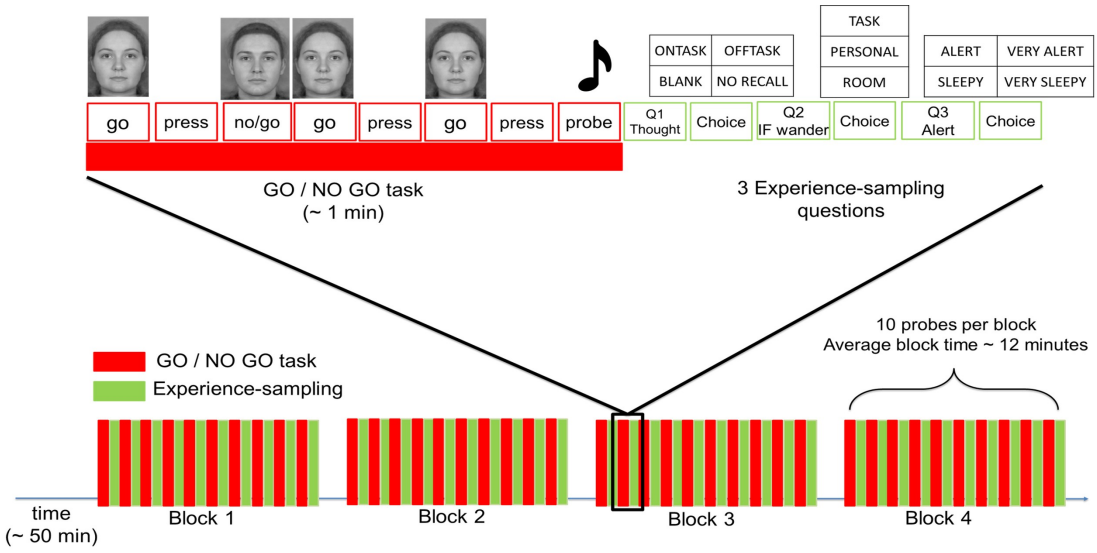

Figure 4.1: Structure of the Experiment Used for Described Dataset

4.3 MRI Recording

Participants were instructed to lie still in the MRI scanner, and with closed eyes in case of rs-fMRI, minimising eye movements and muscle artifacts. Data were collected using a Siemens Skyra 3T MRI system, equipped with a Siemens 20-channel Head/Neck coil, allowing for simultaneous EEG and ECG recordings. Anatomical images were acquired using a T1-weighted MPRAGE sequence with a voxel size of 1.00 mm^3, TR=2.3s, TE=2.07s, and a slice thickness of 1 mm. Functional images were obtained using an Echo Planar Imaging (EPI) sequence with the following parameters: TR=1.56s, TE=0.03s, slice thickness=3 mm, flip angle=70.

For each subject, four separate acquisitions were made corresponding to the 4 blocks of the experiment (Fig. 4.1). That way, each participant underwent four blocks of fMRI recording.

4.4 MRI Preprocessing

All MRI data were preprocessed using the `fmriprep` library, which implements a standardised, BIDS-compliant workflow combining tools from ANTs, FSL, FreeSurfer, and AFNI (Esteban et al., 2019).

4.4.1 Anatomical Data Preprocessing

Structural T1-weighted images were reoriented and resampled to a common RAS orientation and voxel size, if multiple T1w scans were available, they were averaged into a single reference

template. This template underwent skull-stripping using ANTs and tissue segmentation via FSL's FAST to generate gray matter, white matter, and cerebrospinal fluid probability maps. Finally, nonlinear spatial normalization to MNI standard space was performed using ANTs' registration framework.

4.4.2 Functional MRI preprocessing

For each run per block of the experiment, a reference image was created and used for head motion (FSL's `mcflirt`). Then, functional images were aligned to each subject's anatomical T1-weighted scan and normalized to standard space using a single-shot resampling to preserve data quality. Afterwards, confounding time series were computed. Multiple confounds were calculated, including motion parameters, framewise displacement, DVARS, global signals (from CSF, WM, whole brain), and physiological noise regressors via aCompCor and tCompCor. Frames with excessive motion or signal variability are marked as outliers. The final outputs include cleaned BOLD images and confound regressors.

This study specifically focuses on the global signal derived from the whole brain, defined as the mean time course across all brain voxels. This signal, extracted from the confounds output of fMRIPrep, serves as the primary variable of interest in our EEG-fMRI correlation analysis.

Data were processed with a single command across all subjects and runs, with input data structured according to BIDS and requiring at minimum both T1w and BOLD scans. The full preprocessing pipeline is documented in the official `fmriprep` documentation (fMRIPrep Community). This standardised and widely used approach has been implemented in many research and workflows (Wong et al., 2013; Scheeringa et al., 2012), ensuring a robust and uniform method for analysis.

4.5 EEG Recording

EEG data were acquired using the BrainAmp MR plus system (Brain Products, Munich, Germany), equipped with a 64-channel EEG Cap (64Ch Standard BrainCap-MR with multitrodes). Electrode placement followed the international 10-20 system (Fig. 4.2. The ground electrode was positioned in the location of AFz, and the reference was in the location of FCz. The data were recorded with the BrainAmp MR plus DC and bipolar BrainAmp ExG MR amplifiers and the BrainVision Recorder (Version 2.2) software with a resolution of 0.5μV/bit at 5000 Hz and with a low cut-off hardware filter with a time constant of 10s and high cut-off at 250Hz. The EEG and fMRI data acquisition were synchronised using the Brain Products SyncBox.

Recorded triggers in EEG data had the following meanings:

- `T/T 1` – Beginning of each subtask of the Go/NoGo Task;
- `S/S 1` – Time Repetition (TR), occurring every 1.56 s;
- `Q/Q 1` – End of the experience sampling (40 in total, one for each block of the experiment);
- `P/P 1` – Beginning of the experience sampling (also 40 in total);
- `C/C 1` – End of each experimental block (4 in total, one per run);
- `B/B 1` – Beginning of each experimental block (4 in total);
- `Sync On` – Marks the synchronization pulse used to align EEG and scanner clocks at the start of acquisition.

Other triggers that appear before the first `S/S` trigger were not considered, as they seem to relate only to trials preceding the actual task and are outside the scope of interest.

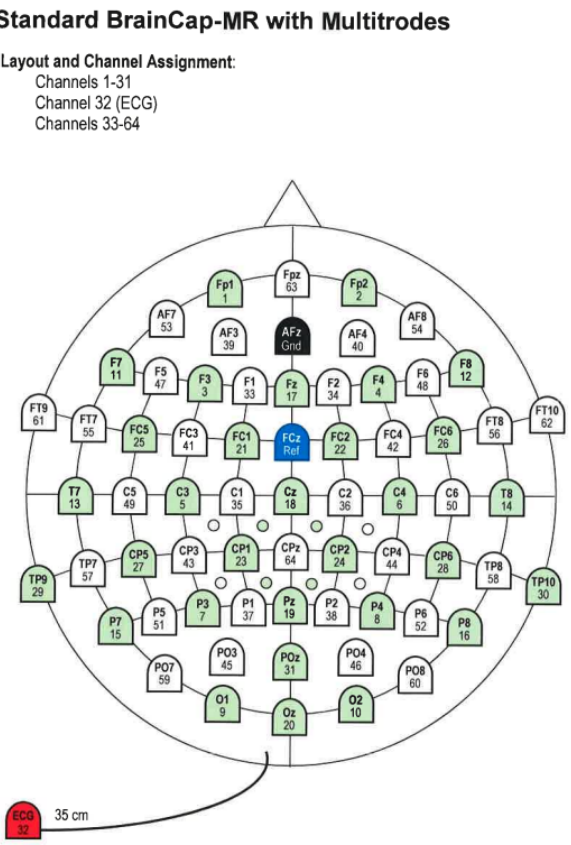

Figure 4.2: EEG Cap Used in the Experiment

4.6 EEG Preprocessing

The following section will detail all preprocessing steps applied to the EEG data described above, including detection of instrumental, environmental, and biological artifacts and their rejection.

4.6.1 Instrumentation Artifact Cleaning

In EEG-fMRI experiments, the scanner environment generates various artifacts. Notably, the switching of magnetic gradients causes significant currents in the EEG leads, resulting in large artifactual voltages. Additionally, vibrations from the scanner induce motion artifacts, which are amplified by the magnetic field. Moreover, besides artifacts generated by general cardiac activity, there can also be pulse artifacts arising from the EEG electrode, which is placed around a vessel or artery. To handle these artifacts it requires specialised analysis techniques.

These artifacts were cleaned using the BrainVision Analyser 2.0.1 software (Brain Products, Munich, Germany), which removes MRI gradient artifacts using an average pulse artifact template procedure (Allen et al., 2000). An average template was created based on markers indicating repetition time from the MRI system (S/S 1, see Fig. 4.3), and then subtracted from the EEG signal to correct for artifacts. After gradient artifact removal, cardioballistic artifact removal was also performed using BrainVision Analyser. Heartbeat event markers were created by detecting R-peaks from the ECG channel. The corrected EEG data and event markers were then exported in `edf` format (Team of Brain Products GmbH).

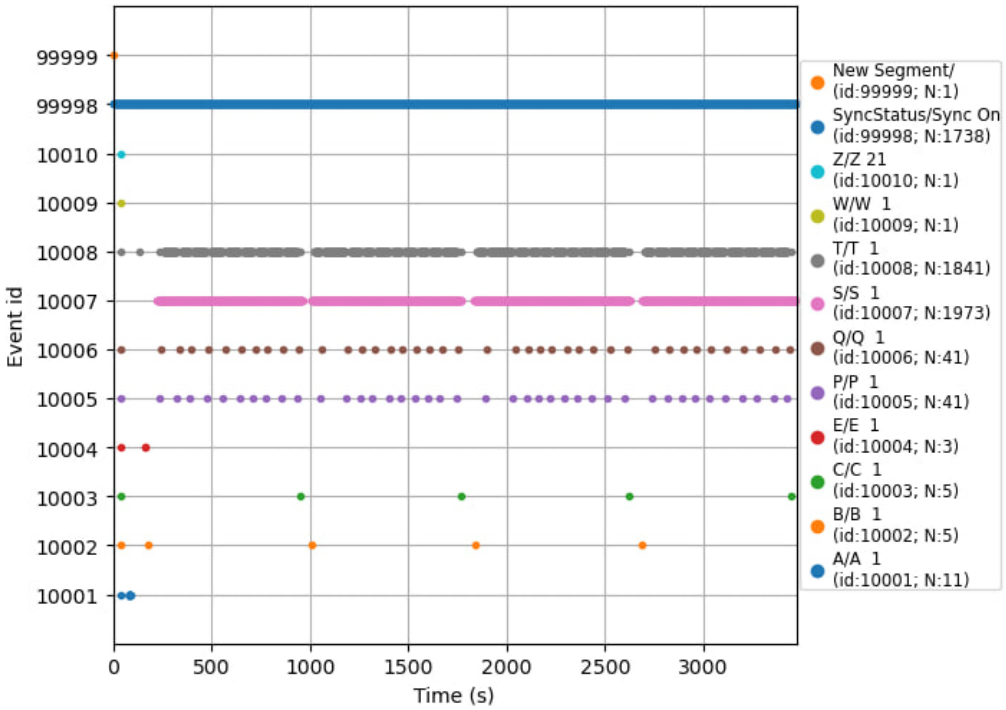

Figure 4.3: Example of Triggers for Subject 219 from EEG data.

Instrumentation artifact removal was applied to the entire EEG recording, which included all four experimental blocks combined into a single sequence. Performing this step on the full sequence is practical, as it does not rely on or generate any `.log` files containing run-specific information and applies the same correction algorithm uniformly across the entire session. Further preprocessing was performed using the `MNE` library in Python.

4.6.2 Data Structuring and Annotation Alignment

For subsequent preprocessing steps, the continuous EEG recording was divided into four segments corresponding to the individual fMRI runs. This segmentation preserved run-specific information, such as bad epochs and bad channels, and enabled precise alignment between EEG and fMRI data. The separation was based on event markers indicating the beginning and end of each experimental block (Fig. 4.1; see also Fig. 4.3 for trigger details).

Besides EEG triggers, there were also triggers which come from the scanner. The scanner triggers not only recorded the experimental timing, but also captured the participants' responses related to their experienced mental state during the task. These behavioural responses were aligned with the EEG events, too. This was done by creating new annotations that combined the triggers recorded in the EEG with the annotations available from the scanner. The scanner annotations were extracted from the `.tsv` files associated with each of the four runs.

By aligning both EEG and scanner triggers, it was possible to determine the start and end of each Go/NoGo task as well as to identify the moments when participants reported mind-blanking and other states. After correctly segmenting the EEG data in correspondence with the fMRI runs and after instrumental artifact removal, the signals were further processed to clean the data from other types of artifacts to isolate neuronal activity as clearly as possible. To further clean the EEG data from residual artifacts, the steps described in the following sections were applied.

4.6.3 BIDS Formatting

Data were formatted using the BIDS formatting convention. BIDS formatting is a standard convention for neuroimaging and behavioural data, including EEG data. This approach allows data to be organised efficiently and clearly, which is generally recommended for storing and analysing such types of data (Pernet et al., 2019). A Python script was implemented to rename the original files into the following format: `sub-`*index_ of_ subject*`_task- gonogo_run-`*index_ of_ run*`_eeg.fif`. This ensures that each run for each subject is formatted consistently, facilitating further processing and storage of additional files.

4.6.4 Bad Channels Removal

As a next preprocessing step, it was necessary to exclude EEG channels that were clearly contaminated by noise or otherwise unusable. These typically included electrodes with flat signals, excessive artifacts, or unstable baseline drift. An example of such channels is shown in Figure 4.4.

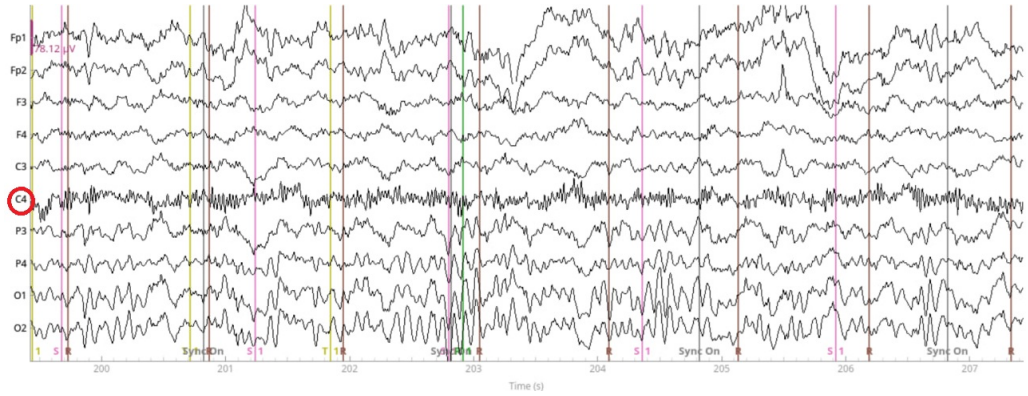

(a) Example of a bad channel for Subject 217, Run 4: **C4**

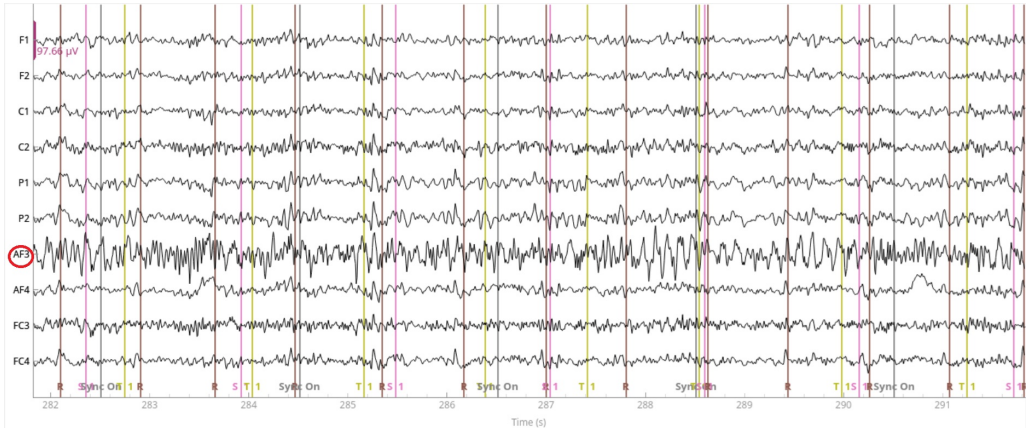

(b) Example of bad channels for Subject 227, Run 4: **AF3**

Figure 4.4: Examples of some bad channels identified in Subject 217 and Subject 227

This step was performed using the `MNE` library in Python. Specifically, the raw EEG data were first band-pass filtered between 0.5 Hz and 45 Hz, and the filtered signal was then plotted from the `.fif` file. This visualization allowed for manual inspection of all 63 EEG channels, along with the 2 ECG channels, across the full duration of each recording.

All identified bad channels for each subject were saved into a single `.json` file. This file contained the list of bad channels for all runs belonging to the same subject. By storing this information in a separate configuration file, it was possible to automatically reload and apply the same bad channel annotations if preprocessing needed to be redone or updated at a later stage.

4.6.5 Cutting The Data Into Epochs

Now, after indicating bad channels and removing them, cutting the data into epochs was required before running the next step of the analysis, particularly ICA.

For each subject, the EEG recordings were uploaded. Then, the continuous EEG signals were band-pass filtered between 0.5 Hz and 45 Hz to remove low-frequency drifts and high-frequency noise, in line with standard preprocessing for EEG studies. An Infinite Impulse Response (IIR) filter was selected instead of the default Finite Impulse Response (FIR) filter, as the recordings triggered warnings indicating that the data length was insufficient for effective FIR filtering. The IIR filter, with its shorter kernel allowed to avoid these warnings.

With the MRI scanner's TR set to 1.56 s, the continuous EEG data was segmented into equal-length epochs of 1.56 seconds. This was done using `mne.make_fixed_length_events`, which generated events at regular intervals matching the TR. These events were then used to define epochs with `mne.Epochs`, resulting in a series of consecutive 1.56-second EEG segments. The final epoched data was saved in `.fif` format for further analysis.

4.6.6 Removing Bad Epochs

After cutting the data into fixed-length epochs, cleaning the epochs contaminated with pronounced artifacts was necessary to detect the genuine neuronal signal. Bad epoch filtering was done manually by visually inspecting the data. Instead of checking all 63 EEG channels individually, PCA was applied to reduce the data to its main 10 components. This made it easier to spot any distortions during an epoch without the need to go through every channel. The list of bad epochs was saved in the same `.json` file as the bad channels, so the whole preprocessing can be reproduced easily later if needed.

Removing bad epochs is a necessary step before running ICA, because noisy segments, like those with excessive muscle activity, eye blinks, or movement artifacts, can distort the ICA decomposition and lead to inaccurate separation of components (Jiang et al., 2019). ICA assumes that the underlying sources are statistically independent and consistent across the recording, but bad epochs introduce high-amplitude, non-stationary noise that can break this assumption (Jiang et al., 2019).

As a result, the ICA algorithm may prioritise fitting those artifacts, which could be present only in a few epochs and not within whole recording, instead of uncovering true neural signals. It will lead to reducing the quality of artifact detection which appear permanently across data and leading to false interpretability of the resulting components. That way, removing bad epochs improves ICA's effectiveness and yields cleaner, and more meaningful components. After this step it can be possible to apply ICA.

4.6.7 Apply ICA

ICA is a statistical method that identifies hidden factors within observed data, assuming that the observed signals are linear mixtures of unknown, non-Gaussian, and mutually independent sources (MNE). That way, if any non-neuronal signal is presented significantly, it will be captured by one of the components.

ICA is applied using the `Picard algorithm` from MNE library, a fast and robust ICA solver well-suited for EEG data. The number of components is set to `n_components=0.9999`, which instructs MNE to retain enough components to explain 99.99% of the variance in the data. The Picard method is chosen because it has good convergence properties and is configured with additional parameters, like `ortho=False` to allow non-orthogonal components and `extended=True` to enable better separation of both sub-Gaussian and super-Gaussian sources, which is useful for detecting eye blinks and cardiac activity (MNE). The output result of ICA was saved in `.fif` file.

4.6.8 Reject Components Which Contain artifacts

Referencing the implementation by senior postdoctoral researcher in Applied Machine Learning Group (Federico Raimondo, 2025), the ICA decomposition results were saved as interactive `.html` reports using the `.fif` files from the previous step. These reports allowed a detailed inspection of the main 20 independent components, showing their spatial topography, ERP/ERF plot, variance across epochs, power spectra, and single-trial time series. This visualization made it easier to identify components representing artifacts.

Components were rejected only when they clearly represented artifacts. Figure 4.5 illustrates two such examples. The top image shows a typical eye blink artifact, identified by strong frontal activation in the topography and high-amplitude deflections in the time series. The bottom image displays a muscle artifact, characterized by broadband high-frequency power in the spectrum plot (above 20 Hz) and noisy oscillatory time series.

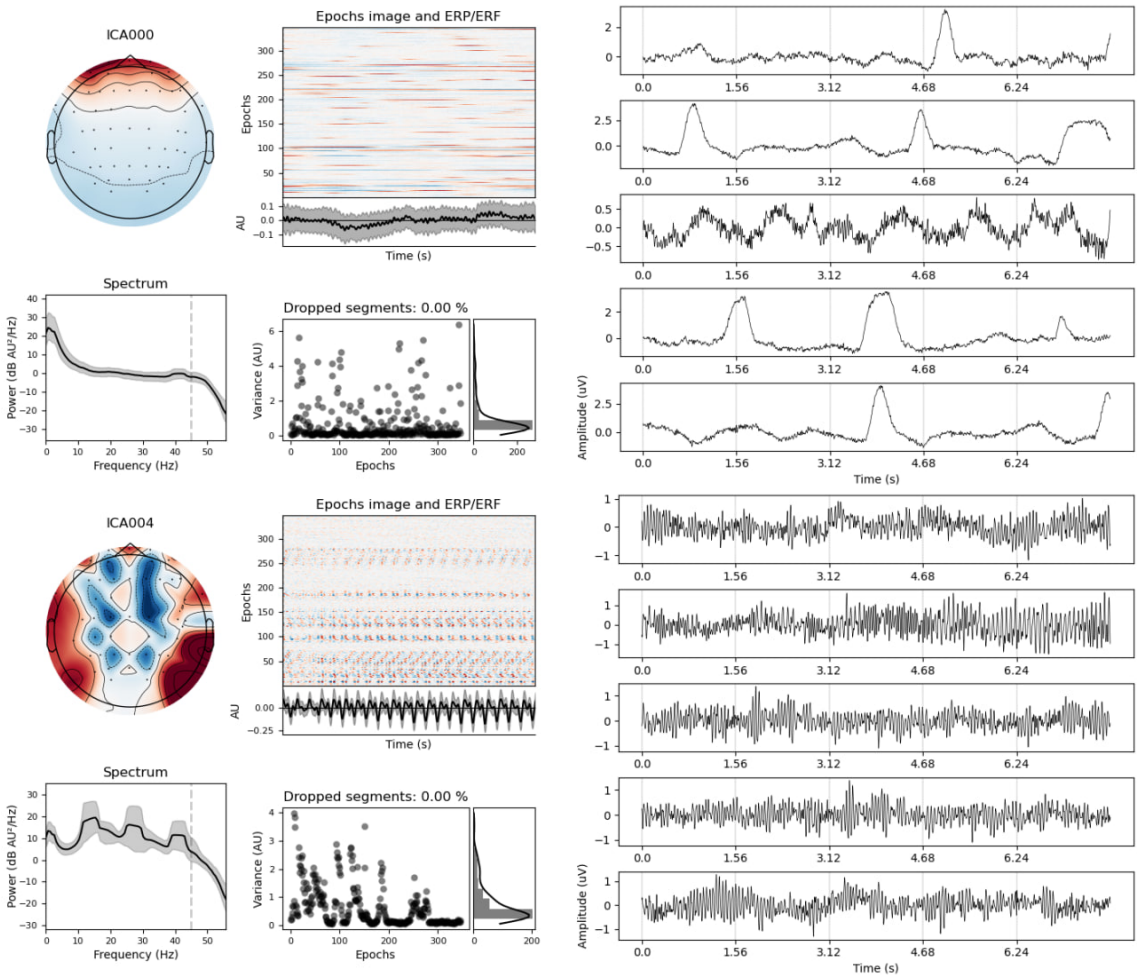

Figure 4.5: ICA examples for artifact identification. **Top**: Example of an eye blink artifact for Subject 217, Run 3, showing strong frontal activation in the scalp topography and large deflections in the time series. **Bottom**: Example of a cyclical muscle artifact for Subject 217, Run 3, characterized by broadband high-frequency power (above ∼20 Hz) in the spectrum plot and noisy oscillatory time series.

Only after rejecting the contaminated components bad channels were interpolated. This ensured that ICA decomposition was not biased by previously corrupted channels. This procedure was repeated for every block of the experiment (run) and every subject in the dataset. After component rejection and interpolation, the EEG data was considered clean from the major artifacts and ready for further analysis.

4.7 Physiological Signal

To understand the causes of increased GSA around MB reports, whether the rise is driven by neuronal or neurovascular activity, it is essential to extract a physiological signal to help disentangle these contributions. Physiological signal refers to any signal that does not originate from neuronal sources. In the initial trials, we aimed to define a broader category of physiological activity that included muscle artifacts, cardiac activity, and eye blinks captured in the EEG signal, treating them as additional physiological components.

To identify these components in the EEG data, ICA was applied with a variance threshold of 0.99 to decompose the EEG signal. The resulting components were then visually inspected and labeled using the MNE library, assigning physiological labels when components corresponded to identifiable artifacts (e.g., eye blinks, muscle activity)(see Fig. 2.4). However, this approach did not work well in practice. ICLabel, which is a supervised machine learning classifier originally implemented in EEGLAB, can label EEG components based on their most likely source. While it performs reasonably well, many components that contained physiological noise also included some valuable neuronal activity. Because of that overlap, rejecting such components would risk losing meaningful brain signals.

Due to these limitations, it was chosen to rely only on ECG as a pure physiological signal. Unlike the previous approach, the ECG is a direct measure of cardiovascular activity and can better reflect true physiological reactions, rather than just artifacts that may not relate to mental states. The ECG signal was processed using the `neurokit2` library, which provides tools for analyzing different types of physiological data. For ECG, neurokit2 uses heart rate variability (HRV) as a main metric, which is known to reflect psychophysiological states and disorders like depression, anxiety, schizophrenia, and post-traumatic stress disorder (Gullett et al., 2023). HRV also can show how flexible the nervous system is in changing arousal levels and that it can be related to emotion regulation (Pham et al., 2021).

For each subject and run, we selected the ECG channel and ran an implemented Python script that extracts ECG amplitude regressors aligned to the fMRI scans. It starts from MRI-artifact corrected EEG files, identifies task segments, splits them into four parts per subject (as was described previously in section EEG Preprocessing), and cleans the corresponding epochs (based on `.json` from EEG preprocessing). Each segment's ECG signal is filtered (0.5–40 Hz) and resampled to 256 Hz. Then, using `neurokit2.ecg_process()`, R-peaks were detected, signal was cleaned, and the heart rate was computed. From this, we extracted the `ECG_Rate` (beats per minute), giving us an instantaneous heart rate signal over time.

That way, the signal was converted to a time vector, then it was z-scored and interpolated to obtain one value per each TR (1.56 s). Bad scans were excluded, as well, as the first 10 volumes (to allow for magnetisation stabilisation), ensuring only clean epochs were used. And the final ECG regressors, which contained one value per fMRI scan, were saved as text files. This resulted in a clean, time-resolved physiological regressor (specifically, heart rate variation) aligned with the fMRI volumes.

4.8 Deriving EEG metrics

To check if any cardiac artifacts remained in the preprocessed EEG data, Pearson correlation was calculated between the extracted ECG signal and each of the 63 EEG channels. This helped to see if there were any remaining links with the physiological signal, which would indicate that the process of EEG cleaning might not have been fully effective. A topographical brain map was then created to show where on the scalp these positive or negative correlations occurred. As visible in Fig. 4.6, none of the areas show either positive or negative correlation, indicating good separation between these two signals.

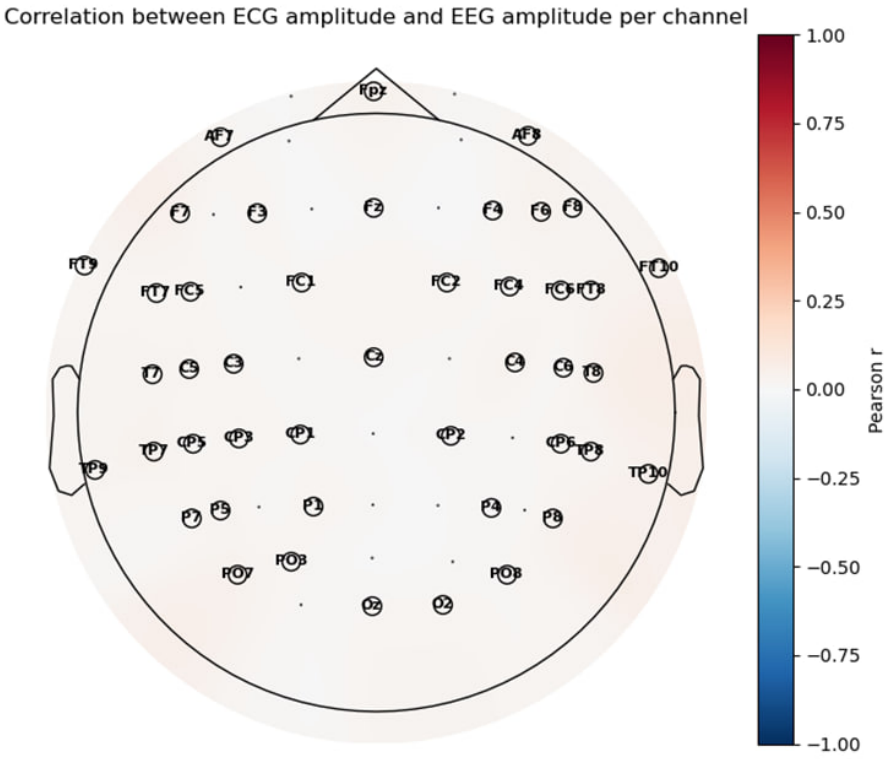

Figure 4.6: Correlation between EEG amplitude and ECG amplitude across all 64 EEG channels. No scalp region exhibited significant positive or negative correlation, suggesting that cardiac-related artifacts were effectively removed from the EEG data. This indicates good separation between neuronal and physiological signals, supporting the reliability of subsequent EEG–fMRI coupling analyses

4.8.1 Delta Oscillations

Since MB is linked to slow-wave activity (Andrillon et al., 2019), the primary EEG band of interest is the delta band. This enabled us to extract the signal related to the neuronal characteristics of MB, which can aid in understanding the extent to which neuronal activity, associated with MB, correlates with GSA. To prepare delta oscillations for fMRI correlation analysis, the pipeline was referenced to the study of Scheeringa et al. (2012), where correlation analysis was implemented for rs-fMRI and alpha bands, and to the study of Bolt et al. (2024), where coupling between GS and physiological signals was studied.

After cleaning the data from the major artifacts, the next step involved extracting neural regressors in the delta frequency range (1–4 Hz). For each subject, the preprocessed epoched files (`.fif`) were loaded, and any bad epochs and channels specified in the corresponding `.json` file were removed. If any bad channels were detected, they were interpolated using spherical spline interpolation to reduce the loss of spatial information. This was done via `epochs.interpolate_bads (reset_bads=True)`.

The data was then resampled to 256 Hz since the signal of interest is enough to process with this frequency rate. Downsampling was done only at this stage, so there is no loss in the signal during epoching and ICA. Moreover, downsampling during epoching can induce longer fixed events due to the smaller sampling frequency, which in the end can lead to the shift of all the data and wrong alignment with the fMRI signal.

To isolate neural activity in the delta band (1-4 Hz), a band-pass filter was applied using the IIR method. This filter was chosen over default methods to avoid warnings related to signal length and to ensure stable filter performance on shorter epochs. Then, to extract regressors the following procedure was implemented for each of 63 EEG channels:

The envelope of the delta activity was computed using Hilbert transform, which provides an analytic signal from which the instantaneous amplitude (envelope) was extracted. This envelope was then normalized using a z-score to make the signal comparable across epochs and channels. The instantaneous amplitude is proportional to the square root of the instantaneous power. Because the sampling rate of the EEG recording was 256 Hz, the Hilbert envelope had a high temporal resolution, resulting in fast, high-frequency amplitude fluctuations.

Since BOLD signals are slower and delayed due to the hemodynamic response, the EEG envelope needed to be matched to the temporal dynamics of fMRI. The EEG envelope was convolved with a canonical "hemodynamic response function" (HRF) to approximate the expected hemodynamic delay. The canonical HRF implemented in SPM was used for this purpose, which models the typical biphasic shape of the BOLD response, sampled at the same resolution as EEG (oversampled to match 256 Hz). The convolution itself was performed using FFT-based fast convolution.

Since data was epoched into the segments which are equal to the repetition time of the scanner, it allows us to simplify the alignment with the fMRI scanner, particularly to obtain only one value per scan. For this, the mean of the convolved signal across time points was taken as the final EEG regressor per epoch. To ensure consistency with fMRI analysis, only epochs beyond the 10th (to exclude unstable initial volumes) were retained. These delta-band regressors were then saved into individual text files per channel, to be later used in general linear models. As a result, the final delta-based power regressor contained one value per fMRI scan, aligned with the number of volumes acquired in each run of the experiment.

4.8.2 Other EEG Bands

To verify the reliability of the analysis, we aimed to perform the same analysis not only for delta but also for other frequency bands, particularly for theta, alpha, and gamma. The processing procedure remains the same despite the change in filter range (Murta et al., 2015; da Silva, 2022):

- Theta Band - 4-8 Hz
- Alpha Band - 8-12 Hz
- Gamma Band - $>$ 30 Hz (Since we had high-pass filtering at 45 Hz, Gamma band was limited from 30-45 Hz)

That way, the script allows easy adaptation to different bands of interest simply by switching filter parameters.

4.9 Retrieve Global Signal Amplitude

Confounds from `fmriprep` are used to obtain one of its outputs — the global signal, which is then correlated with EEG and ECG regressors. For each subject and corresponding run, the preprocessed fMRI global signal was retrieved from the related `.tsv` files. After loading the relevant EEG epochs for each run, bad epochs were discarded. The remaining volume indices were then extracted to ensure that only clear EEG epochs were included.

The global signal was processed by computing the analytic signal using Hilbert transform, and taking the absolute value to obtain its amplitude envelope. This envelope was then standardised using a global z-score transformation to ensure comparability.

To maintain consistency with the EEG-derived regressors, only those fMRI scans corresponding to the accepted EEG epochs were retained. Since epochs are equal to repetition time, it can be done by excluding the corresponding scans which correspond to bad epochs. Furthermore, the first nine volumes of each run were excluded, as they typically contain instability due to scanner

equilibration. The resulting vector was saved as a plain text file. These global signal regressors will be later analysed for the linear correlation with EEG and ECG regressors.

4.10 Retrieving Mind-Blanking Reports

All the processing steps above were applied to the full recording of the experiment. However, in this study, we are specifically interested in the moments when participants reported MB. For that, a separate script was implemented to generate a text file with a boolean mask with `True` for timepoints where MB was reported.

The periods of MB were extracted using task annotations from EEG triggers (see Fig. 4.3). The script segmented the MB events into blocks based on the timing of the task. For each question–response block, it identified the start of the next Go/NoGo block to consider the duration of the answer during the experience-sampling block. Then, it checked which MB onsets happened within these intervals of the question-response block. For every matched MB onset, the script defined the block start as the first Go/NoGo onset following the previous question–response end, and the block end as the current question–response onset.

This allowed to mark periods of Go/NoGo tasks when MB was likely occurring, and use that information to extract the relevant segments from the physiological and neuronal signals. In the same way the masks were retrieved for MW and ONTASK mental states for further analysis.

For additional inspection, MB reports were also analyzed using a complementary extraction procedure based on the approach described by Mortaheb et al. (2022). In this method, the precise onset of each MB report was used, and fixed-length segments surrounding this onset were extracted. Specifically, a window extending 11.7 seconds before and 11.7 seconds after the reported onset was selected. This window captured both the period before and after the reported MB onset, allowing us to examine surrounding neural and physiological activity. Using this approach alongside the task-based segmentation also provided a way to check the consistency of our results across two methods of defining MB epochs.

4.11 Correlation Analysis of EEG and GS

The resulting regressors allowed us to perform correlation analysis using Generalized Linear Models (GLM), particularly Linear Mixed-Effects Models (LMMs), to check the linear relationship between different types of signals.

4.11.1 Design Matrix

Based on the previous steps, regressors were collected for each experiment run and each subject, covering ECG, EEG, and GS amplitude signals. Each regressor contained a number of time points corresponding to the number of fMRI scans in that run. All these regressors were concatenated into one matrix, resulting in a design matrix with 69 columns:

- **Columns 1–63**: EEG amplitude regressors for each of the 63 channels (Fig. 4.2)
- **Column 64**: Global EEG signal (average across all EEG channels)
- **Column 65**: ECG heart rate variability regressors
- **Column 66**: Global signal amplitude regressor
- **Column 67**: Boolean mask for MB (`True` when MB was reported, `False` otherwise)

- **Column 68**: Subject ID number (from sub-217 to sub-244)
- **Column 69**: Run number (from 1 to 4, which corresponds to each block of the experiment)

This resulted in continuous time series for each EEG channel, ECG, and GS amplitude, where each regressor (e.g., F1 EEG channel) aggregated data across all four runs and all subjects into a single column. In other words, each regressor represented the concatenated signal from all fMRI scans for all sessions and subjects. The number of time points in each column matched the total number of scans which were included after preprocessing. These regressors were then used as input for the GLM-analysis, particularly using Linear Mixed-Effects Models (LMMs), implemented in R to explore correlations between EEG and GSA and between ECG and GSA.

As can be seen, in addition to EEG, ECG, and GS amplitude regressors, subject number and run were included as grouping factors in an LMM. Unlike a standard GLM, where subject and run would need to be represented through dummy-coded regressors, here they were modelled as random effects, allowing the model to estimate subject-specific intercepts without explicit dummy coding. Thus, the subject and run columns in the design matrix served only as grouping indices rather than continuous predictors.

In this context, a regressor refers to a single explanatory variable (i.e., a column in the design matrix) used to predict variation in the GSA within the general linear model. For EEG, the GLM-based correlation analysis was done in two ways:

- **Channel-wise**: a separate GLM was fitted for each of the 63 EEG channels, with the amplitude of the given channel entered as a regressor for GSA. This approach allowed the identification of spatially specific relationships between local EEG activity and fluctuations in the GSA,
- **Globally**: in parallel, the GLM was applied to the global delta signal, computed as the mean amplitude across all EEG channels. This provided a single regressor representing large-scale EEG activity, which was then tested against GSA.

Each of these analyses was performed twice: first on the entire dataset, and then only on the timepoints when MB was reported, which obviously resulted in a smaller dataset. For some particular EEG bands, the same analysis was provided to analyse the correlation during MW and ONTASK reports.

4.11.2 Linear Mixed-Effects Model for EEG–GSA Coupling with Subject-Level Random Effects

Since we have multiple subjects and natural variability between them, using an ordinary linear model might not be effective enough, as it could miss meaningful effects by averaging over individuals.

To address this, Linear Mixed-Effects Models (LMMs) were used. These models are designed for regression analyses involving grouped or repeated measures data, like in our case, where we have multiple time points per subject. There are two main types of random effects used in these models:

- Random intercept: all responses in a group (subject) are shifted by a subject-specific constant.
- Random slope: the relationship between predictor and outcome can vary across subjects (e.g., EEG–GS slope is different per subject).

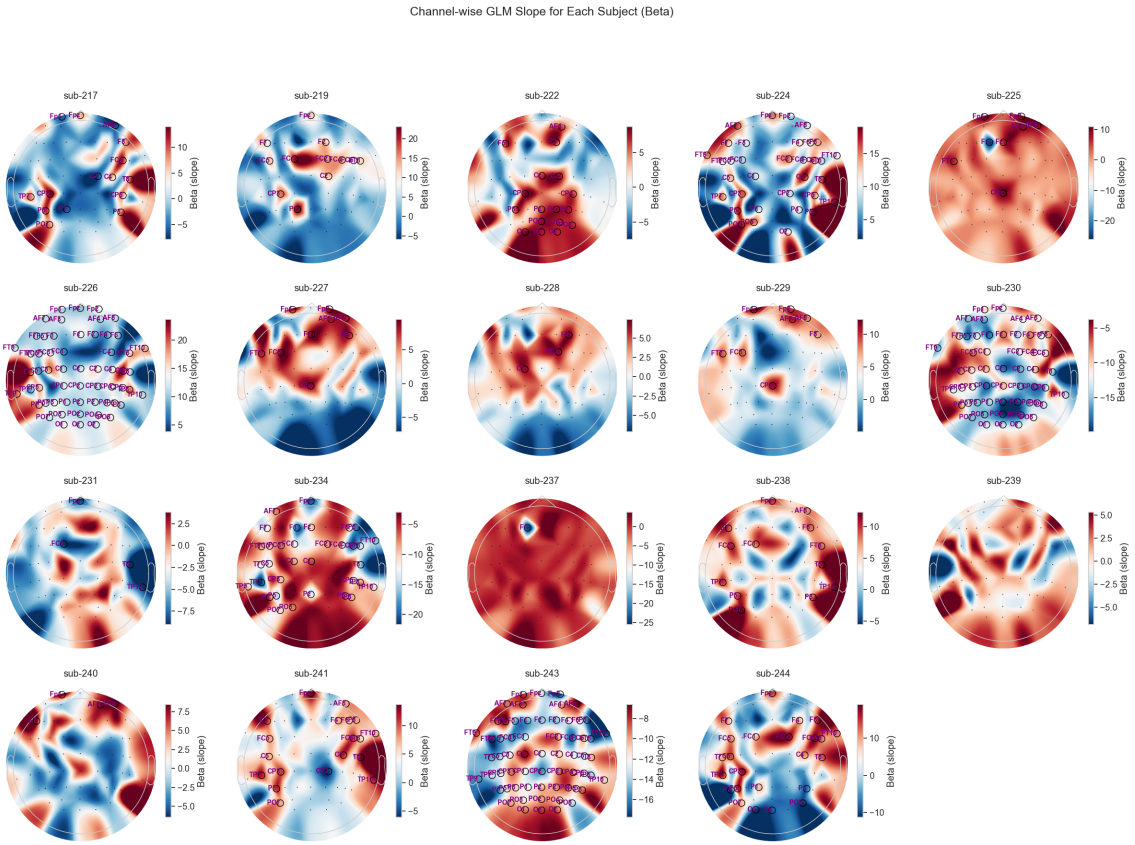

Figure 4.7: GSA and EEG Amplitude Correlation Subject-Wise revealed significant variation across individuals

To understand if subject-specific variability of EEG-GS relationship is present in the data, the correlation between EEG amplitude and global signal amplitude per subject was firstly visualized (Fig. 4.7).

The figure shows noticeable variation across individuals, which suggests that including random slopes may help capture real effects in the data. Because of that, it was initially decided to use a mixed linear model with both **random intercept and random slope**. This model was implemented in `R` using the `lme4` package, which is a standard library for mixed models. Although Python also offers `MixedLM` via `statsmodels`, `R` was chosen due to its wider application for mixed models

The full model, which was tested:

$$\text{global\_signal}_{ij} = \beta_0 + \beta_1 \cdot \text{eeg}_{ij} + u_{0j} + u_{1j} \cdot \text{eeg}_{ij} + \epsilon_{ij} \tag{4.1}$$

where

- $\text{global\_signal}_{ij}$: fMRI global signal amplitude at time point i for subject j
- eeg_{ij}: EEG regressor amplitude at time point i for subject j
- β_0: fixed intercept (global average)
- β_1: fixed slope (global effect of EEG on global signal)
- u_{0j}: subject-specific random intercept (baseline shift)
- u_{1j}: subject-specific random slope (variation in EEG–GS relation)
- ϵ_{ij}: residual error term

To assess the significance of the slope β_1, we extracted p-values from the model output and applied FDR correction to account for multiple comparisons across EEG channels. However, during model fitting, convergence warnings appeared ("Model failed to converge") for models with both random effects. These warnings indicated that the estimated covariance matrix of the random effects was not positive definite and included at least one negative eigenvalue, a sign of a singular fit. This issue suggests overparameterization or insufficient variability in the data to estimate both random effects reliably.

To investigate this further, we restricted the analysis to MB periods, where fewer convergence problems were observed (12 out of 63 channels). We then systematically examined the design matrices and model diagnostics. The fixed effects design matrix was of full rank in all cases, with two predictors (intercept and EEG regressor), confirming that the basic model structure was valid. The random effects design matrix also conformed to expectations, consisting of 38 columns (19 subjects $\times$ 2 random effects: intercept and EEG slope). Thus, structurally, the models were correctly specified.

However, additional diagnostics revealed that the variance of the random slope component was frequently less than 0.0001, a threshold used for the detection of matrix singularity. This lack of variability is a common cause of singular fits. Furthermore, the fixed effects design matrix had a condition number of approximately 150 across all channels, indicating moderate to high multicollinearity. Such multicollinearity can inflate estimation uncertainty and hinder model convergence.

Due to these convergence problems, additional inspection was necessary to understand whether we really benefit from a more complex model (with 2 degrees of freedom) using the log-likelihood ratio tests and its p-value.

This inspection was conducted only on the mind-blanking dataset, since convergence issues were observed for just 12 out of 63 channels. A more complex model, including both random slope and intercept, could still be beneficial for the remaining channels where it converges successfully, potentially outweighing the drawbacks of convergence problems.

The comparison showed that:

- For 22 out of 63 channels, the more complex model provided a significantly better fit
- For the remaining 41 channels, the simpler model was sufficient

This means that for most EEG channels, allowing EEG–GS relationships to vary per subject (random slopes) did not improve model fit. But for a subset (35%), between-subject variability was strong enough to justify a more complex model.

Therefore, we chose the simpler model, including only random intercepts, as our final specification. This model converged reliably for all channels and demonstrated stable behaviour across full and MB-only datasets. Moreover, model comparisons based on log-likelihood ratio tests indicated that the simpler model was better for most EEG channels. In addition, AIC and BIC values were generally lower or comparable for the simpler model, further supporting better performance compared to the model with 2 random effects. These findings suggest that including random slopes does not meaningfully improve model performance in most cases, while introducing convergence issues and instability. While simpler model may underestimate the uncertainty for channels with subject-specific EEG–GS variability (as shown in Figure 4.7), it provides a more robust and stable results, and it still allows for individual differences in baseline global signal amplitude

The final equation for the mixed linear model with random intercept is the following:

$$\text{global\_signal}_{ij} = \beta_0 + \beta_1 \cdot \text{eeg}_{ij} + u_{0j} + \epsilon_{ij} \tag{4.2}$$

- $\text{global\_signal}_{ij}$: fMRI global signal amplitude at time point i for subject j

- eeg_{ij}: EEG regressor amplitude at time point i for subject j
- β_0: fixed intercept (global average)
- β_1: fixed slope (global effect of EEG on global signal)
- u_{0j}: subject-specific random intercept (baseline shift)
- ϵ_{ij}: residual error term

4.11.3 Implementing the Model

Based on these assumptions, a mixed linear model was fitted for each of the 63 EEG channels, and the corresponding beta values and p-values were saved. After fitting the model across all channels, the p-values were FDR corrected for multiple comparisons. It is done because simultaneous testing of the hypothesis can increase the risk of false positives. Particularly, FDR accepts that some false discoveries may occur but keeps their proportion under a chosen threshold, in this study the threshold was considered as 5%, meaning that, on average, no more than 5% of the significant results are expected to be false positives.

In addition, the same model was used to fit the global delta signal with the global signal amplitude, using subject as a random intercept. As with the channel-wise analysis, beta values and corrected p-values were extracted. A topographical map was plotted to visualize the EEG channel-wise results, and a scatter plot with a regression line was created for the global delta signal.

The model was fitted on the entire dataset but separately for each mental state condition: MB, MW, and on-task reports. Additionally, the analysis was performed across all EEG frequency bands of interest, including delta, theta, alpha, and gamma.

4.11.4 Correlation Analysis of ECG and GS

To assess the relationship between physiological activity and GSA, the same mixed linear modeling framework was applied, but restricted to the global level. Unlike EEG, where signals can be analyzed on a channel-wise basis, the ECG data originate from a single channel, and therefore the model was fitted once across the entire dataset.

Specifically, GSA was entered as the dependent variable, while ECG power was used as the main predictor, with subject included as a random intercept to account for inter-individual variability. From this model, beta coefficients and associated p-values were extracted. As in the EEG analysis, the p-values were corrected for multiple comparisons using the false discovery rate (FDR) procedure, with a significance threshold of 5%, ensuring that no more than 5% of the significant results were expected to be false positives on average.

The analysis for EEG was performed only for each MB, since it was the one condition-specific relationship between ECG activity and GSA we wanted to examine. To aid interpretation, the ECG–GSA relationship was visualised using scatter plots with a regression line.

The whole code implementation is available in the corresponding ULiège's GitLab repository (Varvara Strizhneva, 2025).

Some parts of the EEG preprocessing pipeline were based on in-house code developed by a senior postdoctoral researcher in Applied Machine Learning Group. Institute of Neuroscience and Medicine, Brain & Behaviour (INM-7), Research Centre Jülich, Germany. This implementation allowed for saving all intermediate preprocessing results in structured `.json` files and generated `.html` reports for ICA quality inspection. The code is publicly available in a dedicated GitHub repository (Federico Raimondo, 2025).

4.12 Data Inspection

Before preprocessing the fMRI and EEG data, it was important to check the clarity of the EEG recordings. After initial preprocessing - particularly MRI artifact removal and cardioballistic artifact correction, some of the subjects from the dataset showed saturated channels during visual inspection. These saturated channels could not be reconstructed. This issue likely occurred due to amplifier overload, where the EEG amplifier failed to handle the MR environment noise or participant movement, resulting in flat or clipped signals across certain channels. Since this type of corruption rendered large portions of the data unusable, 10 subjects (from sub-205 to sub-216) were excluded from the further analysis.

In the next preprocessing step, after removing scanner-related artifacts, the alignment between EEG and fMRI data was carefully checked. This was necessary to ensure that the timing and segmentation of the two modalities matched correctly. The original EEG file, which included all four fMRI runs, was split into four separate EEG files based on repetition time markers in the EEG. These EEG segments were expected to align perfectly with the four fMRI runs.

To verify this, the total durations of both EEG and fMRI data were calculated and compared. If mismatches were found, the raw data and annotations were rechecked. For five subjects: sub-230, sub-239, sub-240, sub-241, and sub-244, minor misalignments were detected in the fourth run. These were not due to data corruption but to incorrect annotations. Therefore, it was decided to restore the original EEG annotations for these subjects prior to preprocessing, which allowed proper alignment to be achieved across all subjects.

4.13 Personal Contribution

I contributed to the preprocessing and analysis pipeline of both EEG data and global signal confounds. This included the alignment of EEG markers with corresponding fMRI sessions and the extraction of time windows associated with reported mental states (MB, MW, on-task).

Using BrainVision Analyzer software, I performed artifact removal to eliminate both instrumental and physiological noise. I implemented a complete EEG preprocessing pipeline, which included band-pass filtering, bad channel detection and rejection, ICA-based artifact correction, and segmentation into epochs aligned with fixed events. From this cleaned data, I extracted band-specific amplitude features for further analysis.

This approach was adapted from the methodology described by Scheeringa et al. (2012), who analyzed alpha-band oscillations using Hilbert transforms and accounted for delays due to HRF. However, unlike their interpolation-based method, I implemented an alternative approach because I specifically used fixed-length epochs aligned with the fMRI TR; instead of interpolating, I computed the mean signal amplitude per epoch, ensuring consistent alignment with the hemodynamic response.

In addition, I developed a methodology for extracting physiological regressors (ECG) directly from the EEG data. This involved designing the extraction procedure, implementing signal processing steps, and preparing the resulting physiological time series for use in statistical modelling.

For the statistical analysis, I constructed and implemented linear mixed-effects models to investigate relationships between EEG amplitudes, physiological signals, and global signal amplitude. This included model specification, fitting, and evaluation using metrics such as AIC/BIC and likelihood ratio tests. I also created a design matrix for linear mixed-effects analyses across mental states and conducted all statistical testing related to state comparisons.

All neurophysiological data visualisations, including boxplots, scalp maps, and condition-specific comparisons, were designed and implemented by me to support the interpretation of the LMMs' outputs.

As part of the collaborative workflow, I also integrated existing code for cleaning EEG data with automatic .json metadata generation and interactive ICA component visualization via HTML reports, as described in Federico Raimondo (2025). This integration improved both the reproducibility and accuracy of the artifact rejection process. Overall, the preprocessing pipeline combined original contributions with well-established, referenced methods.

Chapter 5

Results

The next chapter will present the results of three main analyses. First, we report the sanity check of Andrillon et al. (2021), which was conducted to ensure the quality and reliability of the preprocessing steps applied to EEG and fMRI data. Second, we describe the behavioural analysis, focusing on participants' reports of mental states and amplitude distribution of different signals across experimental runs, which provides the necessary context for interpreting the data. Finally, the correlation analyses are presented, where the relationships between EEG-derived components, global signal amplitude, and reported mental states are examined, with a particular emphasis on MB.

5.1 Sanity Check

To validate the proposed methodology, a sanity check was conducted referencing the study of Andrillon et al. (2021), which investigated slow-wave activity during wakefulness. In particular, it was aimed to replicate the key analysis relating local slow-wave properties to self-reported mental states at the probe level. The mental states and experiment structure itself were identical to our data; particularly, they studied the following mental reports: MW, MB, and ONTASK.

In the original study, the authors examined whether properties of slow waves, particularly density, amplitude, downward slope, and upward slope, preceding each probe could predict the participants' reported mental state. These analyses were performed independently for each electrode across the scalp, followed by mixed-effects modeling and cluster-based permutation testing (Fig. 5.1).

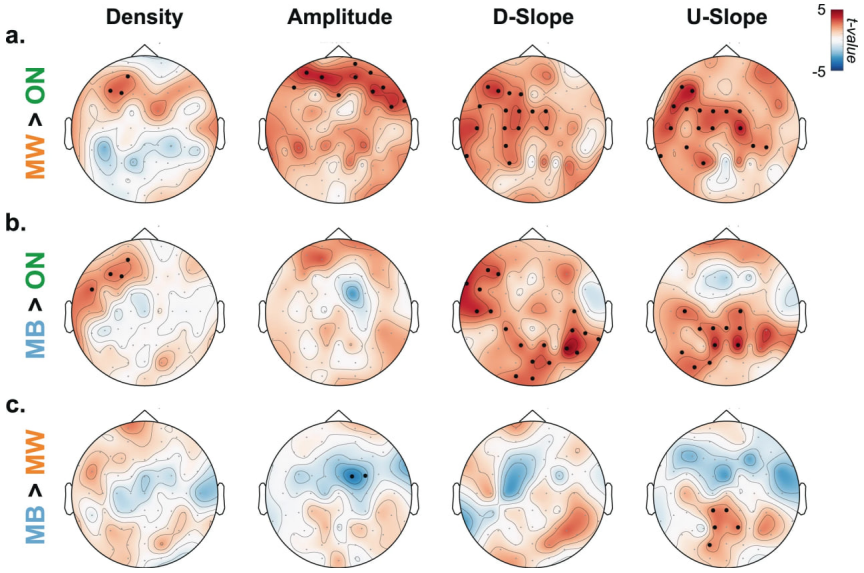

Figure 5.1: Locally, based on each individual electrode, Andrillon et al. (2021) performed mixed-effect analyses, followed by permutation analysis to quantify the impact of slow-wave properties on mental states.

Due to methodological differences in slow-wave detection and its feature extraction, our replication was limited only to analysing the amplitude of delta oscillations during mental state reports, which serves as a proxy for slow-wave activity in the current dataset. We focused on the same pairwise contrasts of mental states as in the original study:

- MW > ON
- MB > ON
- MB > MW

Topographical maps of these contrasts, computed using linear mixed-effects models at each electrode, are presented in Figure 5.2. Despite differences in preprocessing and analytical pipelines, the observed spatial patterns qualitatively resemble those reported by Andrillon et al. (2021). Notably, we observed enhanced delta amplitude over frontal regions relative to ON during MW and a widespread reduction in amplitude for MB relative to both ON and MW conditions.

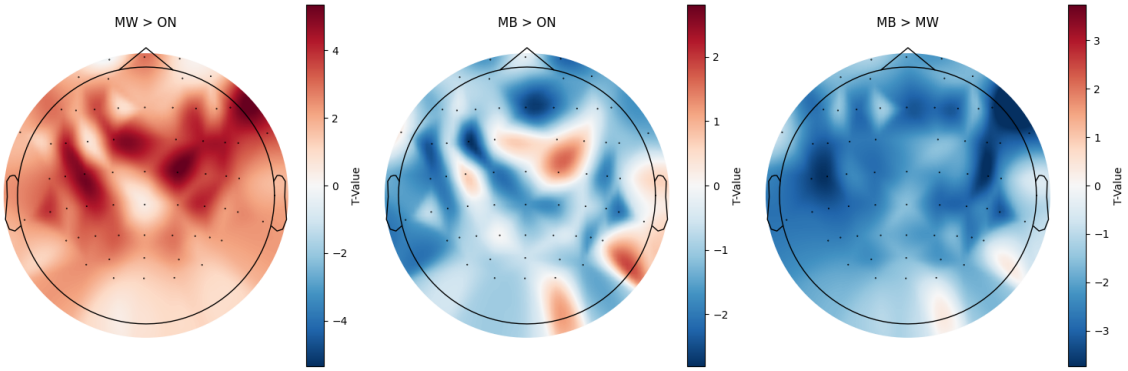

Figure 5.2: Topographical contrasts of delta amplitude for each mental state comparison. Maps reflect t-values from linear mixed-effects models.

It is important to note several methodological differences that could account for discrepancies. First, the duration of the analysis window for each mental state report differed. Whereas Andrillon

et al. (2021) limited their analyses to 20 seconds before the probe, we extended the window to 60 seconds, corresponding to the duration of the one Go/NoGo task of the experiment block. This choice was made to ensure that reported mental states are confidently captured.

Second, our approach to slow-wave extraction diverged from the original pipeline, where a dedicated slow-wave detection algorithm was used to quantify individual events and compute slopes and density. In our case, we relied only on delta-band amplitude.

Nonetheless, the qualitative similarity between the resulting topographical distributions supports the robustness of our analytic approach and confirms that delta-band amplitude captures meaningful cognitive dynamics associated with spontaneous mental states (Fig. 5.1, 5.2).

5.2 Behavioural Analysis

To investigate the periods of the experiment when the mental states of interest were reported, the `events` recorded by the scanner were analysed to assess the frequency of each reported mental state.

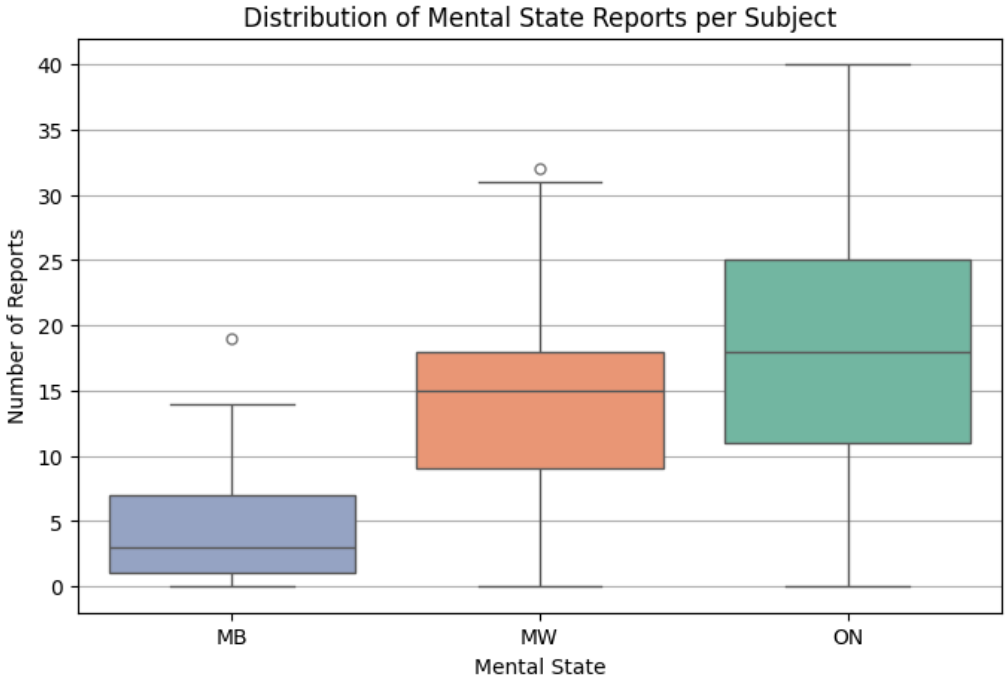

Figure 5.3: Distribution of Reported Mental States Observed across 38 subjects

As shown in Figure 5.3, the most frequently reported mental state was **ONTASK** with total number of reports 740, while **MB** was reported the least with only 157 reports. Using t-test on two related samples of scores, it is possible to test for the null hypothesis that two related or repeated samples have identical average (expected) values. The results showed that indeed MB is significantly less frequent than both ONTASK and MW ((H1: MB $<$ ONTASK) T-stat: 7.315, one-tailed p: 0.000, (H1: MB $<$ MW) T-stat: 6.805, one-tailed p: 0.000), while the frequency of ONTASK and MW do not differ significantly (T-statistic: 1.639, p: 0.110).

This pattern was expected, as participants were instructed to perform a task that required continuous attention, making task-focused (ONTASK) states more prevalent. In contrast, MB episodes are characterised by spontaneous lapses of awareness, faster than other states and often occur during low-stimulation or monotonous periods, making them less frequent in active experiments for some participants (Mortaheb et al., 2022). Moreover, answers which were skipped by subjects were considered as also MB reports, since they can indicate a loss of attention which

caused the report to be missed.

	MB	**MW**	**ONTASK**
sub-205	10	17	10
sub-206	0	3	37
sub-207	11	13	9
sub-208	1	14	24
sub-209	2	6	17
sub-210	14	12	8
sub-212	1	0	38
sub-213	3	20	5
sub-214	7	20	0
sub-215	2	18	13
sub-216	12	8	12
sub-217	4	15	21
sub-218	0	10	30
sub-219	9	13	18
sub-222	4	17	19
sub-223	0	14	26
sub-224	1	30	9
sub-225	6	16	18
sub-226	4	23	13
sub-227	13	8	19
sub-228	1	5	33
sub-229	2	17	21
sub-230	3	9	28
sub-231	7	16	17
sub-232	0	0	40
sub-233	0	17	23
sub-234	5	20	15
sub-235	0	32	8
sub-236	0	15	25
sub-237	1	9	30
sub-238	13	23	4
sub-239	3	31	6
sub-240	12	5	23
sub-241	3	0	37
sub-242	0	23	17
sub-243	19	10	11
sub-244	4	17	19

Table 5.1: Number of reported mental states for each subject, where **MB** - mind blanking, **MW** - mind wandering, **ONTASK** - active task involvement, where ONTASK is the most frequent mental state, while MB is the least frequent state.

In addition to reports on mental states, subjects were also informed about their level of alertness. This allows for the consideration of active mental states alongside lower levels of arousal, potentially leading to an increase in slow-wave activity. The reported alert states across subjects and total number of each state can be observed in the Table 5.2. The Table 5.2 summarises the results of alertness, which are shown only for 19 subjects who were included in the final analysis after data inspection described in Section 4.12. Subjects with corrupted data and those who did not report MB were excluded from the analysis. For MW and ONTASK reports, we included only the same set of subjects considered for MB, even though additional subjects reported MW and ONTASK but not MB. This approach ensured that all comparisons were based on an identical group of participants, thereby maintaining equal statistical power across conditions.

Table 5.2: Alertness State Counts per Subject

Subject	**Alert**	**Sleepy**	**ExAlert**	**ExSleepy**
sub-217	12	22	4	2
sub-219	27	9	1	3
sub-222	8	23	1	8
sub-224	15	21	1	3
sub-225	11	22	1	6
sub-226	19	17	3	1
sub-227	38	2	0	0
sub-228	22	9	8	0
sub-229	24	10	6	0
sub-230	19	11	10	0
sub-231	24	15	1	0
sub-234	20	7	10	3
sub-237	24	10	6	0
sub-238	3	10	0	27
sub-239	11	15	0	14
sub-240	15	17	3	5
sub-241	26	0	14	0
sub-243	7	24	0	9
sub-244	16	11	7	6
Total	**341** (45%)	**255** (34%)	**76** (10%)	**87** (11%)

For further analysis, the following subjects will be used based on the previous steps of data inspection and presence of MB reports: **sub-217, sub-219, sub-222, sub-224, sub-225, sub-226, sub-227, sub-228, sub-229, sub-230, sub-231, sub-234, sub-237, sub-238, sub-239, sub-240, sub-241, sub-243, sub-244**. In total, 19 subjects were analysed.

The following sections will present a series of analyses examining correlations between the amplitudes of neuronal oscillations (delta, theta, alpha, and gamma) and physiological oscillations (ECG) with GS amplitudes. These results are intended to test the hypothesis and to disentangle the contribution of neuronal and physiological components to GS fluctuations during MB. By systematically comparing these relationships, we aim to clarify whether GS increases observed in MB primarily reflect neural slow-wave activity or whether they are more strongly driven by physiological processes.

5.3 Result of Correlation Analysis

In the following analysis, the results of the correlation analysis will be presented, which include:

- Correlation analysis between the amplitude of different EEG bands (delta, theta, gamma, and alpha) and GSA to assess the overall relationship between EEG activity and GSA, and to evaluate potential neuronal contributions to the global signal;
- Correlation analysis between the amplitude of different EEG bands (delta, theta, gamma, and alpha) and ECG with GSA during MB reports to determine whether low-frequency EEG activity is associated with increased GSA or the physiological signal;
- Correlation between the amplitude of different EEG bands (delta, theta, gamma, and alpha) and GSA during MW reports to explore whether spontaneous thinking is reflected in changes in global signal and associated neuronal activity;
- Correlation analysis between the amplitude of different EEG bands (delta, theta, gamma, and alpha) and GSA during On-Task reports to characterize the neuronal profile during focused

cognitive engagement and compare it to mind-blanking and mind-wandering conditions.

To assess the properties of the regressors used in the linear mixed-effects analysis, we first examined their distributions across all experimental runs. As shown in Figure 5.4, the values of the EEG, GS, and physiological (ECG-related) regressors were z-scored, resulting in standardized distributions across runs. The boxplots reveal consistent centring and comparable spread for each regressor type across runs, which shows correctly applied normalisation. Notably, the physiological regressors exhibit a much wider range of outliers, extending from approximately from -7.5 to 10 in z-score units.

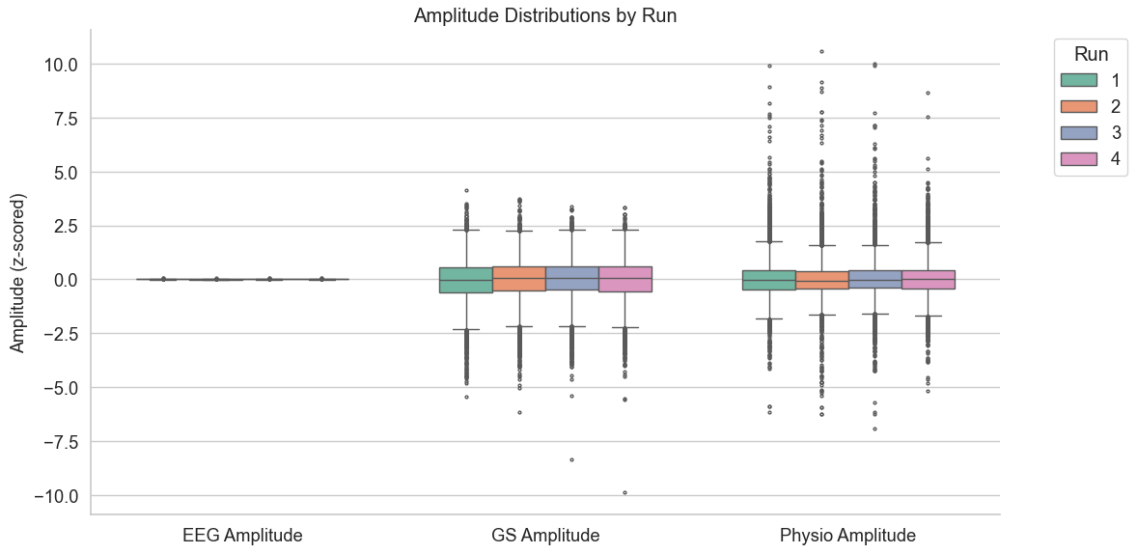

Figure 5.4: Distribution of z-scored amplitude values for EEG, GS, and physiological (ECG) regressors across runs, which shows a wide range of outliers of physiological regressors and low variance of EEG regressors

To further investigate the properties of the EEG regressor in isolation, Figure 5.5 presents a focused distribution analysis of the EEG delta-band amplitude across the four runs. The values are tightly clustered around zero with limited variance and a small number of outliers reaching up to approximately 0.05. This narrow distribution is expected, as the delta regressor reflects a filtered and smoothed band-limited component of the EEG signal, capturing only slow oscillatory fluctuations while excluding broader variability present in the raw EEG with all EEG bands. These results confirm that all regressors were effectively normalized, and their distributions are appropriate for use in linear modeling.

Next, the amplitude variation was examined separately for each EEG frequency band of interest across the three reported cognitive conditions: MB, MW, and On-Task (Fig. 5.6).

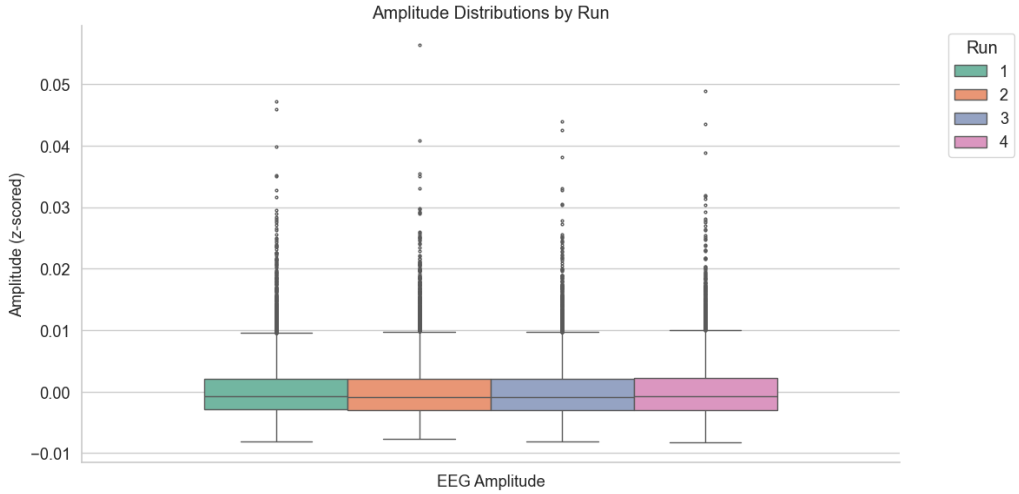

Figure 5.5: Distribution of z-scored delta-band EEG amplitude regressors across runs, showing low variance and minimal outliers

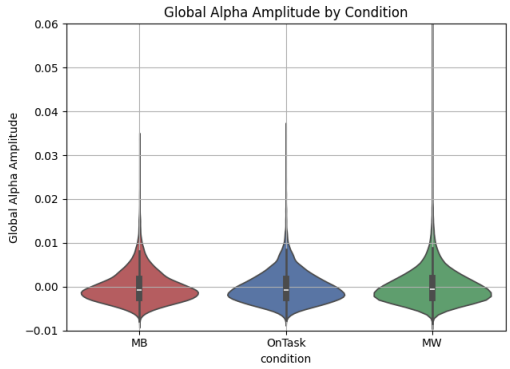

(a) Distribution of Alpha Band Amplitude During Different Conditions

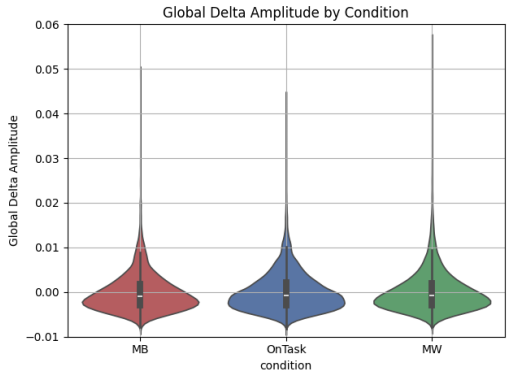

(b) Distribution of Delta Band Amplitude During Different Conditions

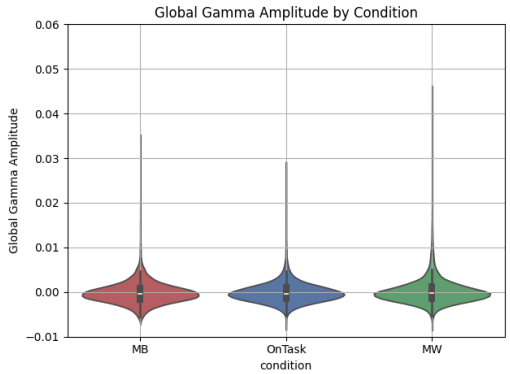

(c) Distribution of Gamma Band Amplitude During Different Conditions

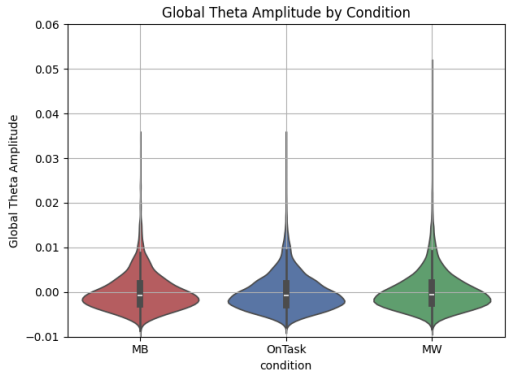

(d) Distribution of Theta Band Amplitude During Different Conditions

Figure 5.6: Distribution of Amplitude for EEG Bands During Different Conditions

For this, each normalised time series was visualised using violin plots with noted variance and mean values. Overall, the distributions show some overlap across conditions, suggesting that differences in global EEG amplitude are hardly distinguishable. However, they still show slightly different spreads, medians, and tails depending on the EEG band. Delta and theta showed the broadest variability, with MW in particular displaying extended positive tails, suggesting occasional bursts of higher low-frequency activity during mind-wandering. Moreover, the broad variability

is also present for the delta band during MB reports. By contrast, alpha exhibited a narrower distribution, though MW displayed slightly more spread than MB and ONTASK. Gamma stood out as the most tightly clustered band, with minimal spread across all states. Across conditions, median values remained near zero in all bands, but the broader tails in MW for delta and theta, and in MB for delta, highlighting the small variability of oscillations of the EEG bands related to state differences.

In addition to EEG-based regressors, similar plots were generated to evaluate amplitude variation in GS and ECG regressors across the same cognitive conditions (Fig. 5.7).

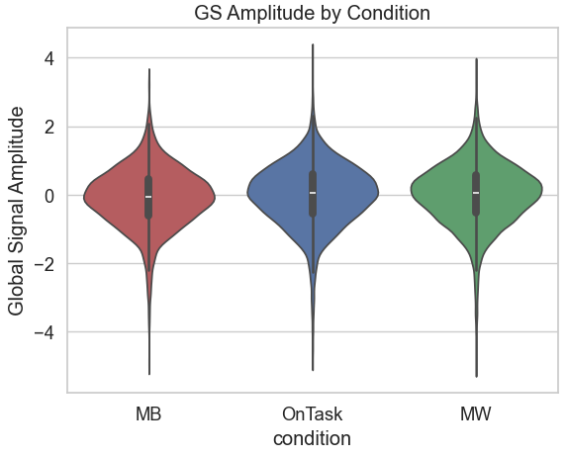

(a) Distribution of GS Amplitude During Different Conditions

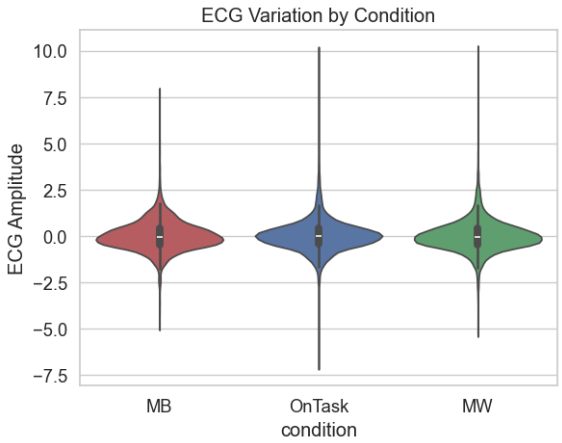

(b) Distribution of ECG Variation During Different Conditions

Figure 5.7: Distribution of Amplitude and Variation for GS and ECG during different Conditions

The violin plots reveal a generally consistent amplitude distribution across conditions, with a slightly wider spread during On-Task and MW. However, no strong shift in central tendency is visually evident. This suggests that GS amplitude alone may not sharply distinguish between cognitive states, but some variability may exist.

The right panel in Fig. 5.7 displays the distribution of ECG amplitude, reflecting physiological variability across the same conditions. Similar to the GS amplitude, ECG variability does not show pronounced condition-specific differences, with overlapping distributions in all three states. Although the effect appears modest, slightly higher tails are observed during MW and MB, which might increase physiological fluctuation during internally oriented states.

As shown in the violin plots, the distribution of GSA values during MB appears shifted

compared to MW and ON-task states. To further examine this, the average GSA per mental state was computed and visualized in Figure 5.8. Although MB showed a trend toward lower GSA values, statistical comparisons did not reach significance. Specifically, the difference between MB and MW yielded t = –1.415, p = 0.160; between MB and ON-task: t = –1.195, p = 0.234. A one-sample t-test also showed that the mean GSA during MB was not significantly different from zero (t = –1.575, p = 0.120). Thus, while a decrease in GSA is observed during MB, the evidence is not strong enough to conclude a reliable difference.

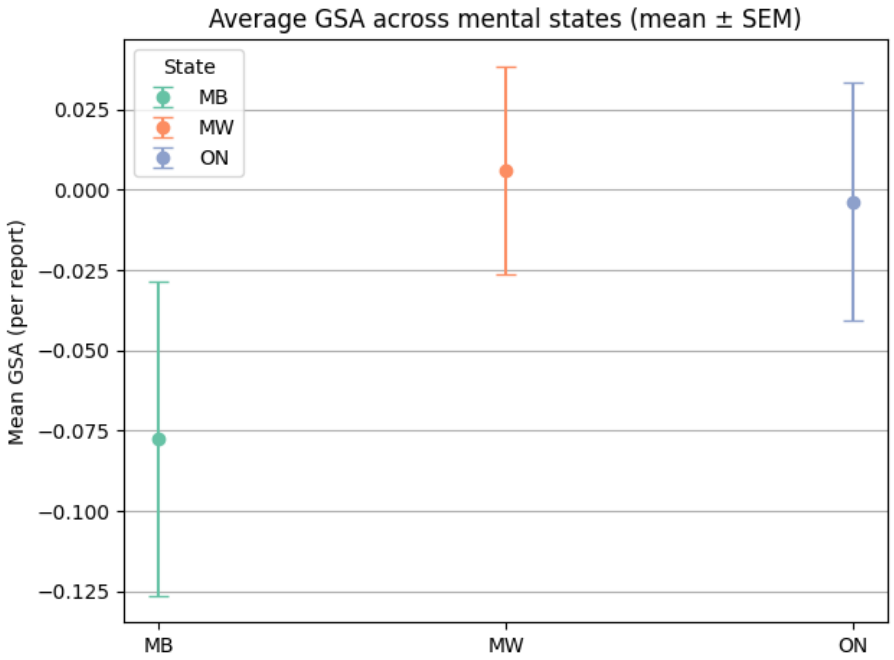

Figure 5.8: Chart of averaged GSA reveals that GSA during MB reports is lower than during other mental states but this difference is not significant (t = –1.575, p = 0.120)

Overall, the distribution analysis shows that although some differences in spread and tails can be noted between bands and states, no clear or systematic distinctions emerge across conditions. Since these descriptive results alone do not provide strong evidence of state-specific amplitude changes, the next step is correlation analyses to explore how neuronal and physiological oscillations relate to GS more directly.

5.3.1 Correlation of Delta Oscillations and GSA

Before examining the correlation, particularly during MB reports, it was decided to assess the overall relationship between delta waves and GS and other wave oscillations to determine if any neuronal activity can be linked to the global signal. The relationship between EEG band activity and global signal amplitude was assessed using a GLM. This analysis used the global signal as the dependent variable, and the EEG band amplitudes were regressors. The GLM output included the slope (beta coefficient), its associated p-value, and confidence intervals. The beta coefficient reflects both the strength and direction of the association, indicating how much the global signal amplitude changes with a one-unit increase in EEG amplitude.

To visualize this relationship spatially, topographical maps were plotted using the beta values for each EEG channel, allowing identification of regions where delta-band power shows either a positive or negative association with the global signal. The scalp map provides a clear overview of these spatial patterns across the entire electrode layout (Fig. 5.9).

On the resulting topomap, significant channels are displayed in purple, representing those for

which the beta values have a p-value < 0.05. As described in Chapter 4, all p-values were corrected for multiple comparisons. This adjustment was necessary because testing several hypotheses simultaneously increases the risk of false positives. By applying correction procedures, the analyses ensured that the proportion of false rejections of the null hypothesis was properly controlled. This indicates that the observed effect can be considered confidently.

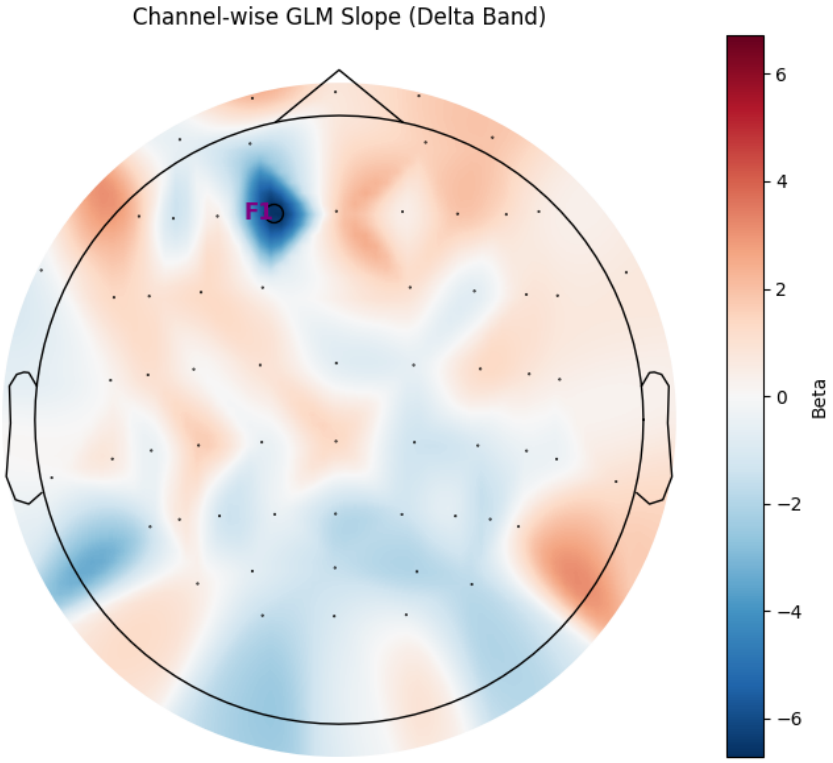

Figure 5.9: GLM Slopes Reveal No Significant Delta-Band EEG Activity

The colourbar next to the topomap represents the beta values from the GLM, which indicate the slope of the relationship between EEG power in each channel and the global fMRI signal. These values quantify how fluctuations in EEG activity are associated with changes in the global signal.

Warm red colours on the map indicate positive slopes, meaning that increases in delta power in those channels are associated with increases in the global signal. Cool blue colours represent negative slopes, indicating an inverse relationship - where higher delta activity corresponds to a reduction in global signal amplitude.

The strongest negative slope was observed in the frontal region, particularly around the F1 channel. In contrast, positive associations were more prominent in occipital and temporal areas. However, it is important to note that only the F1 channel showed a statistically significant result ($p < 0.05$), and therefore, the findings for other channels should be interpreted with caution.

In addition, the channel-wise global correlation between the mean delta signal and the global signal was calculated. For this, a single GLM model was used to compute one beta coefficient and its p-value between the two time series, global delta and global signal. The results show a global slope of 0.1195 and an associated p-value with confidence interval, which suggests non-significance of the observed pattern, as shown in Table 5.3.

Table 5.3: Results of the GLM for global signal amplitude and amplitude of the mean EEG signal in the delta band

Variable	Beta	p-value	CI Lower	CI Upper
global delta signal	0.120	0.914	-2.056	2.295

5.3.2 Correlation of Other EEG Bands and GSA

As mentioned above, it was necessary to check the correlation between other EEG bands of interest, particularly for alpha, gamma and theta EEG bands to reveal any coupling effect between GSA and neuronal components.

Alpha Oscillations

Alpha wave oscillations are typically observed during states of relaxed wakefulness. In our analysis, a negative slope was identified between alpha wave activity and the global signal, with β = -3.65 (Fig. 5.10b). The statistical significance of this relationship is supported by a p-value and confidence interval not crossing the zero, indicating that the observed effect is unlikely to be due to random chance (Table 5.4). This suggests that increased alpha wave activity may be associated with decreased global brain signals during task-based activity.

The topography reveals a widespread pattern of negative slopes, particularly pronounced in parietal, occipital, and posterior temporal regions (e.g., POz, O2, TP8), where increases in alpha power are associated with decreases in the global fMRI signal. This inverse relationship is consistent across almost all EEG channels (Fig. 5.10a).

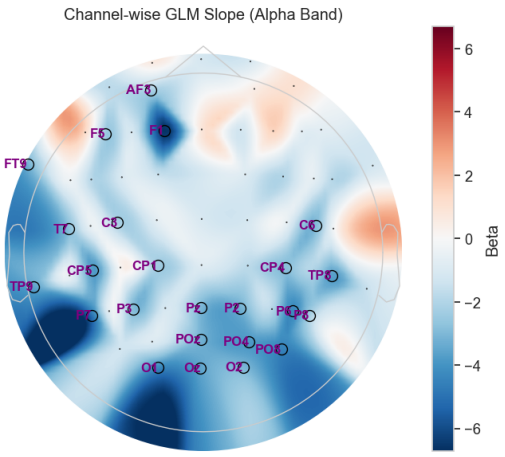

(a) GLM Slopes Reveal Significant Alpha-Band EEG Suppression in Parietal, Occipital and Posterior Temporal Regions, which shows local negative correlation with GSA

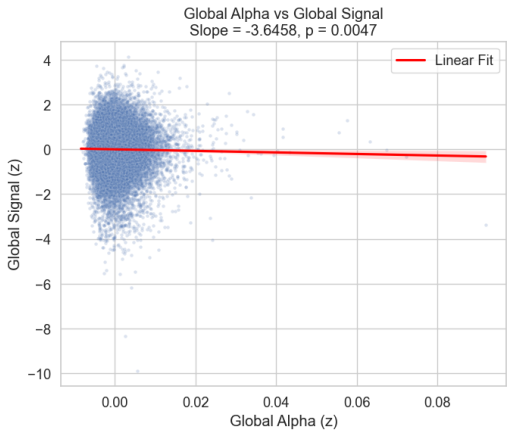

(b) Linear regression between global alpha amplitude and GSA

Figure 5.10: Alpha-band EEG–fMRI relationship. **(a)** Beta values across EEG channels reflect channel-wise GLM slopes with the global signal amplitude. **(b)** Linear model fit between global alpha amplitude and global signal amplitude across time points

Theta Oscillations

The GLM for global theta amplitude the linear relationship between EEG amplitude and the fMRI global signal amplitude. Although the fitted linear model yielded a positive slope (β =

Table 5.4: Results of the GLM for global signal amplitude and amplitude of the mean EEG signal in alpha band

Variable	Beta	p-value	CI Lower	CI Upper
global alpha signal	-3.646	0.005	-6.173	-1.119

1.81), the association did not reach statistical significance (p = 0.1239), indicating that, at the whole-brain level, fluctuations in theta-band power were not reliably associated with fluctuations in the global signal (Table 5.5).

The left graph presents the spatial distribution of GLM slopes for the theta band across individual EEG channels. The topography reveals a heterogeneous pattern, with both positive and negative slopes depending on the scalp region. Stronger positive associations were observed over frontal, parietal, and temporal areas, particularly around channels Fp2, AF4, P8 and CPz (Fig. 5.11).

Together, these results suggest that there is no significant global association between theta activity and the global fMRI signal. However, regional patterns may still reflect localised interactions between global signal amplitude and theta wave amplitude.

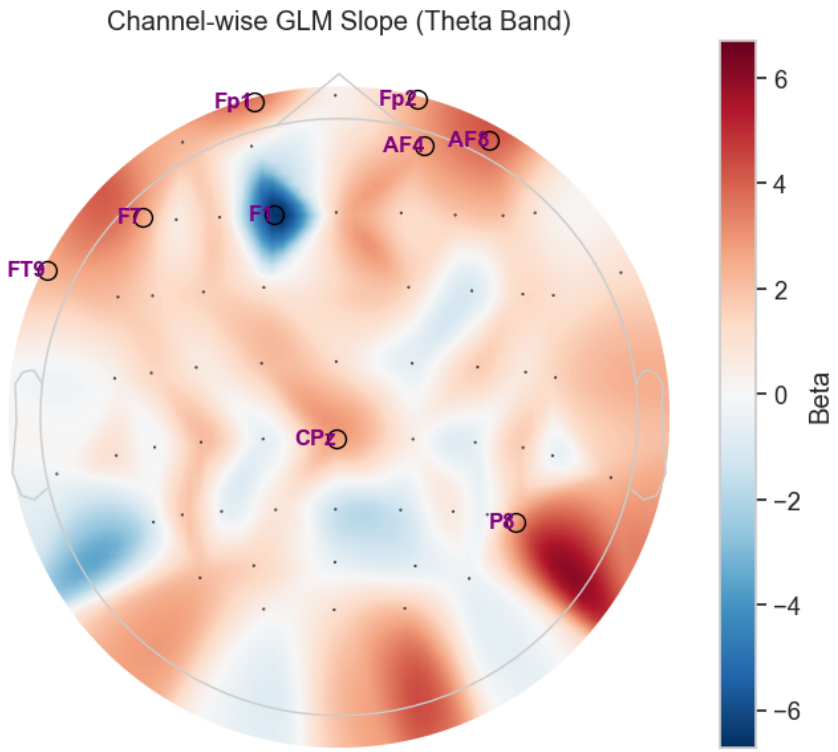

Figure 5.11: GLM Outputs Reveal Frontal Dominance in Theta-Band EEG Activity

Table 5.5: Results of the GLM for GSA and amplitude of the mean EEG signal in theta band

Variable	Beta	p-value	CI Lower	CI Upper
global theta signal	1.807	0.124	-0.495	4.109

Gamma Oscillations

The GLM output for globally averaged gamma power and the global fMRI signal shows the linear relationship between them. The estimated slope is negative ($\beta = -0.609$), but the association

did not reach statistical significance ($p = 0.746$), suggesting no reliable linear coupling between whole-scalp gamma activity and global signal fluctuations (Table 5.6).

In contrast, the left panel presents the spatial distribution of GLM slopes for gamma-band power across individual EEG channels, where channels marked in purple indicate statistically significant associations ($p < 0.05$), highlighting regions where the observed effects are unlikely to be due to chance (Fig. 5.12).

Significant negative associations were most prominent in frontocentral and parietal regions (FC2, F7, CP3), while positive slopes reached significance in left and right temporal lobes, including TP8, C6, TP9 and P7. This spatial dissociation implies that, although the global effect is not significant, local gamma–fMRI interactions are present and vary by anatomical location.

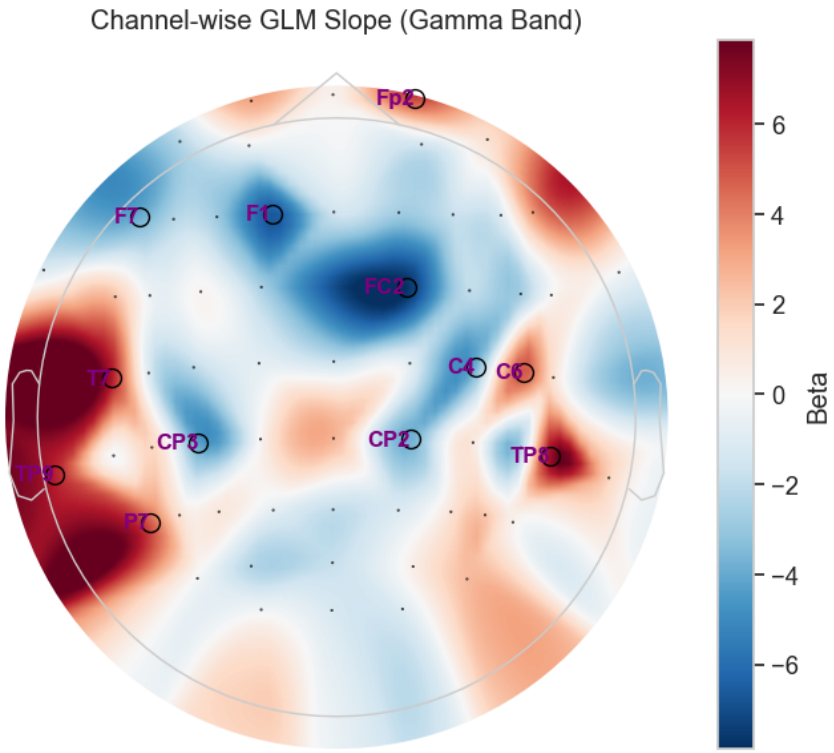

Figure 5.12: GLM Slopes Indicate Frontal-Central Gamma Reduction

Table 5.6: Results of the GLM for GSA and amplitude of the mean EEG signal in gamma band

Variable	Beta	*p*-value	CI Lower	CI Upper
global gamma signal	-0.609	0.746	-4.292	3.073

Notably, the F1 channel consistently displays an extreme negative slope, regardless of the cognitive condition or frequency band analysed across all four frequency bands- gamma, alpha, theta, and delta. This repeated prominence suggests that the effect seen at F1 is not driven by underlying neuronal activity, but is more likely an artifact.

To further investigate the suspiciously strong negative slope observed at channel F1, its behaviour was cross-checked in individual subjects who showed the most prominent effects (Fig. 4.7), specifically sub-225, sub-234, sub-237, and sub-230. In subjects 225 and 237, the F1 channel exhibited flat, suggesting possible electrode malfunction. However, in subjects 234 and 230, the F1 channel appeared to have normal signal characteristics, without any noticeable artifacts. Therefore, even with removal and interpolating this channel, it did not fully resolve the issue or explain the abnormal slope at F1 across the group.

5.3.3 Correlation of Delta Oscillations and GSA During MB Reports

To retrieve the correlation between delta-band EEG power and the global fMRI signal specifically during MB reports, only the time segments corresponding to MB episodes were included in the GLM analysis, as described in the Methods Chapter 4. This included the time window of around 60 seconds, which corresponds to one Go/NoGo task of the block.

The left panel shows the linear relationship between the global delta power (z-scored and averaged across all channels) and the global fMRI signal during MB episodes (Fig. 5.13b. A significant negative association was observed (slope = –10.13, p = 0.0012), indicating that higher delta power during MB is reliably associated with lower global signal amplitude (Table 5.7).

The right panel presents the channel-wise GLM slopes for the delta band, which are also limited to MB periods (Fig. 5.13a). Most electrodes exhibit negative slopes, powerful effects over parietal, central, and occipital regions. Channels highlighted in purple represent statistically significant effects ($p < 0.05$), showing that the inverse coupling between delta activity and the global fMRI signal is spatially widespread and robust during MB.

Table 5.7: Results of the GLM for GSA and amplitude of the mean EEG signal in delta band during MB

Variable	Beta	*p*-value	CI Lower	CI Upper
global delta signal	-10.134	0.001	-16.243	-4.024

The table above summarises the GLM output for the global delta regressors. The beta coefficient (–10.13) indicates an inverse association. The confidence interval (CI) ranges from –16.24 to –4.02, meaning that with 95% confidence, the true effect lies within this interval and does not cross zero, further confirming statistical significance. This also leads to the conclusion that higher delta amplitude during MB is reliably associated with lower global signal amplitude, and that this relationship is unlikely to have occurred by chance.

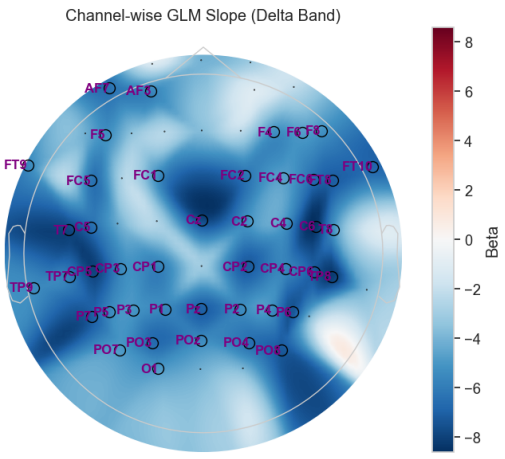

(a) GLM Slopes Reveal Significant Delta-Band EEG Suppression in Parietal, Occipital, Posterior and Temporal Regions, which shows local negative correlation with GSA during MB reports

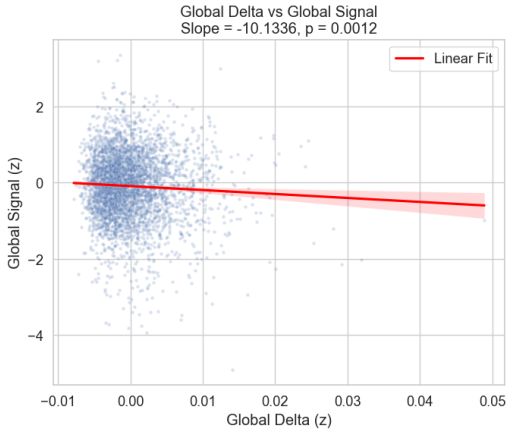

(b) Results of the GLM for GSA and mean EEG signal amplitude in delta band during MB reports reveal global negative correlation with GSA

Figure 5.13: Delta-band EEG–fMRI relationship during MB. **(a)** Beta values across EEG channels reflect channel-wise GLM slopes with the global signal. **(b)** Linear model fit between global delta amplitude and GSA across time points during MB reports

5.3.4 Correlation of Other EEG Bands with GSA During MB Reports

As discussed in Chapter 1, MB is typically associated with increased delta and theta frequency bands activity. In contrast, cognitive states characterised by higher arousal and attention are often linked to elevated gamma band activity. Given these opposing functional associations, delta/theta and gamma bands would be expected to show an inverse relationship with the global signal amplitude, reflecting their opposite roles in brain state regulation.

Theta Oscillations During MB

The linear fit between global theta power (averaged across electrodes; MB segments only) and the global fMRI signal revealed that the slope is negative (–4.58) but did not reach statistical significance ($p = 0.1536$). This indicates that theta fluctuations, when pooled across the scalp, are not reliably related to global signal amplitude during reported MB (Table 5.8).

The Figure 5.14a displays the channel-wise GLM slopes for theta power during MB. The map is dominated by widespread negative effects, most clearly over posterior regions. A small set of electrodes reached statistical significance (highlighted in purple), clustering over left posterior (e.g., CP5/P7 region) and right posterior temporo-parietal/occipital sites (e.g., TP8, P6, PO8 region). These localised effects suggest that, despite the absence of a robust whole-scalp theta–GS relationship, posterior theta activity may contribute selectively to MB-related variance in the global signal.

Table 5.8: Results of the GLM for GSA and mean EEG signal amplitude in theta band during MB

Variable	Beta	*p*-value	CI Lower	CI Upper
global theta signal	-4.581	0.154	-10.872	1.711

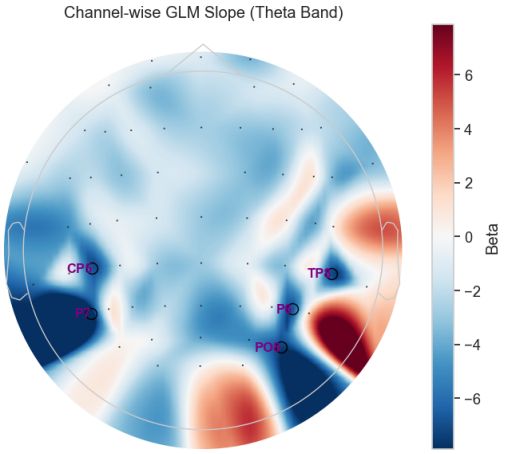

(a) Theta-band: Topographical distribution of GLM beta values during MB revealed negative correlations over posterior regions

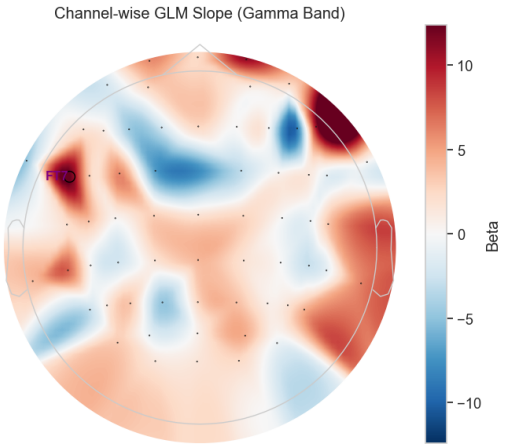

(b) Gamma-band: Topographical distribution of GLM beta values during MB reveals no significant correlation with GSA

Figure 5.14: Topographical distribution of GLM beta values across EEG channels during MB reports. **(a)** Theta band. **(b)** Gamma band.

Gamma Oscillations MB

GLM output revealed that while the fitted slope is positive ($\beta = 2.817$), the association is not statistically significant ($p = 0.608$), as shown in Table 5.9. This suggests that there is no reliable coupling between gamma-band EEG activity and global signal fluctuations during MB episodes.

Table 5.9: Results of the GLM for GSA and mean EEG signal amplitude in the gamma band during MB

Variable	Beta	*p*-value	CI Lower	CI Upper
global gamma signal	2.817	0.608	-7.944	13.578

The 95% confidence interval spans from –7.94 to 13.58, crossing zero, further confirming the lack of statistical significance. Although the direction of the effect is positive, the wide interval and high p-value imply a high degree of uncertainty, and the result is likely driven by noise rather than any true underlying relationship.

The left panel presents the channel-wise GLM slope distribution for gamma-band activity during MB (Fig. 5.14b). Unlike lower-frequency bands (delta or theta), the gamma map does not reveal any consistent spatial coupling pattern between gamma power and the global signal. Only a single electrode (FT7), located over the left temporal area, showed a statistically significant effect ($p < 0.05$). However, since no other neighbouring channels reflect a similar trend, this finding should be interpreted cautiously, as it may result from residual noise rather than a neural oscillation.

Correlation of ECG Amplitude and GSA

To assess the relationship between physiological activity and global signal amplitude, the same approach was applied as with EEG: an LMM was used, where the beta coefficient reflects the strength and direction of the association between ECG amplitude and the global fMRI signal.

As shown in Figure 5.15, ECG values in the dataset show a significant variance, ranging broadly from negative to positive values. This wide spread on the x-axis, which was seen on the Figure 5.7 as well, visually exaggerates the slope of the linear fit, making the relationship between ECG amplitude and GSA appear steeper than it actually is. In reality, the model indicates that an increase of 1 unit in ECG is associated with only a 0.09 unit change (increase) in the fMRI GSA.

Although the linear trend appears pronounced on the plot, this is primarily due to the large variance in ECG rather than a strong effect size. The true effect is modest but statistically reliable, as supported by the extremely low p-value and a narrow 95% confidence interval that does not include zero (Table 5.13).

Table 5.10: Modestly Positive Linear fit between ECG variation and GSA across time points during MB

Variable	Beta	*p*-value	CI Lower	CI Upper
ECG signal	0.096	8.463e-48	0.083	0.109

Even though the visual trend may suggest a strong effect, the actual magnitude of the relationship is small. Nevertheless, the result is statistically significant, indicating that ECG fluctuations contribute subtly but consistently to variations in the global signal amplitude.

5.3.5 Correlation of ECG and Global Signal during MB Reports

As well as for EEG regressors to link ECG variation and fMRI GSA, during MB reports, only data segments corresponding to MB reports were included in the analysis to ensure condition-specific interpretation.

As shown in Figure 5.16, the linear trend between ECG amplitude and GSA appears visually

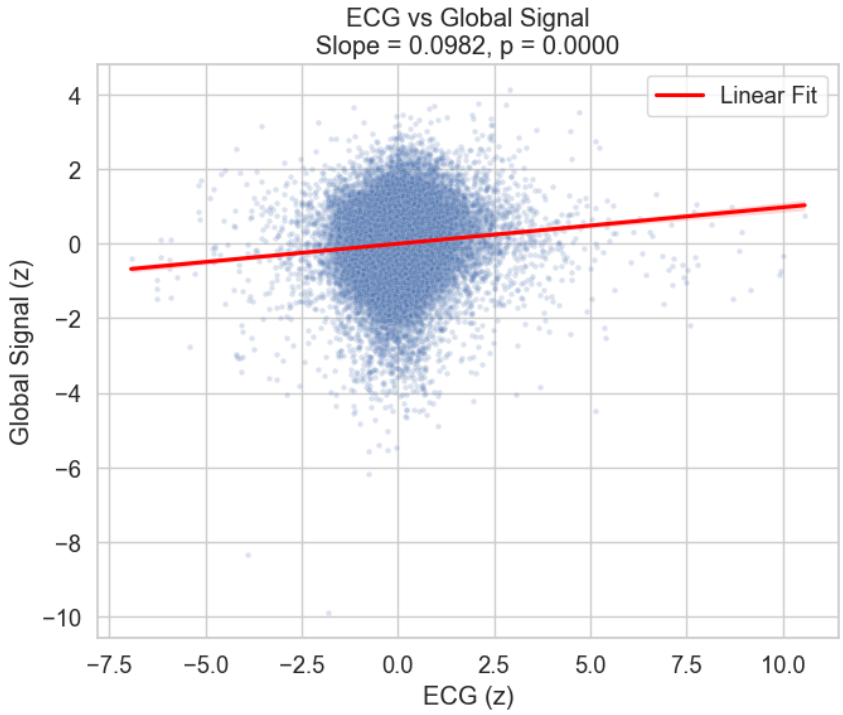

Figure 5.15: Modestly Positive Linear fit between ECG variation and GSA across time points

prominent. However, the actual slope is quite modest ($\beta = 0.094$), indicating that a 1-unit increase in ECG amplitude is associated with a 0.094-unit increase in global signal amplitude. This effect, while small in magnitude, is statistically significant, as confirmed by the very low p-value ($p = 1.18 \times 10^{-8}$).

Table 5.11: Results of the GLM for GSA and ECG signal amplitude during MB

Variable	Beta	p-value	CI Lower	CI Upper
ECG signal	0.094	1.182e-8	0.061	0.126

The 95% confidence interval (CI: 0.061–0.126) does not cross zero, also supporting the reliability of the observed effect. While the slope is relatively small, the consistent and significant relationship indicates that ECG activity still slightly contributes to global signal amplitude fluctuations during MB.

5.3.6 Correlation of EEG Oscillations Bands with GSA During MW Reports

MW episodes also exhibit general coupling with low-frequency EEG bands, particularly theta, alpha, and delta, which have been previously associated with inattentiveness and spontaneous thought. To explore this relationship, both global EEG amplitude and channel-wise GLM slopes were analyzed in relation to the global fMRI signal during MW reports.

The Figure 5.17 presents linear regression plots between the global signal amplitude and z-scored EEG power for each frequency band. Although all three regressors show slopes in either positive (theta, delta) or negative (alpha) directions, none of these associations reached statistical significance, with p-values well above 0.05 threshold. This suggests that, at the global EEG level, there is no reliable modulation of global signal amplitude during MW periods by any of the three frequency bands.

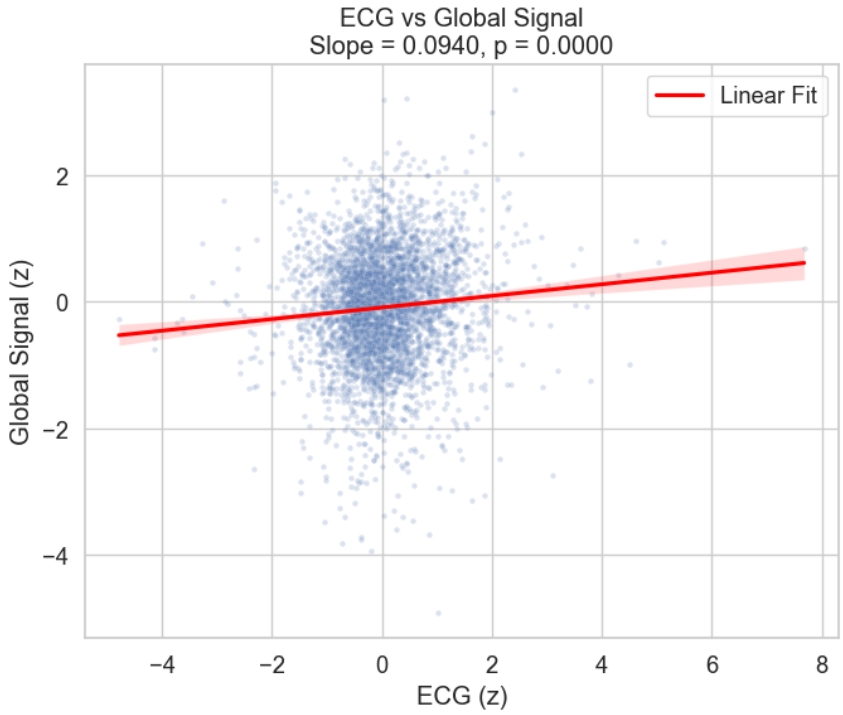

Figure 5.16: Linear model fit between ECG variation and GSA across time points during MB reports

The set of topographic maps (Fig. 5.18) shows the spatial distribution of GLM slopes across EEG channels for each frequency band. As observed, no significant spatial pattern appears in any of the maps. During spontaneous mental activity associated with MW, low-frequency EEG power does not reliably track fluctuations in the global fMRI signal — either globally or locally.

The GLM results for global EEG amplitude during MW (Table 5.12) further support the lack of significant associations between low-frequency EEG activity and global signal amplitude. For all three regressors—alpha, theta, and delta—the p-values are well above 0.05, indicating that none of the relationships are statistically reliable. The beta coefficients range from –1.89 (alpha) to +1.89 (delta), but all 95% confidence intervals include zero, suggesting a high degree of uncertainty around the estimated effects. Notably, while the slope direction varies (positive for delta and theta, negative for alpha), the magnitude remains modest. These results confirm that global EEG amplitude fluctuations in these frequency bands do not meaningfully link with GSA during MW episodes.

Table 5.12: GLM results for the association between global EEG band amplitude and global signal amplitude during MW

Variable	Beta	p-value	CI Lower	CI Upper
global alpha signal	–1.887	0.330	–5.679	1.906
global theta signal	1.737	0.347	–1.882	5.357
global delta signal	1.888	0.288	–1.592	5.368

Together, these results contrast with findings from MB condition, where delta and theta bands showed more consistent spatial and statistical coupling with the global signal. In MW, the EEG–GSA relationship appears insignificant for all EEG bands - theta, alpha and delta.

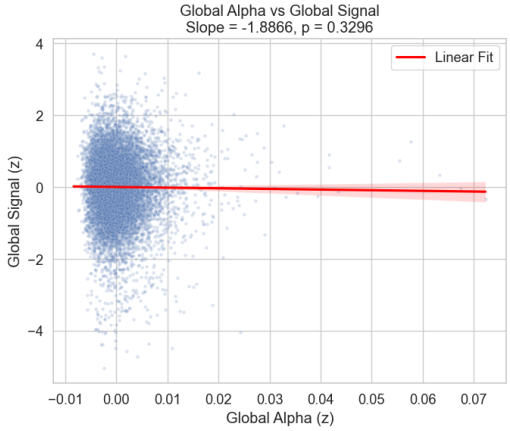

(a) Linear model fit between global alpha amplitude and GSA across time points during MW reports

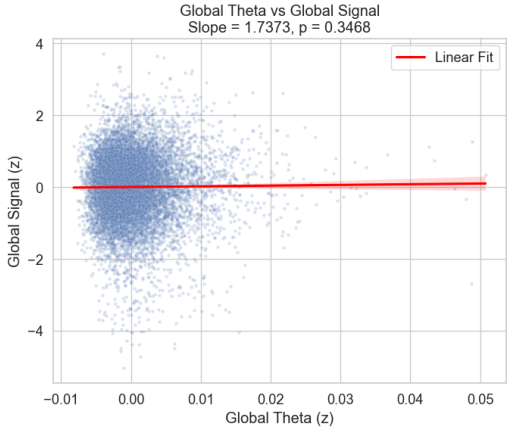

(b) Linear model fit between global theta amplitude and GSA across time points during MW reports

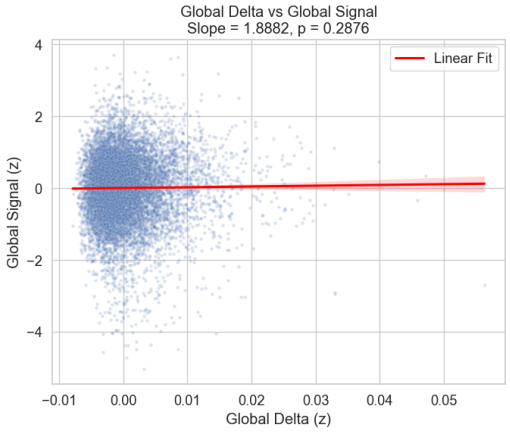

(c) Linear model fit between global delta amplitude and GSA across time points during MW reports

Figure 5.17: Linear model fit between low-frequency EEG bands' amplitude and GSA across time points during MW reports

5.3.7 Correlation of Alpha Oscillations and Global Signal During ON-TASK Reports

While MB remains the primary state of interest in this study, analysing On-Task reports provides an important contrast condition. On-Task states are characterised by sustained attention to external stimuli, and are expected to be associated with slow wave suppression in overall neuronal oscillations. By comparing this condition with internally oriented states like MB and MW, it is possible to clarify state-specific neural dynamics between EEG–fMRI coupling.

The topography reveals a posterior–anterior gradient: posterior regions (especially occipital and parieto-occipital lobes) display significant negative associations. In contrast, more frontal sites tend toward positive slopes. Channels such as O1, PO8, PO4, P6, and P3 show statistically significant negative relationships with the global signal. A significant positive relationship is observed for Fz and CP3 channel (Fig. 5.19a).

The graph on the right illustrates the linear association between GSA and mean alpha signal amplitude. The regression slope is negative (β = –0.97), but not statistically significant (p = 0.6855), indicating that global alpha activity was not reliably related to global fMRI signal amplitude fluctuations during periods of active task engagement (Fig. 5.19b).

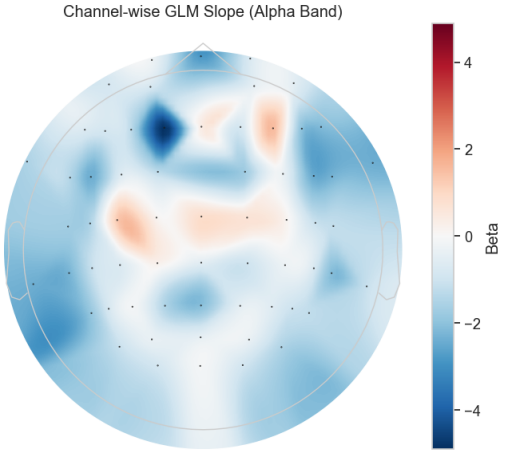

(a) Topographical distribution of GLM beta values alpha-band EEG during MW reports did not reveal any significant correlation with GSA

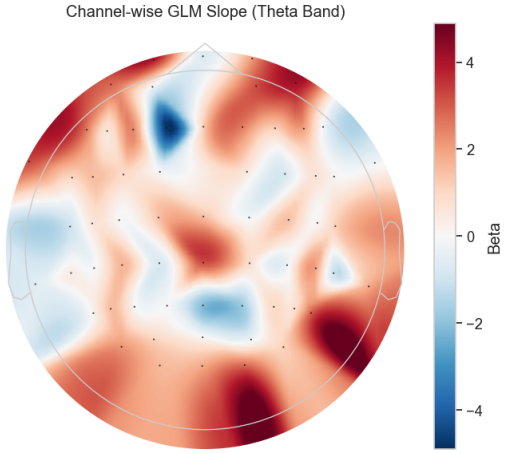

(b) Topographical distribution of GLM beta values theta-band EEG during MW reports did not reveal any significant correlation with GSA

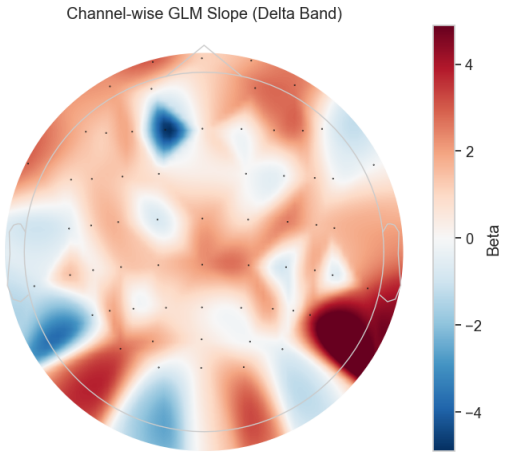

(c) Topographical distribution of GLM beta values delta-band EEG during MW reports did not reveal any significant correlation with GSA

Figure 5.18: Topographical distribution of GLM beta values for low-frequency EEG bands' regressors during MW reports

In this context, a significant negative slope in the posterior lobe, but the absence of a significant global relationship, suggests that only localised neural modulations between alpha wave amplitude and GSA can occur during the task.

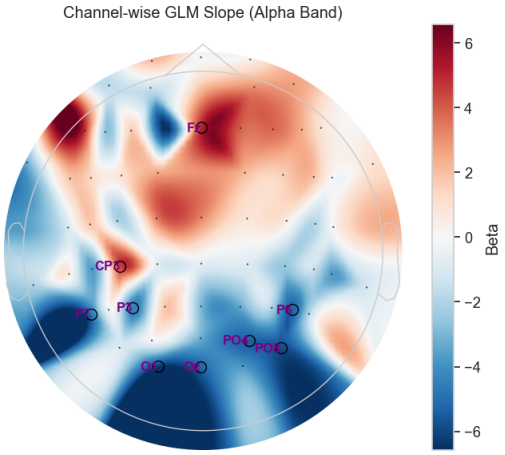

(a) GLM output indicates occipital and parieto-occipital Decrease in Alpha-Band during ONTASK reports

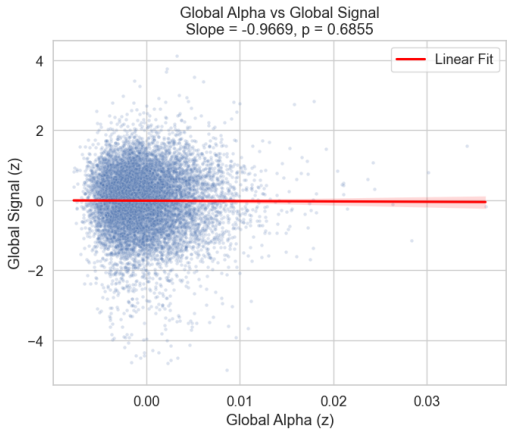

(b) Results of the GLM for GSA and mean EEG signal amplitude in the alpha band during ONTASK reports show no significant correlation

Figure 5.19: Alpha-band EEG–fMRI relationship during MB. **(a)** Beta values across EEG channels reflect channel-wise GLM slopes with the global signal. **(b)** Linear model fit between global alpha amplitude and GSA across time points during ONTASK reports

Table 5.13: Results of the GLM for GSA and global alpha signal amplitude during ONTASK reports

Variable	Beta	p-value	CI Lower	CI Upper
global alpha signal	-0.967	0.686	-5.647	3.713

Chapter 6

Discussion

The aim of this study was to investigate the underlying mechanisms of MB, with a specific focus on whether it is primarily driven by neuronal or physiological oscillations. In particular, we sought to clarify what contributes to the observed increase in GSA during MB reports, described by Mortaheb et al. (2022), by identifying which components are correlated with GSA during this mental state.

Our hypothesis was that GSA reflects a combination of neuronal and neurovascular signals, and that it is possible to disentangle their relative contributions. To address this, we analysed both neuronal and physiological components separately during periods of MB.

The key finding of our analysis revealed that the neuronal signal associated with MB, primarily characterised by delta-band activity, was negatively correlated with GSA. This suggests that during MB, GSA is suppressed in relation to slow-wave neuronal activity. In contrast, the ECG-derived signal showed a positive, even though weak, correlation with GSA.

These results support the idea that the increase in GSA previously observed during MB is not driven only by delta-band neural activity but may instead reflect physiological contributions or a dissociation between neuronal downstates and neurovascular fluctuations.

6.1 Findings according to GSA-EEG coupling results

The GS in fMRI, typically defined as the average BOLD signal across all brain voxels at each time point, has long been a topic of debate in the neuroimaging community (Liu et al., 2017). Historically, it was considered a nuisance variable, primarily reflecting noise from non-neuronal sources. However, recent findings have suggested that GS may also contain meaningful neuronal information, particularly related to vigilance and arousal (Li et al., 2019a; Liu et al., 2017).

Non-neuronal components of GS can arise from both structured and random sources. Structured sources include physiological processes such as respiration, cardiac activity, and head motion, as well as scanner-related fluctuations. These influences can introduce low-frequency oscillations and confounds into the BOLD signal, especially in rs-fMRI, because task-based analysis can better isolate task-related activity. Since GS can be related to various artifacts, GSR is frequently applied as a denoising step in both rs-fMRI and task-based fMRI preprocessing pipelines (Power et al., 2018). This is motivated by findings of high correlation between GS and respiratory patterns, and to a lesser extent, cardiac cycles (Shmueli et al., 2007).

Despite these associations with physiological noise, several studies have demonstrated that GS also captures aspects of brain state. Wong et al. (2013) showed that GSA, defined as the standard deviation of the GS, negatively correlates with EEG vigilance markers: higher arousal was associated with lower GSA. This effect was further modulated by caffeine administration,

which decreased GSA and increased alertness. Other studies have reported similar patterns, with GSA increasing during light sleep (Fukunaga et al., 2006), sleep deprivation (Yeo et al., 2015).

Recent studies have also reported correlations between GSA and specific EEG frequency bands. For example, Wong et al. demonstrated a positive relationship between delta power and GSA, while others have observed similar negative associations with alpha power during resting-state (Chang et al., 2013; Tagliazucchi et al., 2012).

Thus, GSA has become a candidate biomarker for vigilance-related neural states in rs-fMRI. However, evidence for the role of GS in task-based fMRI remains more limited. While GS in task contexts has been shown to reflect widespread spatial coherence at low frequencies, its use as a covariate is often avoided due to concerns that regressing it out may induce artificial anti-correlations, which will lead to wrong interpretation.

In the present study, we extend this work by examining how GS amplitude is coupled with the amplitude of EEG waves during an active task context. By linking GSA with concurrent EEG measures, our findings could provide insight into whether task-based GS fluctuations reflect neuronal oscillatory dynamics or physiological processes such as ECG variation. The relationship between GSA and EEG band-limited amplitude was provided across various frequencies: delta, theta, alpha, and gamma. Using a linear model (Linear Mixed-Effects Models (LMMs)), both global and channel-level correlations were assessed along reports of different mental states, allowing us to extend and support the findings from prior literature.

Delta oscillations are typically dominant during sleep but can occasionally be observed during wakefulness, particularly in states of low arousal or inattentiveness, so delta activity is usually suppressed, particularly during periods of external attentional engagement and high arousal. In the context of the current task-based experiment, delta activity did not show any significant relationship with global fMRI signal fluctuations.

Topographical mapping of the channel-wise GLM slopes revealed no significant associations between delta-band amplitude and GSA across the scalp (Fig. 5.9). Although a prominent negative slope was observed over the F1 channel, this effect is likely due to residual artifacts rather than a true neurophysiological pattern.

Similarly, the global delta signal, defined as the mean delta amplitude averaged across all EEG channels, was not significantly related to GSA (Table 5.3). Furthermore, the lack of any significant correlations, whether looking at the global delta signal as a whole or at delta activity in specific brain regions, suggests that delta oscillations did not have a consistent or meaningful role in the brain functions relevant to the task-based experiment.

One potential explanation lies in the nature of the experiment itself. As shown in Figure 5.3, subjects most frequently reported being in the ONTASK state, which typically reflects high levels of attention and engagement, and at the same time suppression of delta wave activity. Additionally, alertness ratings revealed that nearly 45% of responses indicated an "alert" state, again suggesting that participants were involved throughout most of the experiment.

In a situation that requires a lot of mental activity, strong delta brain activity, which is usually linked to sleepiness or internal thoughts, is not likely to appear. So, the fact that there is no clear link between delta oscillations and GSA might just mean that slow-wave activity is reduced when a person is focused on external tasks.

The other band which can be associated with slow-wave activity is the theta band. Theta oscillations are typically associated with meditative, drowsy, or light sleep states, but they are not predominant during the deepest stages of sleep. During task-based experiments, especially those with long durations or monotonous demands, increased theta activity may reflect reduced alertness or transitions toward drowsiness.

In the present analysis, the amplitude of the global theta signal (mean theta amplitude across all EEG channels) did not exhibit a statistically significant correlation with the GSA (Table 5.5). This suggests that, at a whole-brain level, theta power fluctuations were not strongly coupled with

changes in the global signal during the task.

However, global averaging may obscure localised effects. When examining the channel-wise GLM slope topography (Fig. 5.11), several electrodes, particularly over the frontal and fronto-temporal regions, displayed positive slopes, indicating that increases in theta amplitude at those sites tend to co-occur with increases in GSA. One notable parietal area (CPz) site also exhibited a positive slope.

Interestingly, the spatial distribution of theta-band slopes resembles that observed in the delta-band topography (Fig. 5.9), with a mix of positive and negative slopes across the scalp and similar frontal prominence. This suggests that while neither band showed robust global effects, both may have overlapping spatial patterns across the task-based experiment.

Overall, the findings imply that theta–GSA coupling is weak at the global level but may exist in region-specific patterns, particularly in areas associated with attention regulation and cognitive control. These results support previous findings related to the global alertness suppression observed during lower GSA (Wong et al., 2013).

The other band of interest was the alpha. Alpha oscillations are typically associated with relaxed wakefulness and reduced attentional demands. Prior studies have shown that higher alpha power has been linked to increased anti-correlation between DMN and dorsal attention network (DAN) during resting-state, often corresponding to a lower global signal amplitude (Chang et al., 2013; Tagliazucchi et al., 2012).

Consistent with these findings, the current analysis revealed a significant negative relationship between the global amplitude of alpha activity and the GSA, as shown in Figure 5.10b and supported by the values in the Table 5.4. This result suggests that higher GSA is associated with reduced alpha power, even in a task-based context. The presence of this effect across mental states reports aligns with resting-state observations, extending the relevance of this effect also to cognitive tasks.

At the spatial level, the channel-wise GLM results (Figure 5.10a) further support this pattern: all electrodes with statistically significant slopes ($p < 0.05$) exhibited negative beta values, primarily distributed across the frontal, parietal, temporal, and occipital lobes. This widespread distribution mirrors the global finding and suggests that the alpha–GSA coupling is not localised but broadly expressed across the scalp. These findings show an inverse relationship between GSA and alpha power.

Importantly, this observation also links task-based and resting-state paradigms. Much of the previous literature linking EEG activity to GSA has focused on the resting state. These results suggest that global signal amplitude is sensitive not just to specific EEG bands, but to the broader experimental context, like task-based experiments.

During particular on-task reports, more interesting patterns appeared. While the overall link between alpha power and GSA was not significant, specific brain areas showed both positive and negative relationships, suggesting localised changes in attention and engagement (Fig. 5.19).

In this study, higher alpha amplitude was linked to lower GSA, supporting past research of Wong et al. (2013). Theta amplitude was positively connected to GSA and was also consistent with previous findings by Wong et al. (2013) regarding the positive relationship between mean GSA and mean EEG amplitude in the theta band.

To cross-check if GSA is linked in general to more high-frequency bands, and not only to alpha, it was correlated with gamma waves, which are often associated with cognitive processes such as sustained attention, conscious awareness, and active information processing. Given this functional role, elevated gamma activity is typically expected during task-based paradigms that demand mental focus and engagement.

In our dataset, however, global gamma amplitude (averaged across all EEG channels) did not show a significant linear relationship with GSA, as shown in Table 5.6. The resulting slope

($\beta = -0.61$, $p = 0.7457$) was small and non-significant, suggesting a lack of global coupling between gamma oscillations and fMRI global signal fluctuations during task periods. Additionally, the dense cluster of points around the lower amplitude values reflects a generally weak gamma signal, consistent with earlier violin plots (Fig. 5.6c).

Despite the null result at the global level, spatial patterns in the channel-wise GLM beta values (Fig. 5.12) offer additional insights. Several regions, particularly within the frontal and temporal lobes, exhibit positive slopes, whereas negative associations cluster more around central and parietal areas. These regional variations suggest that the relationship between gamma power and GSA may be more localised and not adequately captured by global averaging.

Notably, channels such as F7, CP3, C4, and CP2 show more pronounced and potentially reliable slopes. In comparison, some of the observed topographical variation might reflect residual muscle-related artifacts (especially in high-frequency bands like gamma), which were not cleaned due to the overlap with neuronal activity. In sum, although the gamma band does not appear to contribute substantially to GSA on a global scale, localised channel-level associations suggest that gamma activity may modulate the global signal in specific brain regions.

During isolated MW reports, there were no clear links between GSA and EEG amplitudes, either overall (Fig. 5.17) or in specific brain regions (Fig. 5.18), across any EEG frequency bands. This might be because MW is varied and includes different thoughts and attention shifts, which may involve different brain processes.

Globally, only alpha oscillations show a significant inverse relationship, whereas on the channel level, theta and gamma waves are linked to specific scalp areas. This occurs because global EEG amplitude averages signals across all channels, smoothing out local differences. When some channels exhibit positive correlation and others negative or none, the overall effect can cancel out.

In contrast, alpha activity tends to be more spatially coherent, particularly across occipital and parietal regions. Therefore, a strong effect in one direction can persist even after global averaging, explaining the observed significant negative global correlation for alpha.

In the case of theta, a mostly positive relationship is seen in the frontal and fronto-temporal lobes. A localised relationship between GSA and theta amplitude here may reflect changes in vigilance, especially during long tasks. It is possible to clarify that theta-band oscillations, which are mainly linked to drowsiness, attentional disengagement, or internal mental states, are reflected in fMRI signal fluctuations.

The absence of a correlation between delta oscillations and GSA across the experiment can be interpreted in a similar way as for gamma oscillations. Although residual artifacts, such as slow eye blinks, may overlap with neuronal activity, their impact should be minimal due to the standard EEG preprocessing pipeline. Therefore, the observed lack of association is more likely related to the relatively low prominence of delta waves during the active experimental task, rather than being driven by unremoved physiological noise.

In addition to neuronal fluctuations, physiological processes also contributed to variations in GSA. In this study, ECG variability was used as a marker of physiological activity. As previously discussed, ECG is sensitive to changes in mental states and is frequently employed to assess physiological responses to cognitive demands or external stimuli. The correlation analysis revealed a small but positive association between ECG variation and GSA (Table 5.13), with a relatively wide confidence interval. This finding is consistent with the work of Shmueli et al. (2007), who demonstrated that GS contains a substantial physiological component. The modest correlation magnitude observed here may be partly explained by the larger variance in ECG values (ranging from approximately 7.5 to 10, see Fig. 5.15) compared to GSA (ranging from approximately –10 to 4). In such cases, even a small regression slope (0.0982) can reflect meaningful changes in GSA, given the broader dynamic range of ECG fluctuations.

The channel-specific coupling with GSA indicates localised neuronal interactions. This supports the hypothesis that the global signal is not just noise but can carry regionally specific neuronal information, particularly in task-related contexts. These results also show that the GS in fMRI is

influenced by multiple factors, including physical components and brain activity that depends on mental state and alertness.

6.2 Investigations According to MB

MB is linked to slow-wave EEG activity, particularly theta and delta waves (Andrillon et al., 2021), which are associated with drowsiness, attentional lapses, and low vigilance. In the study by Mortaheb et al. (2022), an increase in GSA was observed during MB reports. However, based on the Background chapter 2, it remains unclear whether this GS increase reflects physiological or neuronal processes, as the origins of GS are still debated.

To address this question, we used the relationship between EEG band-specific amplitude and ECG variation with GSA as a window into the underlying mechanisms of MB. By focusing on how delta, theta, and gamma activity relate to GSA specifically during MB reports, we aim to clarify which components contribute to the GSA changes observed during these episodes.

We investigated the role of gamma oscillations in MB reports. Unlike delta and theta oscillations, which have shown a positive relationship with MB, gamma activity is linked to different neuronal functions. Therefore, we expected to observe a relationship between gamma and GSA that is opposite to the relationship between low-frequency bands. Together, these analyses will help clarify the underlying mechanisms contributing to MB.

Our results show a consistent pattern for delta activity. As shown in Figure 5.13, delta band amplitude exhibits a negative relationship with GSA during MB reports both globally and at the channel level. Nearly all electrodes across the scalp show negative GLM slopes, with no evidence of positive associations. This widespread pattern results in a significant negative correlation at the global level (Table 5.7).

This finding is particularly interesting since MB has been previously linked to increased delta power Andrillon et al. (2021), and at the same time with the higher GSA reports Mortaheb et al. (2022). However, the opposite pattern occurs in the current data: greater GSA is associated with reduced delta amplitude. Since MB is linked to increased delta and theta activity and higher GSA, this negative delta–GSA link may suggest that the suppression of GSA can be expected during MB reports, which contradicts the previous findings.

One possible explanation lies in the nature of GSA itself. While delta activity is a well-established marker of neuronal disengagement and reduced cognitive processing, GSA is a more complex signal, integrating both neuronal and physiological components. The inverse delta–GSA relationship during MB might therefore indicate that GSA increases during MB are not primarily driven by slow-wave neural activity but reflect non-neuronal physiological contributions. Moreover, the findings of Mortaheb et al. (2022) were obtained in a resting-state context, whereas the present results come from a task-based fMRI paradigm. This distinction is important because task demands can modulate both neuronal and physiological contributions to GSA. In a task-based setting, fluctuations in attention and cognitive engagement are more dynamic, and levels of alertness tend to remain relatively high. Indeed, in the current dataset, most reports were accompanied by self-reports of being "alert" (see Table 5.2). This higher baseline alertness may attenuate the slow-wave neural activity typically linked to MB during rest, thereby altering the GSA–EEG relationship.

Furthermore, this result contrasts with the resting-state findings of Wong et al. (2013), who reported a positive correlation between delta power and GSA. This divergence may come from differences in the experimental context as well. While Wong et al. (2013) analysed spontaneous resting-state activity, the current study examines MB periods within an active task, potentially altering delta activity's functional role. These observations support the idea that the nature and drivers of GSA are context-dependent, varying according to whether the brain is in a resting state or engaged in an active cognitive task.

For theta-band activity, the results present a more complex picture. While no significant

global-level correlation with GSA was found during MB, channel-wise analysis reveals localised negative associations, particularly over the left and right temporal regions (Fig. 5.14a). These patterns support those observed for delta wave oscillations during MB, suggesting that local theta suppression may also co-occur with increased GSA during MB.

This finding notably contrasts theta–GSA relationships observed during the entire experiment period, where positive correlations were identified, especially in frontal and fronto-temporal areas (Fig. 5.11). This divergence may indicate that the relationship between GSA and theta activity is state-dependent, shifting based on whether the brain is engaged in task processing (ONTASK) or a passive state (MB). A similar state-dependent pattern emerges for delta oscillations. Here, delta power was significantly negatively correlated with GSA, indicating that higher GSA values during the experiment were associated with lower delta activity. This pattern is consistent suggests that slow-wave activity contributed less to GSA under these experimental conditions. These findings highlight the specific relationship between GSA and EEG amplitude. GSA may reflect differences depending on mental state. The same analysis was also performed using a shorter time window of 23.4 seconds (11.7 seconds before and after MB onset), following the approach described by Mortaheb et al. (2022). The results of this complementary analysis are presented in Appendix A (Fig. A.1a, A.1b). While the shorter window reproduced the same negative trend observed in the topographical maps and at the global level, the effects did not reach statistical significance. This lack of significance can be largely attributed to the lower variance of the EEG signal in this reduced time window, as shown in Figure 5.5, which reduced the statistical power of the analysis.

To explore whether GSA might also be linked to faster neural oscillations during MB, we examined gamma-band amplitude. However, both the global and channel-wise analyses failed to reveal any robust associations (Fig. 5.14b). Although some channels show positive slopes, the overall p-values are high, making these connections unreliable.

The gamma-band results during MB should be viewed carefully because of the lack of strong findings and the chance of residual artifacts. Currently, there is no solid evidence to connect GSA and gamma activity during MB reports.

To examine whether the observed increase in GSA during MB reports could be attributed to physiological components, the general relationship between GSA and ECG variability across the entire experiment was first investigated. As shown in Figure 5.15, although the slope of the regression line is relatively small ($\beta = 0.098$), the associated p-value is highly significant ($p < 0.00001$), indicating a reliable positive relationship between GSA and ECG variation (Table 5.13). As discussed for ECG-GSA correlation within the whole experiment, the modest correlation can be explained due to the high variance of ECG regressors, which will reflect meaningful changes in GSA.

This analysis was then explicitly repeated for the time points corresponding to MB reports (Fig. 5.16). The results showed a very similar slope ($\beta = 0.094$), again with a highly significant p-value, confirming the consistency of this effect (Table 5.11).

The close match between the slope values in the whole dataset and the MB-specific subset suggests that the relationship between ECG and GSA remains stable regardless of the reported mental state. The similarity between slope values in the whole dataset and the MB-specific subset suggests that ECG–GSA coupling is present during MB episodes, but it may also occur in other states. To further examine this relationship, an additional analysis was performed using a shorter time window of 23.4 seconds (11.7 seconds before and after MB onset), following the approach of Mortaheb et al. (2022). This complementary analysis, presented in Appendix A (Fig. A.2), revealed even more pronounced physiological contributions to GSA during MB. The shorter window reduced the variance of the ECG data compared to the longer 60-second window, thereby amplifying the observed coupling. These findings strengthen the interpretation that increases in GSA during MB are largely driven by physiological processes, particularly ECG-related fluctuations, and that the magnitude of this effect can be sensitive to the temporal scale of analysis.

While previous studies suggested that GSA increases during MB, it was shown that this rise reflected was significantly due to physiological contributions. Our results suggest that the elevated

GSA observed during MB may be primarily driven by physiological components, as evidenced by the negative coupling between delta-band amplitude and GSA, and the lack of strong positive neuronal associations for theta and negative associations with gamma bands. This suggests that while MB is associated with increased low-frequency neuronal activity, these oscillations may actively suppress global BOLD fluctuations, rather than drive them. In contrast, physiological signals such as ECG may contribute modestly to GSA increases, indicating that the global signal during MB reflects a composite of neuronal disengagement and background physiological dynamics.

Our findings suggest that the MB state is shaped not only by slow-wave neural activity but also by physiological processes. In the recent work of Andrillon et al. (2024), the authors questioned what MB truly reflects, and in this work, it was highlighted that physiological factors may contribute to its occurrence. MB could represent a state characterized by disengagement from mental content and a loss of effective communication between neural assemblies. This aligns with observation seen in this study that MB is associated with strong suppression of delta oscillations, alongside a positive relationship between GSA and ECG measures. Such coupling between GSA and physiological signals supports the idea that part of the GSA increase during MB originates from non-neuronal sources. Furthermore, as reported by Andrillon et al. (2024), MB cannot be reliably induced voluntarily — deliberate attempts to "empty the mind" tend to introduce distinct neural activation patterns rather than spontaneous MB. This supports the interpretation that the link between ECG and GSA during MB may reflect reduced neural integration and diminished mental content, and can be seen also as signature of spontaneous MB.

6.3 Limitations

Several limitations should be acknowledged in this study. First, our approach to measuring specific EEG band activity differed from methods used in previous studies such as Andrillon et al. (2021) and Scheeringa et al. (2012). While those studies often extracted individual slow waves, either by identifying negative peaks in the filtered signal or by isolating relevant components through ICA, our method involved applying a bandpass filter to retain the full signal within the frequency range of interest. This choice was made to preserve as much neuronal information as possible, but it may also have allowed residual non-neuronal activity (physiological noise) to remain in the data.

Second, our analysis focused only on the amplitude of the filtered EEG signal. Other important features of slow waves, such as density, downward slope, and upward slope, were not computed. As a result, our findings do not cover all the properties linked with GSA. However, this decision was aligned with the specific aim of the study, which focused on understanding the relationship between GSA and EEG amplitude as two amplitude-based measures. Also, the time window used to define the EEG segment preceding each probe response was set to one minute, compared to a 20-second window in previous work. We aimed to increase the likelihood of capturing the reported mental state within the selected period, particularly for states like MB that may fluctuate over time. However, a longer window may also introduce variability. To address this, we repeated the same analysis using a shorter time window of 23.4 seconds, consistent with previous studies. The outcomes of this control analysis are reported in the Appendix. Results showed that ECG variation remained positively associated with GSA, supporting earlier findings linked to longer MB episodes. Delta-band amplitude also exhibited a negative trend with GSA both globally and at the channel level, though these effects did not reach statistical significance.

Third, the GLM used in this analysis included random intercepts to account for variability in baseline GSA levels across participants. However, the model assumed fixed slopes, meaning the relationship between EEG amplitudes and GSA was treated as consistent across all subjects. While this captures individual differences in overall signal levels, it does not model potential variability in how strongly EEG features relate to GSA across participants. This simplification may limit sensitivity to subject-specific neural dynamics.

Finally, our findings are correlational and do not establish causality between neuronal activity and GSA. Based on our analysis, we cannot infer the presence of neuronal components in specific

mental states; we can only confirm whether a coupling effect exists between correlated metrics. Furthermore, the interpretation of increased GSA during MB was constrained by the fact that this study examined only a task-based experiment, without a resting-state condition.

Chapter 7

Conclusion

Spontaneous mental states, such as mind-wandering and mind-blanking (MB), have been associated with specific neural patterns—most notably, increased slow-wave activity in the delta and theta bands. Previous work of Wong et al. (2013) demonstrated that GSA in resting-state fMRI positively correlates with low-frequency EEG activity, raising the possibility that GSA may reflect underlying slow-wave neural processes. Additionally, Mortaheb et al. (2022) found that MB reports are accompanied by increased GSA. However, the global signal remains a debated measure, as it may contain both neuronal and non-neuronal (e.g., physiological or instrumental) sources. This raises an important question: Is the observed increase in GSA during MB truly driven by neuronal slow-wave activity?

To investigate this, we analyzed multimodal data from EEG, fMRI, and ECG recordings. We extracted key signal features, including GSA from fMRI, heart rate variability from ECG, and amplitude of EEG bands (delta, theta, alpha, gamma). Linear mixed-effects models were applied to examine relationships between these physiological and neural signals, especially during MB, MW, and On-Task reports.

Our results showed that, contrary to expectations, GSA during MB was significantly negatively correlated with delta and theta amplitude, and positively associated with ECG variability. Across the full dataset (independent of mental state), GSA correlated positively with theta and negatively with alpha. These findings suggest that while MB is associated with slow-wave EEG activity, the concurrent increase in GSA may not directly reflect these neuronal patterns. Instead, the global signal likely reflects a more complex mixture of physiological and neural components, with cardiovascular contributions (as measured by ECG) playing a notable role during MB.

These findings suggest that the rise in global signal amplitude during MB may not be directly explained by increases in slow-wave neural activity, as previously assumed. Instead, the observed positive relationship between GSA and ECG variability during MB points to a possible physiological contribution. While global relationships across the full dataset show consistent neural patterns, such as a positive link between GSA and theta and a negative link with alpha, the specific pattern during MB highlights that physiological signals may also play a role. This implies that MB might not be purely a neuronal phenomenon, but rather one that also involves changes in physiological states, underscoring the complex, multi-source nature of the global signal.

For future work, additional features of the EEG signal beyond amplitude, such as phase or shape of the slow-wave, could be explored to better understand their relationship with GSA. In this study, ECG was the only physiological measure considered, but other signals like muscle activity (EMG) and respiration may also contribute to GSA changes, particularly during MB episodes. Furthermore, it would be valuable to investigate the characteristics of MB across different experimental conditions, as variations in task structure may influence the neural and physiological profiles associated with this mental state. Especially, during rs-fMRI, since the possible divergence in the expected results could be driven by different experimental settings and active cognitive engagement.

AI usage acknowledgment

The writing of this thesis used AI tools, mainly for grammar correction and rephrasing, with the aim of ensuring lexical accuracy in the specified terminology and context. Specifically, Grammarly and ChatGPT were used for this purpose. ChatGPT was also used for debugging and resolving errors during code development.

Appendix A

Supplementary results

To assess the robustness of our results, we addressed a key concern related to the length of the analysis time window. In the main analysis, we used an extended window (1 minute) equal to the whole Go/NoGo block, which could potentially introduce variability and deviate from prior studies. To evaluate this, we repeated the GLM analysis using a shorter window of 23.4 seconds (11.7 seconds before and after the MB onset), as described in the article of Mortaheb et al. (2022). The same regressors and GLM specification were used, allowing a direct comparison between the two approaches.

The results are shown in Figures A.1a–A.2. Figure A.1a displays the spatial distribution of the GLM beta values across EEG channels, reflecting the relationship between delta-band amplitude and GSA during MB reports. Although the overall trend suggests a decrease in delta amplitude, particularly over frontal, central, and occipital areas, these effects were not statistically significant. This is further supported by the linear model fit shown in Figure A.1b, where the observed negative trend between delta amplitude and GSA did not reach significance due to a high resulting p-value.

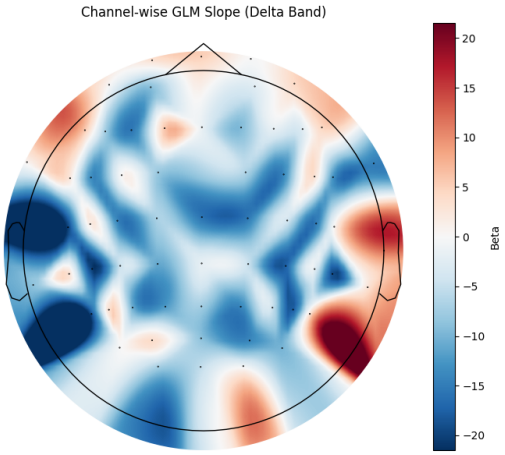

(a) GLM output indicates not significant frontal, occipital and central Decrease in Delta-Band during MB reports with alternative time-window (23.4 sec)

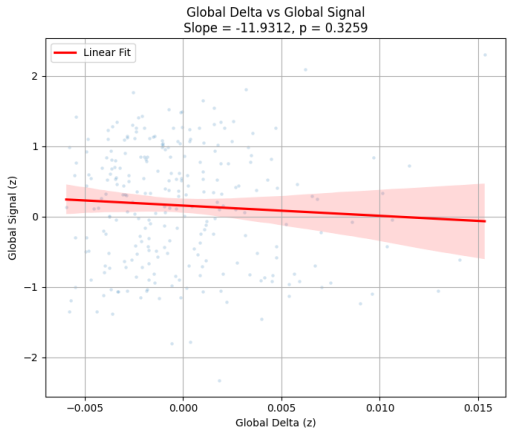

(b) Results of the GLM for GSA and mean EEG signal amplitude in the delta band during MB reports with the 23.4 sec time window show a negative trend, which is not considered a significant correlation due to its resulting big p-value

Figure A.1: Delta-band EEG–fMRI relationship during MB with different time windows (23.4 sec). **(a)** Beta values across EEG channels reflect channel-wise GLM slopes with the global signal. **(b)** Linear model fit between global alpha amplitude and GSA across time points during ONTASK reports

In contrast, ECG variation continued to show a positive correlation with GSA during this

shorter window, as illustrated in Figure A.2. This effect was even more pronounced compared to the longer time window, reinforcing previous findings and highlighting the importance of accounting for physiological confounds such as ECG in MB mechanisms.

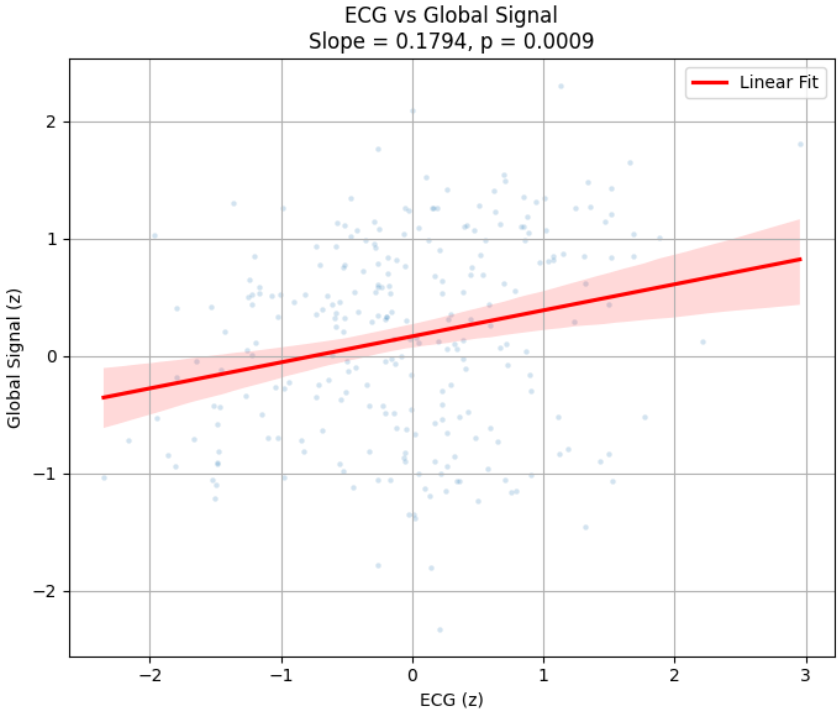

Figure A.2: Linear model fit between ECG variation and GSA across time points during an alternative time window of MB reports revealed a stronger positive correlation between ECG variation and GSA compared to a longer time window, confirming the confounds about ECG correlation with GSA

Glossary

cerebral blood flow (CBF) The blood supply to the brain in a given period of time. 18

cerebral blood volume (CBV) The total volume of blood in the cerebral vasculature at a given time. 18

cerebral metabolic rate of oxygen ($CMRO_2$) The rate at which oxygen is consumed by the brain. 18

Generalized Linear Models (GLM) is an extension of traditional linear regression, which enables the relationship between the linear predictor and the response variable to be defined through a link function. Additionally, it allows the variance of each measurement to depend on its predicted value, providing greater flexibility. 40

global signal (GS) A time series of signal intensity averaged across all brain voxels, reflecting a combination of neural and physiological sources, often treated as a nuisance variable but increasingly recognised for its potential functional relevance. 13

global signal amplitude (GSA) The standard deviation or variability of the global signal over time, used as a measure of its magnitude. 12

heart rate variability (HRV) A measure of the variation in time intervals between consecutive heartbeats, reflecting autonomic nervous system activity and often used as an indicator of physiological arousal and stress levels. 37

Hilbert transform An operation that enables making an analytic signal based on some original real-valued signal, therefore we can express it in exponential notation and get rid of identical positive and negative values. 39

Linear Mixed-Effects Models (LMMs) A statistical model containing both fixed effects and random effects. A linear mixed-effects model extends GLM by adding random effects to account for variation across groups. 40, 41, 69

mind-blanking (MB) A spontaneous cognitive state characterised by a temporary absence of reportable mental content, in which individuals experience the mind as "going blank," often associated with reduced cortical arousal and altered brain connectivity patterns. 12

mind-wandering (MW) A form of spontaneous thought in which attention drifts away from the external environment toward self-generated mental activity, typically involving internally oriented and unconstrained thinking. 12

slow waves Low-frequency brain oscillations observed in EEG, associated with deep NREM sleep and states of reduced cortical arousal, and characterized by synchronized neuronal activity. 12

Bibliography

Philip J. Allen, Oliver Josephs, and Robert Turner. A Method for Removing Imaging Artifact from Continuous EEG Recorded during Functional MRI. *NeuroImage*, 12(2):230–239, August 2000. ISSN 1053-8119. doi: 10.1006/nimg.2000.0599. URL https://www.sciencedirect.com/science/article/pii/S1053811900905998.

N. C. Andreasen, D. S. O'Leary, T. Cizadlo, S. Arndt, K. Rezai, G. L. Watkins, L. L. Ponto, and R. D. Hichwa. Remembering the past: two facets of episodic memory explored with positron emission tomography. *The American Journal of Psychiatry*, 152(11):1576–1585, November 1995. ISSN 0002-953X. doi: 10.1176/ajp.152.11.1576.

Thomas Andrillon, Andreas Trier Poulsen, Lars Kai Hansen, Damien Léger, and Sid Kouider. Neural Markers of Responsiveness to the Environment in Human Sleep. *The Journal of Neuroscience*, 36(24):6583–6596, June 2016. ISSN 0270-6474. doi: 10.1523/JNEUROSCI.0902-16.2016. URL https://www.ncbi.nlm.nih.gov/pmc/articles/PMC6601917/.

Thomas Andrillon, Jennifer Windt, Tim Silk, Sean P. A. Drummond, Mark A. Bellgrove, and Naotsugu Tsuchiya. Does the Mind Wander When the Brain Takes a Break? Local Sleep in Wakefulness, Attentional Lapses and Mind-Wandering. *Frontiers in Neuroscience*, 13:949, September 2019. doi: 10.3389/fnins.2019.00949. URL https://pmc.ncbi.nlm.nih.gov/articles/PMC6753166/.

Thomas Andrillon, Angus Burns, Teigane Mackay, Jennifer Windt, and Naotsugu Tsuchiya. Predicting lapses of attention with sleep-like slow waves. *Nature Communications*, 12(1):3657, June 2021. ISSN 2041-1723. doi: 10.1038/s41467-021-23890-7. URL https://www.nature.com/articles/s41467-021-23890-7. Publisher: Nature Publishing Group.

Thomas Andrillon, Antoine Lutz, Jennifer Windt, and Athena Demertzi. Where is my Mind?: A Neurocognitive Investigation of Mind Blanking, October 2024. URL https://osf.io/xmtga.

David Attwell, Alastair M. Buchan, Serge Charpak, Martin Lauritzen, Brian A. MacVicar, and Eric A. Newman. Glial and neuronal control of brain blood flow. *Nature*, 468(7321):232–243, November 2010. ISSN 1476-4687. doi: 10.1038/nature09613. URL https://doi.org/10.1038/nature09613.

J. R. Binder, J. A. Frost, T. A. Hammeke, P. S. Bellgowan, S. M. Rao, and R. W. Cox. Conceptual processing during the conscious resting state. A functional MRI study. *Journal of Cognitive Neuroscience*, 11(1):80–95, January 1999. ISSN 0898-929X. doi: 10.1162/089892999563265.

Taylor Bolt, Shiyu Wang, Jason S. Nomi, Roni Setton, Benjamin P. Gold, Blaise deB. Frederick, B.T. Thomas Yeo, J. Jean Chen, Dante Picchioni, R. Nathan Spreng, Shella D. Keilholz, Lucina Q. Uddin, and Catie Chang. Widespread Autonomic Physiological Coupling Across the Brain-Body Axis. *bioRxiv*, page 2023.01.19.524818, July 2024. ISSN 2692-8205. doi: 10.1101/2023.01.19.524818. URL https://www.ncbi.nlm.nih.gov/pmc/articles/PMC11312447/.

Paradeisios Alexandros Boulakis and Athena Demertzi. Relating mind-blanking to the content and dynamics of spontaneous thinking. *Current Opinion in Behavioral Sciences*, 61:101481, February 2025. ISSN 23521546. doi: 10.1016/j.cobeha.2024.101481. URL https://linkinghub.elsevier.com/retrieve/pii/S2352154624001323.

Paradeisios Alexandros Boulakis, Sepehr Mortaheb, Laurens Van Calster, Steve Majerus, and Athena Demertzi. Whole-Brain Deactivations Precede Uninduced Mind-Blanking Reports. *The Journal of Neuroscience*, 43(40):6807–6815, October 2023. ISSN 0270-6474, 1529-2401. doi: 10.1523/JNEUROSCI.0696-23.2023. URL https://www.jneurosci.org/lookup/doi/10.1523/JNEUROSCI.0696-23.2023.

Felicity Callard, Jonathan Smallwood, Julian Golchert, and Daniel S. Margulies. The era of the wandering mind? twenty-first century research on self-generated mental activity. *Frontiers in Psychology*, 4:891, 2013. doi: 10.3389/fpsyg.2013.00891. URL https://doi.org/10.3389/fpsyg.2013.00891.

Mary A. Carskadon and William C. Dement. Normal Human Sleep: An Overview. In *Principles and Practice of Sleep Medicine*, pages 13–23. Elsevier, 2005. ISBN 978-0-7216-0797-9. doi: 10.1016/B0-72-160797-7/50009-4. URL https://linkinghub.elsevier.com/retrieve/pii/B0721607977500094.

Catie Chang, Zhongming Liu, Michael C. Chen, Xiao Liu, and Jeff H. Duyn. EEG correlates of time-varying BOLD functional connectivity. *NeuroImage*, 72:227–236, May 2013. ISSN 1053-8119. doi: 10.1016/j.neuroimage.2013.01.049. URL https://www.sciencedirect.com/science/article/pii/S1053811913000967.

Muhammad E. H. Chowdhury, Amith Khandakar, Karen J. Mullinger, Nasser Al-Emadi, and Richard Bowtell. Simultaneous EEG-fMRI: Evaluating the Effect of the EEG Cap-Cabling Configuration on the Gradient Artifact. *Frontiers in Neuroscience*, 13, July 2019. ISSN 1662-453X. doi: 10.3389/fnins.2019.00690. URL https://www.frontiersin.org/journals/neuroscience/articles/10.3389/fnins.2019.00690/full. Publisher: Frontiers.

Kalina Christoff, Zachary C. Irving, Kieran C. R. Fox, R. Nathan Spreng, and Jessica R. Andrews-Hanna. Mind-wandering as spontaneous thought: a dynamic framework. *Nature Reviews Neuroscience*, 17(11):718–731, 2016. ISSN 1471-0048. doi: 10.1038/nrn.2016.113. URL https://www.nature.com/articles/nrn.2016.113.

R. J. Croft and R. J. Barry. Removal of ocular artifact from the EEG: a review. *Neurophysiologie Clinique/Clinical Neurophysiology*, 30(1):5–19, February 2000. ISSN 0987-7053. doi: 10.1016/S0987-7053(00)00055-1. URL https://www.sciencedirect.com/science/article/pii/S0987705300000551.

Fernando Lopes da Silva. EEG: Origin and Measurement. In Christoph Mulert and Louis Lemieux, editors, *EEG - fMRI: Physiological Basis, Technique, and Applications*, pages 23–48. Springer International Publishing, Cham, 2022. ISBN 978-3-031-07121-8. doi: 10.1007/978-3-031-07121-8_2. URL https://doi.org/10.1007/978-3-031-07121-8_2.

Oscar Esteban, Christopher J. Markiewicz, Ross W. Blair, Craig A. Moodie, A. Ilkay Isik, Asier Erramuzpe, James D. Kent, Mathias Goncalves, Elizabeth DuPre, Madeleine Snyder, Hiroyuki Oya, Satrajit S. Ghosh, Jessey Wright, Joke Durnez, Russell A. Poldrack, and Krzysztof J. Gorgolewski. fMRIPrep: a robust preprocessing pipeline for functional MRI. *Nature Methods*, 16(1):111–116, January 2019. ISSN 1548-7105. doi: 10.1038/s41592-018-0235-4. URL https://www.nature.com/articles/s41592-018-0235-4. Publisher: Nature Publishing Group.

Federico Raimondo. EEG cleaner. https://github.com/fraimondo/eeg_cleaner, 2025.

fMRIPrep Community. Processing pipeline details for fmriprep. https://fmriprep.org/en/stable/workflows.html.

David Foulkes and Stephan Fleisher. Mental activity in relaxed wakefulness. *Journal of Abnormal Psychology*, 84(1):66–75, February 1975. ISSN 1939-1846, 0021-843X. doi: 10.1037/h0076164. URL https://doi.apa.org/doi/10.1037/h0076164.

Michael D. Fox, Dongyang Zhang, Abraham Z. Snyder, and Marcus E. Raichle. The Global Signal and Observed Anticorrelated Resting State Brain Networks. *Journal of Neurophysiology*, 101(6):3270–3283, June 2009. ISSN 0022-3077. doi: 10.1152/jn.90777.2008. URL https://www.ncbi.nlm.nih.gov/pmc/articles/PMC2694109/.

Masaki Fukunaga, Silvina G. Horovitz, Peter van Gelderen, Jacco A. de Zwart, J. Martijn Jansma, Vasiliki N. Ikonomidou, Renxin Chu, Roel H. R. Deckers, David A. Leopold, and Jeff H. Duyn. Large-amplitude, spatially correlated fluctuations in BOLD fMRI signals during extended rest and early sleep stages. *Magnetic Resonance Imaging*, 24(8):979–992, October 2006. ISSN 0730-725X. doi: 10.1016/j.mri.2006.04.018.

Nancy Gullett, Zuzanna Zajkowska, Annabel Walsh, Ross Harper, and Valeria Mondelli. Heart rate variability (HRV) as a way to understand associations between the autonomic nervous system (ANS) and affective states: A critical review of the literature. *International Journal of Psychophysiology*, 192:35–42, October 2023. ISSN 0167-8760. doi: 10.1016/j.ijpsycho.2023.08.001. URL https://www.sciencedirect.com/science/article/pii/S0167876023004853.

Scott A. Huettel, Allen W. Song, and Gregory McCarthy. *Functional magnetic resonance imaging*. Sinauer Associates, Sunderland, Mass, 2004. ISBN 978-0-87893-288-7 978-0-87893-289-4.

Xiao Jiang, Gui-Bin Bian, and Zean Tian. Removal of Artifacts from EEG Signals: A Review. *Sensors (Basel, Switzerland)*, 19(5):987, February 2019. ISSN 1424-8220. doi: 10.3390/s19050987. URL https://www.ncbi.nlm.nih.gov/pmc/articles/PMC6427454/.

João Jorge, Wietske van der Zwaag, and Patrícia Figueiredo. EEG–fMRI integration for the study of human brain function. *NeuroImage*, 102:24–34, November 2014. ISSN 1053-8119. doi: 10.1016/j.neuroimage.2013.05.114. URL https://www.sciencedirect.com/science/article/pii/S1053811913006174.

Toshikazu Kawagoe, Keiichi Onoda, and Shuhei Yamaguchi. Different pre-scanning instructions induce distinct psychological and resting brain states during functional magnetic resonance imaging. *European Journal of Neuroscience*, 47(1):77–82, January 2018. ISSN 0953-816X, 1460-9568. doi: 10.1111/ejn.13787. URL https://onlinelibrary.wiley.com/doi/10.1111/ejn.13787.

Toshikazu Kawagoe, Keiichi Onoda, and Shuhei Yamaguchi. The neural correlates of "mind blanking": When the mind goes away. *Human Brain Mapping*, 40(17):4934–4940, August 2019. ISSN 1065-9471. doi: 10.1002/hbm.24748. URL https://www.ncbi.nlm.nih.gov/pmc/articles/PMC6865483/.

Jingwei Li, Taylor Bolt, Danilo Bzdok, Jason S. Nomi, B. T. Thomas Yeo, R. Nathan Spreng, and Lucina Q. Uddin. Topography and behavioral relevance of the global signal in the human brain. *Scientific Reports*, 9(1):14286, October 2019a. ISSN 2045-2322. doi: 10.1038/s41598-019-50750-8. URL https://www.nature.com/articles/s41598-019-50750-8. Publisher: Nature Publishing Group.

Jingwei Li, Ru Kong, Raphaël Liégeois, Csaba Orban, Yanrui Tan, Nanbo Sun, Avram J. Holmes, Mert R. Sabuncu, Tian Ge, and B.T. Thomas Yeo. Global Signal Regression Strengthens Association between Resting-State Functional Connectivity and Behavior. *NeuroImage*, 196:126–141, August 2019b. ISSN 1053-8119. doi: 10.1016/j.neuroimage.2019.04.016. URL https://www.ncbi.nlm.nih.gov/pmc/articles/PMC6585462/.

Thomas T. Liu, Alican Nalci, and Maryam Falahpour. The Global Signal in fMRI: Nuisance or Information? *NeuroImage*, 150:213–229, April 2017. ISSN 1053-8119. doi: 10.1016/j.neuroimage.2017.02.036. URL https://www.ncbi.nlm.nih.gov/pmc/articles/PMC5406229/.

Erik K. St Louis, Lauren C. Frey, Jeffrey W. Britton, Lauren C. Frey, Jennifer L. Hopp, Pearce Korb, Mohamad Z. Koubeissi, William E. Lievens, Elia M. Pestana-Knight, and Erik K. St Louis. The Normal EEG. In *Electroencephalography (EEG): An Introductory Text and Atlas of Normal and Abnormal Findings in Adults, Children, and Infants [Internet]*. American Epilepsy Society, 2016. URL https://www.ncbi.nlm.nih.gov/books/NBK390343/.

Cornelia McCormick, Clive R. Rosenthal, Thomas D. Miller, and Eleanor A. Maguire. Mind-Wandering in People with Hippocampal Damage. *The Journal of Neuroscience*, 38(11):2745–2754, March 2018. ISSN 0270-6474. doi: 10.1523/JNEUROSCI.1812-17.2018. URL https://www.ncbi.nlm.nih.gov/pmc/articles/PMC5851780/.

MNE. MNE documentation. https://mne.tools/stable/generated/mne.preprocessing.ICA.html.

Sepehr Mortaheb, Laurens Van Calster, Federico Raimondo, Manousos A. Klados, Paradeisios Alexandros Boulakis, Kleio Georgoula, Steve Majerus, Dimitri Van De Ville, and Athena Demertzi. Mind blanking is a distinct mental state linked to a recurrent brain profile of globally positive connectivity during ongoing mentation. *Proceedings of the National Academy of Sciences*, 119(41):e2200511119, October 2022. ISSN 0027-8424, 1091-6490. doi: 10.1073/pnas.2200511119. URL https://pnas.org/doi/10.1073/pnas.2200511119.

Kevin Murphy, Rasmus M. Birn, and Peter A. Bandettini. Resting-state FMRI confounds and cleanup. *NeuroImage*, 80:349–359, October 2013. ISSN 1053-8119. doi: 10.1016/j.neuroimage.2013.04.001. URL https://www.ncbi.nlm.nih.gov/pmc/articles/PMC3720818/.

Teresa Murta, Marco Leite, David W. Carmichael, Patrícia Figueiredo, and Louis Lemieux. Electrophysiological correlates of the BOLD signal for EEG-informed fMRI. *Human Brain Mapping*, 36(1):391–414, 2015. ISSN 1097-0193. doi: 10.1002/hbm.22623. URL https://onlinelibrary.wiley.com/doi/abs/10.1002/hbm.22623. _eprint: https://onlinelibrary.wiley.com/doi/pdf/10.1002/hbm.22623.

Ernst Niedermeyer and F. H. Lopes da Silva. *Electroencephalography: Basic Principles, Clinical Applications, and Related Fields*. Lippincott Williams & Wilkins, 2005. ISBN 978-0-7817-5126-1. Google-Books-ID: tndqYGPHQdEC.

Cyril R. Pernet, Stefan Appelhoff, Krzysztof J. Gorgolewski, Guillaume Flandin, Christophe Phillips, Arnaud Delorme, and Robert Oostenveld. EEG-BIDS, an extension to the brain imaging data structure for electroencephalography. *Scientific Data*, 6(1):103, June 2019. ISSN 2052-4463. doi: 10.1038/s41597-019-0104-8. URL https://www.nature.com/articles/s41597-019-0104-8. Publisher: Nature Publishing Group.

Tam Pham, Zen Juen Lau, S. H. Annabel Chen, and Dominique Makowski. Heart Rate Variability in Psychology: A Review of HRV Indices and an Analysis Tutorial. *Sensors*, 21(12):3998, January 2021. ISSN 1424-8220. doi: 10.3390/s21123998. URL https://www.mdpi.com/1424-8220/21/12/3998. Number: 12 Publisher: Multidisciplinary Digital Publishing Institute.

Jonathan D. Power, Mark Plitt, Stephen J. Gotts, Prantik Kundu, Valerie Voon, Peter A. Bandettini, and Alex Martin. Ridding fMRI data of motion-related influences: Removal of signals with distinct spatial and physical bases in multiecho data. *Proceedings of the National Academy of Sciences*, 115(9):E2105–E2114, February 2018. doi: 10.1073/pnas.1720985115. URL https://www.pnas.org/doi/full/10.1073/pnas.1720985115. Publisher: Proceedings of the National Academy of Sciences.

Radboud University Nijmegen. Radboud faces database. https://rafd.nl/.

Robert N. S. Sachdev, Nicolas Gaspard, Jason L. Gerrard, Lawrence J. Hirsch, Dennis D. Spencer, and Hitten P. Zaveri. Delta rhythm in wakefulness: evidence from intracranial recordings in human beings. *Journal of Neurophysiology*, 114(2):1248–1254, August 2015. ISSN 0022-3077. doi: 10.1152/jn.00249.2015. URL https://www.ncbi.nlm.nih.gov/pmc/articles/PMC4725112/.

René Scheeringa, Karl Magnus Petersson, Andreas Kleinschmidt, Ole Jensen, and Marcel C.M. Bastiaansen. EEG Alpha Power Modulation of fMRI Resting-State Connectivity. *Brain Connectivity*, 2(5):254–264, October 2012. ISSN 2158-0014, 2158-0022. doi: 10.1089/brain.2012.0088. URL http://www.liebertpub.com/doi/10.1089/brain.2012.0088.

Marieke L. Schölvinck, Alexander Maier, Frank Q. Ye, Jeff H. Duyn, and David A. Leopold. Neural basis of global resting-state fMRI activity. *Proceedings of the National Academy of Sciences of the United States of America*, 107(22):10238–10243, June 2010. ISSN 0027-8424. doi: 10.1073/pnas.0913110107. URL https://www.ncbi.nlm.nih.gov/pmc/articles/PMC2890438/.

Karin Shmueli, Peter van Gelderen, Jacco A. de Zwart, Silvina G. Horovitz, Masaki Fukunaga, J. Martijn Jansma, and Jeff H. Duyn. Low-frequency fluctuations in the cardiac rate as a source of variance in the resting-state fMRI BOLD signal. *NeuroImage*, 38(2):306–320, November 2007. ISSN 1053-8119. doi: 10.1016/j.neuroimage.2007.07.037.

G. L. Shulman, J. A. Fiez, M. Corbetta, R. L. Buckner, F. M. Miezin, M. E. Raichle, and S. E. Petersen. Common Blood Flow Changes across Visual Tasks: II. Decreases in Cerebral Cortex. *Journal of Cognitive Neuroscience*, 9(5):648–663, 1997. ISSN 0898-929X. doi: 10.1162/jocn.1997.9.5.648.

Jonathan Smallwood. Distinguishing how from why the mind wanders: A process–occurrence framework for self-generated mental activity. *Psychological Bulletin 139*, 3:519–35, 2013. doi: 10.1037/a0030010. URL https://doi.org/10.1037/a0030010.

Enzo Tagliazucchi, Frederic Von Wegner, Astrid Morzelewski, Verena Brodbeck, and Helmut Laufs. Dynamic BOLD functional connectivity in humans and its electrophysiological correlates. *Frontiers in Human Neuroscience*, 6, December 2012. ISSN 1662-5161. doi: 10.3389/fnhum.2012.00339. URL https://www.frontiersin.org/journals/human-neuroscience/articles/10.3389/fnhum.2012.00339/full. Publisher: Frontiers.

Team of Brain Products GmbH. Brainvision analyzer 2. https://www.brainproducts.com/solutions/analyzer/.

Varvara Strizhneva. Thesis. https://gitlab.uliege.be/Varvara.Strizhneva/thesis, 2025.

Vladyslav V. Vyazovskiy and Kenneth D. Harris. Sleep and the single neuron: the role of global slow oscillations in individual cell rest. *Nature reviews. Neuroscience*, 14(6):443–451, June 2013. ISSN 1471-003X. doi: 10.1038/nrn3494. URL https://www.ncbi.nlm.nih.gov/pmc/articles/PMC3972489/.

Vladyslav V. Vyazovskiy, Umberto Olcese, Erin C. Hanlon, Yuval Nir, Chiara Cirelli, and Giulio Tononi. Local sleep in awake rats. *Nature*, 472(7344):443–447, April 2011. ISSN 1476-4687. doi: 10.1038/nature10009. URL https://www.nature.com/articles/nature10009.

Tracy Warbrick. Simultaneous EEG-fMRI: What Have We Learned and What Does the Future Hold? *Sensors (Basel, Switzerland)*, 22(6):2262, March 2022. ISSN 1424-8220. doi: 10.3390/s22062262. URL https://www.ncbi.nlm.nih.gov/pmc/articles/PMC8952790/.

Adrian Frank Ward and Daniel M. Wegner. Mind-blanking: when the mind goes away. *Frontiers in Psychology*, 4, September 2013. ISSN 1664-1078. doi: 10.3389/fpsyg.2013.00650. URL https://www.frontiersin.org/journals/psychology/articles/10.3389/fpsyg.2013.00650/full. Publisher: Frontiers.

Chi Wah Wong, Valur Olafsson, Omer Tal, and Thomas T. Liu. Anti-correlated Networks, Global Signal Regression, and the Effects of Caffeine in Resting-State Functional MRI. *NeuroImage*, 63(1):356–364, October 2012. ISSN 1053-8119. doi: 10.1016/j.neuroimage.2012.06.035. URL https://www.ncbi.nlm.nih.gov/pmc/articles/PMC3444518/.

Chi Wah Wong, Valur Olafsson, Omer Tal, and Thomas T. Liu. The amplitude of the resting-state fMRI global signal is related to EEG vigilance measures. *NeuroImage*, 83:10.1016/j.neuroimage.2013.07.057, December 2013. ISSN 1053-8119. doi: 10.1016/j.neuroimage.2013.07.057. URL https://www.ncbi.nlm.nih.gov/pmc/articles/PMC3815994/.

Aiping Liu Soojin Lee Xiang Chen Xu Zhang Martin J. McKeown Z. Jane Wang Xun Chen, Xueyuan Xu. (PDF) Removal of Muscle Artifacts from Few-Channel EEG Recordings Based on Multivariate Empirical Mode Decomposition and Independent Vector Analysis. *ResearchGate*, February 2025. doi: 10.1049/el.2018.0191. URL https://www.researchgate.net/publication/325315013_Removal_of_Muscle_Artifacts_from_Few-Channel_EEG_Recordings_Based_on_Multivariate_Empirical_Mode_Decomposition_and_Independent_Vector_Analysis.

B. T. Thomas Yeo, Jesisca Tandi, and Michael W. L. Chee. Functional connectivity during rested wakefulness predicts vulnerability to sleep deprivation. *NeuroImage*, 111:147–158, May 2015. ISSN 1053-8119. doi: 10.1016/j.neuroimage.2015.02.018. URL https://www.sciencedirect.com/science/article/pii/S1053811915001196.